

Nanotechnological Characterisation of Biomaterials – Structural and Biophysical Investigations



Dissertation
der Fakultät für Geowissenschaften
der Ludwig-Maximilians-Universität München

Stefan Strasser

München, 10. September 2007

Advising supervisor:

Prof. Dr. Wolfgang M. Heckl

Second supervisor:

PD Dr. Albert Zink

Date of Disputation:

13. December 2007

Table of Contents

| | |
|---|-----------|
| 1. Summary..... | 4 |
| 2. Introduction | 6 |
| 3. Measuring Bioelasticity – A Nanotechnological Approach | 8 |
| 3.1 Atomic Force Microscopy | 8 |
| 3.1.1 Imaging Modes..... | 9 |
| 3.1.1.1 Contact Mode | 10 |
| 3.1.1.2 Non-Contact Mode..... | 10 |
| 3.1.1.3 Intermittent Contact Mode | 11 |
| 3.1.2 Force Spectroscopy | 11 |
| 3.1.3 Elasticity Calculations..... | 13 |
| 3.1.3.1 Contact Mechanics | 13 |
| 3.1.3.2 Evaluation of Force Spectroscopy Data..... | 16 |
| 3.2 Collagen Studies by Nanotechnological Methods..... | 19 |
| 3.2.1 Formation of Collagen Fibrils..... | 19 |
| 3.2.1.1 <i>In vivo</i> Self-Assembly of Collagen | 20 |
| 3.2.1.2 <i>In vitro</i> Self-Assembly of Collagen | 22 |
| 3.2.2 Structural Properties of Single Collagen Fibrils..... | 24 |
| 3.2.2.1 Microdissection of Single Collagen Fibrils..... | 25 |
| 3.2.2.2 Elasticity Measurements on Dissected Collagen Fibrils..... | 26 |
| 3.2.3 <i>In situ</i> Collagen Applications and Properties of Bone Tissue..... | 29 |
| 3.2.3.1 Interface between Biomaterials and Biological Systems..... | 29 |
| 3.2.3.2 Properties of Complex Organic and Anorganic Biomaterials..... | 31 |
| 3.3 Nanotechnology in the Forensic Science..... | 35 |
| 3.3.1 Chronological Reconstruction of Crimes | 35 |
| 3.3.2 Age Determination of Blood Spots..... | 36 |
| 3.3.2.1 Morphology of Aged Blood | 37 |
| 3.3.2.2 Elasticity of Aged Blood..... | 38 |
| 4. References..... | 41 |
| 5. Publications..... | 47 |
| 5.1 Controlled Self-Assembly of Collagen Fibrils by an Automated Dialysis System | 48 |
| 5.2 Structural Investigations on Native Collagen Type I Fibrils | 54 |
| 5.3 Implant Surface Coatings with Bone Sialoprotein, Collagen and Fibronectin and their Effects on Cells derived from Human Maxillar Bone..... | 61 |
| 5.4 Age Determination of Blood Spots in Forensic Medicine By Force Spectroscopy | 69 |
| 6. Outlook..... | 77 |
| 7. Appendix..... | 78 |
| 8. Acknowledgements | 82 |
| 9. Curriculum Vitae | 83 |

1. Summary

These studies were conducted in order to determine structural and elastic properties of biomaterials and their influence on complex biological structures as well as time dependent degradation processes. Morphological investigations were based on Atomic Force Microscope (AFM) and Scanning Electron Microscope (SEM) images. Elastic properties of the biomaterials were evaluated by means of force spectroscopy measurements performed with an AFM. The feasibility of the methods was proven by the preparation of highly ordered biomolecules and subsequent structural and elastical analysis.

For the *in vitro* investigation of acid soluble D-periodic collagen fibrils a novel, fully automated system for self-assembly was developed. For the separation of acid from collagen molecules in order to initiate and maintain self-assembly, a dialysis process was used. Improvement of performance and reproducibility of the fibril preparation was accomplished by controlling the process with the recently developed automated dialysis system. The functionality of the system was demonstrated by a repeated successful preparation of different collagen types.

Collagen type I fibrils which occur naturally as a compound were used for elaborate structural investigations with nanotechnological methods. During the last years differences in the elasticity between core and shell were discussed controversially. The inner structure of mature fibrils was revealed by AFM topographs, which were taken after a microdissection step. From this data it was evident that the core of the fibrils exhibits the same morphological and structural properties as the shell. In addition to the structural investigations we performed elasticity measurements of both core and shell of the collagen fibrils. The AFM based nanoindentation experiments resulted in a similar value of Youngs modulus for both regions. Therefore a fluid core, as proposed in the literature, could not be confirmed by our spatially resolved elasticity measurements. However the results indicate a somewhat lower adhesion of the shell, which point to different degrees of cross linking of the inner and outer regions.

The role of collagen and adjacent organic and anorganic material in complex biological tissue was investigated by examining fresh vertebral bones from pigs and ancient skeletal material. The high stiffness and toughness of bone is assumed to be mediated by protein filaments, which act as a glue between collagen structures in the calcium hydroxyapatite matrix. This "bone-glue" prevents bone from cracking when high mechanical stress is applied. Samples of an ancient Egyptian mummy were prepared and imaged with the SEM in order to study the lifetime of proteins acting as elasticity mediator. Thereby we could successfully visualize filamentous structures of the supposed size, which were bridging the microcracks in the fresh porcine samples as well as in ancient human vertebrae.

For the comparison of the influence of collagen and other surface coatings on the healing time after implant surgeries, morphological investigations of differently functionalized substrates were conducted with the AFM. Both the bare thin films and thin films with cells adsorbed on them were investigated. Differences in uniformity of the functionalizing layers with minor effects on the cell growth were identified.

The degradation of biological substances plays an important role in forensic science, in particular for the chronological reconstruction of crimes. In this context we presented a novel tool to estimate the age of bloodstains. Fresh blood spots were deposited on a glass slide and imaged with the AFM as a function of time in order to examine morphological alterations over time. In addition time resolved elasticity measurements based on AFM force spectroscopy were performed. We did not detect any

morphological differences of the blood spot, however the elasticity values exhibited a significant hardening of the blood within the investigation period. Our data clearly demonstrated the potential of this method for the age estimation of bloodstains for forensic applications.

2. Introduction

Through structural arrangement of polymeric and ceramic components biological materials achieve remarkable mechanical strength despite their small mass. Biomaterials are either primarily ceramic (tooth enamel, mollusc shell), polymeric (insect exoskeleton, plant cell walls), or composites (antler, bone). Virtually all biological materials are composites combining different properties of the basic components and offer a variety of hierarchical structures [1]. Therefore profound knowledge of the interaction of single constituents in a multi-component material is of outstanding interest. To understand nature's architecture and principles detailed knowledge about biological assemblies and elastical properties is required. While microscopic studies reveal that biological composites can be comprised of as many as five [2] or six [3] distinct substructures (ex. mineral platelets, protein interlayers, collagen fibrils, fibres and lamellae), the influence and interaction of these on the overall mechanical properties is not well understood [1]. Nacre for example consists of 97% calcium carbonate (aragonite modification) embedded in an organic matrix, but has a 3000 times higher tensile strength than calcium carbonate [4]. In brachiopod shells stacked arrangements of organic layers in an organic matrix with crystallites decrease the probability of crack formation and increase stability and hardness. This is attained by the interconnection of flexible and hard constituents and by an hierarchical structure of the shell [5].

Material synthesis in present nanotechnology is based on two fundamentally different approaches, the top down and bottom up principle. A number of physical technologies are used to produce nanoscaled structures like Nano-Electro-Mechanical-Systems (NEMS) using top down principles. The second approach to assemble nanoscaled systems uses elementary building blocks, such as atoms or molecules. Functional units arise step by step by controlled assembly processes. In nature complex structures emerge through self-assembly starting at the molecular level. For the understanding of the structure function relationship in biocomposites, in most cases it is not sufficient to investigate the synthesis only. Also the hierarchical structure and the mechanical properties of single components and their mutual interaction have to be investigated.

During the last years innovations in the field of Scanning Probe Microscopy (SPM) provided valuable insights in the understanding of biological processes. Nowadays, biological materials can be imaged in their natural environment. The most important scanning probe microscope suitable for biological samples is the Atomic Force Microscope (AFM). Here, samples are not imaged in a conventional sense, rather the AFM creates an image of the sample by mechanical interaction with a sharp tip and detection of the force between tip and sample. Images of biological as well as many other materials with resolution down to the molecular and atomic scale can be obtained. Besides imaging this versatile tool allows also for the manipulation of matter on the nanometer scale. The dissection of plasmids in liquid with the AFM was first shown by Hansma et al. [6]. Thalhammer et al. demonstrated the possibility to use the AFM tip as a nanoshuffle to extract minute amounts of DNA for subsequent analysis [7]. Furthermore, the AFM is capable of measuring elasticity and tensile moduli. Elongation and relaxation profiles of single collagen fibrils were recorded, thereby demonstrating a large extensibility and a significant reserve of elasticity [8]. Crosslinks

on a low organisation level of collagen were tested by pulling substructures out of the aggregation.

In order to predict mechanical properties of specific composite materials one has to understand the interconnection, i.e. elastic properties and the mutual interaction of each single constituent in heterogeneous assemblies. For the understanding of single component properties in composites and their contribution to the overall mechanical characteristics of compounds, modern nanotechnology provides unmatched insights. Nanotechnology serves many different fields in science by providing an atomistic understanding. Properties of single molecules and their interaction with adjacent molecules in compounds can be measured directly, not as an ensemble average as with other conventional techniques.

We implemented a new automated system for self-assembly of biomolecules especially collagen fibrils, which were subsequently investigated with the AFM by performing microdissection and elasticity measurements. Structural properties and alterations of biopolymers in complex organic and inorganic matrices were examined. To support forensic medicine, both AFM based force spectroscopy and morphological investigations were conducted on blood samples in a time resolved manner. Investigations of cell growth of osteoblasts on different substrates in order to explore the influence of implant coatings on the healing time after surgery could be supported by providing high resolution images of the substrate coatings and subsequently grown cells. With the Scanning Electron Microscope (SEM) structural properties of ancient and fresh mammalian bone samples at the molecular level were able to provide insights in assembly and degradation processes of microstructured collagenous tissue.

3. Measuring Bioelasticity – A Nanotechnological Approach

Over the years material sciences gave important insights for the understanding of material properties which are of fundamental interest for technological applications. Normally elastic properties are determined by pulling, bending or indentation experiments. For elasticity measurements on the molecular level the measurement tools for macroscopic samples are not suitable: the resolution is insufficient and contact areas are too large to test macromolecules and microstructured biocomposites. The influence of single components on the overall mechanical properties can be investigated only on the microscopic and molecular level. The capabilities of the AFM to image, manipulate and measure mechanical properties of materials in their natural environment without extraordinary requirements on the sample properties, predestines it for applications in material science.

3.1 Atomic Force Microscopy

In the 1980's a new type of nearfield microscope initiated a revolution in the field of imaging a wide variety of samples on the nanometer scale. In 1982 Gerd Binnig, Heinrich Rohrer, Christoph Gerber and Eddie Weibel developed the Scanning Tunneling Microscope (STM) at the research laboratories of IBM in Zurich. The breakthrough was an image of a 7x7 reconstructed silicon (111) surface where atomic resolution was obtained for the first time [9]. A few years later a microscope derived from the STM was invented by Gerd Binnig, Calvin F. Quate and Christoph Gerber at IBM, the Atomic Force Microscope (AFM) [10]. In contrast to the STM, the AFM does not require electrically conducting samples, thus facilitates the investigation of non-conducting samples as normally encountered in biology. The STM operates with a very sharp tip, ideally terminated by a single atom at the apex, which is scanned across the sample surface line by line. Between tip and sample a small bias voltage is applied, so that at the end of the tip a field of 10^7 V/cm and more can be found [11]. By means of the quantum mechanical tunneling effect electrons can be transmitted through the barrier which is not allowed by classical mechanics. This gives rise to a highly distant dependent current which is used as an extremely sensitive measure for the probe sample distance. The AFM also requires a tip which scans the surface line by line, see Fig. 1. However in the case of the AFM it is not necessary to apply a voltage between tip and sample surface. The tip is mounted to a cantilever with a distinct spring constant. This assembly is used to measure the resulting force between tip and surface. As a consequence of sample topography the cantilever bending varies according to the lateral position. Depending on the operational mode some quantity is kept constant by means of a feed-back loop which controls the tip sample distance. Eventually the extension of the z-piezo is used to reconstruct the sample topography. Typically the cantilever bending is detected with a laser based light pointer. The laser is focussed on the backside of the cantilever where it is reflected onto a 4-quadrant photodiode. The laser induces a photovoltage in the quadrants of the photodiode. Vertical movements and torsions can be measured by evaluation of the appropriate

difference signal of the individual quadrants. This difference signal of the photodiode is used as an input signal for a feedback loop. In order to follow the sample topography the cantilever is moved by the z-piezo in vertical directions. Also the movements in x- and y-directions during the linewise scanning process are accomplished by piezos, in most cases stacked piezo assemblies or tubes are used. Piezos are ceramic materials which are extending and contracting when an electric field is applied. Normally PZT (lead zirconium titanate) is used as piezoelectric material.

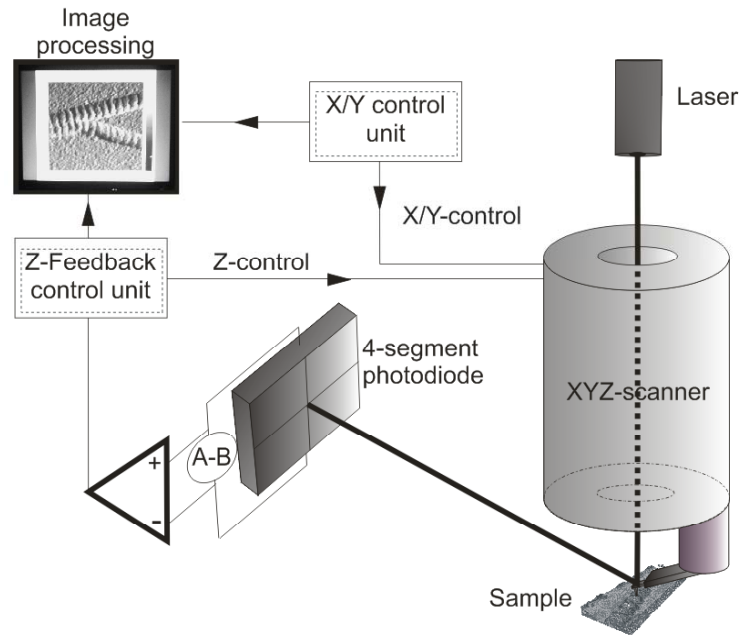


Fig. 1: Sketch of the operating principle of the Atomic Force Microscope

A Si-chip with a cantilever and a very sharp tip is fixed to a piezo tube which fulfils the scanning motion across the sample in x/y-direction and vertical to the sample in z-direction. The deflection is measured with a 4 segment photodiode. The difference signal A-B between upper and lower section of the photodiode is held constant by the feed back loop during imaging in contact mode. The image is created with the signals of the x/y controller, the signal of the z-feedback loop (photodiode signal) and the z-control of the scanner (adapted from [12]).

3.1.1 Imaging Modes

Depending on the samples properties and the required resolution a particular imaging mode has to be chosen. For soft samples the applied force must not be too high, which means mechanical contact between probe and sample should be avoided. Hence the non-contact mode should be used, otherwise the sample will be irreversibly altered during imaging. The contact mode should be chosen, when very high resolution down to the atomic scale is required and the sample offers sufficient hardness. Both advantages, feasibility for soft materials and high resolution capability are combined in the intermittent-contact mode. In the following chapter the most commonly used imaging modes of the AFM are explained in more detail.

Independent of the imaging mode the image results from convolution of the tip geometry with sample topography, as illustrated in Fig. 2. If the diameter of the tip apex becomes comparable to sample features, protrusions appear significantly broader and pits smaller than they actually are. This well known artefact is called “convolution effect”.

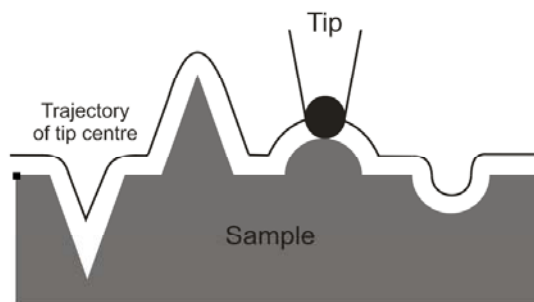


Fig. 2: Trajectory of an AFM tip over a sample surface. Protrusions appear broader, whereas pits are imaged smaller than they are. The resulting image originates from convolution of tip and sample geometry.

3.1.1.1 Contact Mode

In contact mode mechanical contact between the apex of the tip and the outer surface layer of the sample is established, cf. Fig. 2. While imaging hydrophilic surfaces at relative humidities greater than 30%, at least one monolayer of water is condensed on the surface and the tip moves through an adhesive water layer. Since condensation of water in the space between tip and sample surface is energetically favourable, water layers result in an attractive contribution to the total tip sample force.

Generally, the contact mode is subdivided into two modes, the constant force mode and the constant height mode [13]. In the constant force mode the photodiode signal is kept constant by a feedback loop. During the linewise scanning process a set-point force is maintained by holding the cantilever bending constant. In order to achieve this for each image pixel, the z-piezo moves the cantilever in vertical directions. Thus, the z-position of the piezo as a function of lateral position (x, y) corresponds to the topography. Whereas for the constant height mode the feedback control loop is deactivated. This is only recommended for very flat and hard samples. In the constant height mode the topography information is encoded in the photodiode signal, the so called error signal, which is a measure for the cantilever bending. Due to the strong interaction between tip and sample high resolution can be obtained.

3.1.1.2 Non-Contact Mode

In the non-contact mode the tip is not in contact with the sample, but several tens of nanometers away. Far away from the sample the cantilever is oscillated near its resonant frequency by means of applying an alternating voltage to the z-piezo. Upon

approaching the tip to the sample the amplitude of the oscillation will be reduced and the eigen-frequency of the cantilever changed due to interaction forces, see Fig. 3. Here the frequency shift is held constant during imaging. In this mode the total interaction force between tip and sample is smaller as compared to the contact mode and therefore the resolution is reduced. Normally soft samples are imaged with the non-contact mode, as no lateral forces are applied to the sample and no sample deformations are induced.

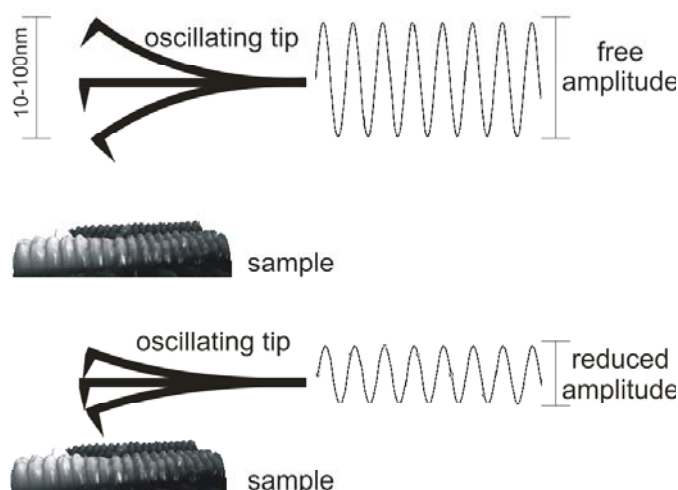


Fig. 3: Principle of non-contact mode. The upper sketch shows the oscillation far away from the sample surface. The sketch below illustrates the reduced oscillation when the tip has been approached to the sample.

3.1.1.3 Intermittent Contact Mode

The intermittent contact mode combines the advantages of the contact mode and the non-contact mode. In the non-contact mode the tip oscillation is excited near its resonant frequency relatively far away from the sample surface. When the amplitude is increased the tip briefly touches the sample every time it passes the lower reversal point of the oscillation, as depicted in Fig. 3. This mode has the advantages that frictional forces can be almost completely avoided and normally higher resolution than in the non-contact mode can be obtained. Alteration and destruction of the sample is often observed when the contact time is too long. This opens up a way to avoid sample destruction by keeping the interaction time between tip and sample short enough.

3.1.2 Force Spectroscopy

Compared to many other microscopical methods as conventional light microscopy, scanning electron microscopy or Transmission Electron Microscopy (TEM), atomic

force microscopy offers the opportunity to locally manipulate and probe elastic properties of the sample.

For the acquisition of force displacement curves, the z-piezo must be ramped along the vertical direction perpendicular to the sample surface and the tip is used as a nanoindenter. In principle there are two modes of recording force-displacement curves. The static mode is characterised by a linearly ramped approach to the sample. The cantilever bending is recorded by means of the photodiode signal as a function of z-piezo extension. In the dynamic mode the AFM is operated in non-contact mode, and the cantilever is oscillating near its resonant frequency. Then the amplitude of the oscillation is recorded as a function of tip-sample distance during approaching and withdrawing. In general force distance curves can be divided into 3 regions, the zero line, the non-contact line and the contact line. When the tip is far away from the sample and the cantilever deflection is nearly zero, the respective bending is assigned to the zero line. When the tip is pushed against the surface and indents into the sample, the contact region of the force displacement curve is recorded. The non-contact line contains the jump-into-contact and the jump-out-of-contact domain. Attractive forces can be distinguished by means of the non-contact line. Attractive forces are mainly Van der Waals or Coulomb forces, whereas repulsive forces are double layer, hydration and steric forces [13]. Fig. 4 displays a typical force-distance curve. The different regions as described above (jump-into-contact and jump-out-of-contact) can be seen in the approach as well as in the retraction curve.

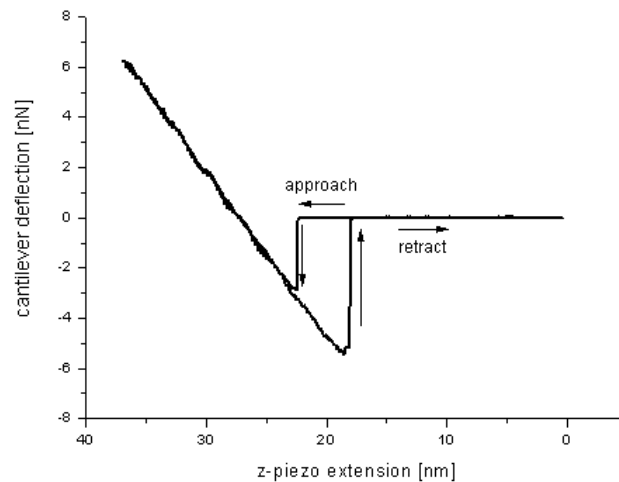


Fig. 4: Force displacement curve on a sample with attractive surface forces.

Depending on the elastic properties of the sample the indentation varies at constant loading forces. In the simplest case there are no or negligible surface forces between tip and sample. In the indentation experiment only elastic properties of the substrate material are measured. When only elastic forces occur during the measurements the force curve can be modelled by a theory developed by Hertz and Sneddon [14, 15]. On rigid surfaces the indentation of the tip is assumed to be zero. As can be seen in Fig. 5,

where curves with different Young's moduli are modelled based on the Hertzian theory in the contact regime. The more elastic the sample is the more the tip penetrates into the sample.

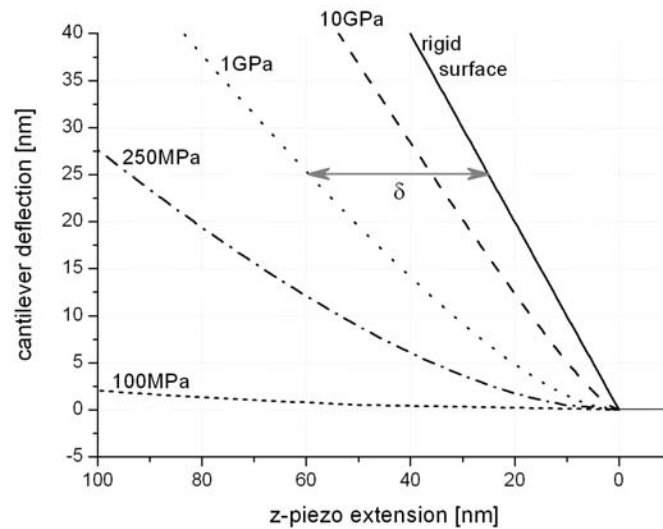


Fig. 5: Force distance curves of various samples with different elasticity modelled with the Hertzian theory in the contact regime. The AFM tip can not penetrate into the rigid sample surface, therefore the cantilever deflection corresponds to the extension of the z-piezo. The softer the sample the more the tip penetrates into the sample. As a consequence the slope becomes smoother.

3.1.3 Elasticity Calculations

At the end of the nineteenth century Heinrich Hertz started his investigations of contact mechanics [14]. He considered the distribution of contact pressure and elastic displacements in two bodies which were pressed against each other. The area of contact was proposed to be elliptical. Hertz worked with glass lenses and investigated optical interference effects. Based on his knowledge about electrostatic potentials and his experience with optical interference he developed his theory of the contact mechanics of two elastic bodies [16].

3.1.3.1 Contact Mechanics

When a force is applied between two elastic bodies, the mechanical stress is mainly concentrated within the contact region. The stress decreases rapidly with increasing distance from the center of contact. In general, the dimensions of the samples are large compared to the contact area. Therefore the sample can be approximated as elastic half space [16].

For force spectroscopy measurements on samples with ideal elastic properties the approach and withdrawal curve would be identical. In case of ideally plastic samples, the curves do not overlap at all and the indentation pit formed during the penetration remains. The great majority of materials exhibit a combination of both properties. The Hertz theory only takes into account elastical properties and neglects additional surface forces such as adhesion. If surface forces play a role during the measurements other models as e.g. Maugis Dugdale (MD), Derjaguin-Müller-Toporov (DMT) or Johnson-Kendall-Roberts (JKR) have to be applied. Fig. 6 displays the geometry of a spherical tip interacting with a flat sample.

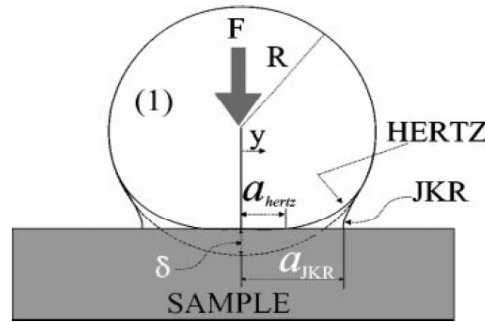


Fig. 6: Interaction of an elastic sphere with a flat surface. F is the loading force, R the radius of the sphere, y the distance from the center of the contact area, δ the penetration depth, a_{Hertz} and a_{JKR} are the contact radius with respect to the Hertz and the JKR theories, (taken from [13]).

Following the ideas of Cappella and Dietler [13], the contact radius a , where a sphere with the radius R is pressed against a flat surface is given by:

$$a = \sqrt[3]{\frac{RF}{K}}. \quad (3.1)$$

Here, the reduced or effective Youngs modulus [17] takes into account that elastic deformations take place in the sample as well as in the indenter. Youngs modulus E_s and Poisson ratio ν_s for the sample as well as for the indenter (index i) determine the effective modulus, which is defined by:

$$\frac{1}{K} = \frac{3}{4} \cdot \left(\frac{1 - \nu_s^2}{E_s} + \frac{1 - \nu_i^2}{E_i} \right). \quad (3.2)$$

In case of a very hard tip, the effective modulus is dominated by the sample material and the second term of equation (3.2) is then negligible; combined with equation (3.1) it results to:

$$F = \frac{4}{3R} \cdot \left(\frac{E_s}{1 - \nu_s^2} \right) \cdot a^3. \quad (3.3)$$

Sneddon extended the model for rigid punches and flat surfaces under the assumption of an elastic half space [15]. In case of rigid axisymmetric punches, where $f(x)$ describes the punch profile, according to Sneddon the force can be estimated by:

$$F = \frac{3}{2} Ka \int_0^1 \frac{x^2 f'(x)}{\sqrt{1-x^2}} dx. \quad (3.4)$$

As stated above, the Hertz and Sneddon model can only be applied when additional surface forces can be neglected, otherwise a more generalized theory has to be applied. A detailed description can be found in reference [13].

For systems with low adhesion forces and small tip radii the theory after Dejarguin, Müller and Toporov (DMT) [18] is most appropriate. It takes into account that forces between the two bodies produce a “finite area of contact”. The DMT model describes adhesive forces around the contact radius while the surface is not deformed by adhesion [19]. Upon retraction of the tip this force increases until the tip snaps out of contact. The adhesion force at zero load can be expressed by the adhesion work W at contact by the following equation with the indentation depth and the contact radius equals to zero:

$$F_{ad} = 2\pi RW \quad (3.5)$$

The adhesion force enters the calculation via the contact radius which is increased according to the DMT-theory. The contact radius has following term:

$$a = \sqrt[3]{(F + 2\pi RW) \frac{R}{K}}. \quad (3.6)$$

The indentation as well as the pressure is identical to the Hertz model.

Johnson Kendall and Roberts (JKR) theory is to be preferred when soft samples with high adhesion are measured with large tip radii [20]. This model only takes short range forces within the contact region into account, which are able to deform the sample upon withdraw. According to the JKR model the force when the indenter detaches is given by:

$$F_{ad} = \frac{3}{2} \pi RW. \quad (3.7)$$

The contact radius can be written as:

$$a = \sqrt[3]{\frac{R}{K} \left[F + 3RW\pi + \sqrt{6RWF\pi + (3RW\pi)^2} \right]}. \quad (3.8)$$

Pashley et al. [21] introduced an expression to estimate the surface forces inside and outside the contact area. The parameter φ_P is directly proportional to the height h of the specimen neck which is formed before the tip detaches during retraction and indirectly proportional to the typical atomic dimension z_0 , φ_P is given by:

$$\varphi_P = \frac{h}{z_0} \cong \sqrt[3]{\frac{RW^2}{K^2 z_0^3}}. \quad (3.9)$$

Müller et al. [22] used this parameter as a criterion for the selection of the appropriate theory. For $\varphi_P < 0.3$, in case of hard samples, small radius and low surface energies the

DMT theory is applicable, whereas for $\phi_P > 3$, in case of soft samples, large radii and high surface energies the JKR model is preferable.

The most extensive theory to model surface interactions was introduced by Maugis [23]. It is applicable for large rigid spheres with high surface energies as well as for small soft bodies with low surface energies, but also for intermediate cases. A dimensionless parameter was introduced to fully describe the sample properties:

$$\lambda = 2 \cdot \sigma_0 \cdot \left(\frac{\pi W K^2}{R} \right)^{-\frac{1}{3}}. \quad (3.10)$$

Whereas σ_0 is the surface stress at the edge of the indenter. For soft, large and adhesive bodies λ is high, whereas for small and hard bodies the value of λ is small. Maugis introduced several supplementary dimensionless parameters corresponding to the contact radius, the adhesion force which is modelled as constant additional stress over the annular region, and the indentation depth.

For $\lambda \rightarrow 0$ the Maugis theory converges to the DMT model and for $\lambda \rightarrow \infty$ to the JKR theory. In all other cases, solving the Maugis model is not trivial and at least some parameters have to be known. It can not be solved analytically and requires elaborate numerical calculations.

All theories described above are continuum elastic theories and hence require smooth surfaces without plastic or viscoelastic deformations. The exact derivations of the equations and theories can be found in detail in the respective literature as cited above and are reviewed by Cappella and Dietler [13]. Although in the Hertzian theory surface interactions are not taken into account. Nevertheless it is useful when high loads are applied, surface forces are not too high and only elastic properties of the sample are to be measured. However depending on the experimental conditions, the sample properties of interest, and the required accuracy, the respective model has to be chosen accordingly.

3.1.3.2 Evaluation of Force Spectroscopy Data

Independent on the model which is used for the evaluation of the force spectra it has to be fitted to the experimental curves. For our data we used the Hertz model to deduce Youngs modulus. Since these experiments were indentation based and no repulsive surface forces were identified, adhesion forces play a minor role for our elasticity calculations.

According to the Hertzian theory for small indentations of an infinitely hard parabolic tip into an elastic half space the normal force F can be described by the following equations [15, 24, 25]:

$$F_{\text{paraboloid}} = \frac{4}{3} \cdot \frac{E}{(1 - \nu^2)} \cdot \delta^{\frac{3}{2}} \cdot \sqrt{R}, \quad (3.11)$$

$$F_{cone} = \frac{\pi}{2} \cdot \frac{E}{(1-\nu^2)} \cdot \delta^2 \cdot \tan(\alpha), \quad (3.12)$$

where δ is the indentation depth, E is Youngs modulus, ν is the Poisson ratio, α is the cone angle (half of the opening angle), and R is the tip radius. In case of incompressible materials the ν is 0.5. The applied force can be derived from the deflection of the cantilever which is considered as a tightened spring obeying Hooke's Law:

$$F = k_c \cdot d, \quad (3.13)$$

where k_c is the spring constant and d stands for the deflection of the cantilever. The cantilever deflection depends on the indentation of the tip into the sample. The extension z of the piezo tube normal to the sample surface accounts for the deflection of the cantilever d and the indentation depth δ of the tip into the sample:

$$z = d + \delta \quad (3.14)$$

By combination of equations (3.11), (3.13), and (3.14), Youngs modulus can be expressed for hard samples with small indentations as follows:

$$E_{paraboloid} = \frac{3 \cdot k_c \cdot (d - d_0) \cdot (1 - \nu^2)}{4 \cdot \sqrt{R} \cdot [(z - z_0) - (d - d_0)]^{3/2}}. \quad (3.15)$$

For soft samples with large indentations of the pyramidal cone of the AFM tip Youngs modulus can be expressed by:

$$E_{cone} = \frac{k_c \cdot (d - d_0) \cdot 2 \cdot (1 - \nu^2)}{\pi \cdot \tan(\alpha) \cdot [(z - z_0) - (d - d_0)]^2} \quad (3.16)$$

where d_0 and z_0 are the corresponding values of the cantilever deflection and the z-piezo extension at the contact point. Now equations (3.14) and (3.15) can be rewritten in the contact regime for hard samples as,

$$z = \left[\frac{3 \cdot k_c \cdot (d - d_0) \cdot (1 - \nu^2)}{4 \cdot \sqrt{R} \cdot E} \right]^{2/3} + (d - d_0) + z_0 \quad (3.17)$$

and for soft samples as:

$$z = \left[\frac{2 \cdot k_c \cdot (d - d_0) \cdot (1 - \nu^2)}{\pi \cdot \tan(\alpha) \cdot E} \right]^{1/2} + (d - d_0) + z_0. \quad (3.18)$$

Evaluation of Youngs modulus is performed through Levenberg Marquardt iterations for a distinct fitting range in the contact region. To exclude surface effects during the iteration the fit range does not include the contact point. Fig. 7 displays a force distance spectrum (grey curve) recorded on a several hundred nanometer thick collagen gel. The dashed black curve is simulated with the values (E , z_0) from the fitting procedure.

The fit is excellent, deviations between the simulated and the measured curve are negligible.

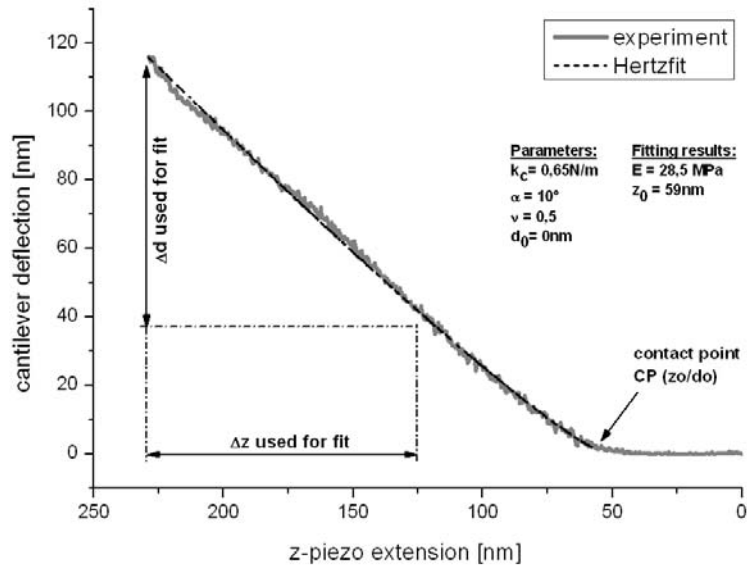


Fig. 7: Force spectroscopy on a collagen gel to demonstrate the applicability of the Hertzian model to these measurements. Fit parameters are Young's modulus E and the contact point z_0 , yielding values of $E = 28.5 \text{ MPa}$ and $z_0 = 59 \text{ nm}$.

3.2 Collagen Studies by Nanotechnological Methods

Collagen is the major structural protein in our body, which makes up for approximately 25% of all proteins and at least 20 distinct collagen types exist. Collagen molecules in the extracellular matrix are responsible for the strength of tendons, support skin and internal organs, as well as bones and teeth by adding mineral crystals. The collagen molecules, a right-handed triple helix, are comprised of three single collagen helices. The triple helix consists of two $\alpha 1(I)$ chains and one $\alpha 2(I)$ chain, where each chain has characteristic sequences of Gly-X-Y, where X and Y stand for any amino acid and Gly for glycine. Glycine has the smallest side chain, only a single hydrogen atom. Therefore a tight packing is possible, when every third amino acid is glycine and the residue (side chain) is inside the helical structure [26]. Irregularities during the assembly of collagen fibrils can cause severe diseases. Scurvy can develop as a consequence of vitamin deficiency (lack of ascorbic acid). Vitamine C plays an important role during the hydroxylation of proline and lysine and deficiency results in a disturbed assembly of collagen fibrils. Patients may suffer from gingival bleeding, dermatitis, joint inflammation, gastroenteritis, diarrhoea, fever and so on. A latency period of the disease of several months leads to a delayed onset of the symptoms [27]. The Ehlers Danlos Syndrom is caused by an accumulation of non-triple helical collagen chains in the endoplasmic reticulum and thus a slower rate of secretion during the collagen assembly. The formation of important cross-links is disturbed. [27]. The pathology of this genetic disease is hyper skin elasticity, extreme joint extendibility and functional disturbance of internal organs. Low bone mass and fragility is also caused by a genetic disorder called osteogenesis imperfecta. Two genes which encode the α chains of collagen type I are mutated. Most mutations of genes in the collagen assembly lead to a substitution of glycyl residues by cysteinyl residues, thereby inducing a disturbed formation of the triple helix [28]. Collagen molecules become fragile and complex structures as skin, tendons or blood vessels tend to rupture if cross-linking is inhibited during self-assembly.

The AFM offers many advantages for studying the structure, organisation and bioassembly of fibrous and other proteins under natural conditions. Cryo-AFM experiments were conducted on segmental-long-spacing (SLS) collagen crystals which may be important for the assembly of calcified tissue [29]. Collagen type I and FLS collagen fibrils were extensively studied and insights in bioassembly of this complex structure [29] were gained by means of AFM results. However, one of the most important aspects, the influence of the substructure on overall mechanical properties of mature fibrils, has not been clarified yet.

3.2.1 Formation of Collagen Fibrils

The collagen helix (α -chain) is left handed and the repeating distance is 0.96 nm. The collagen molecule has a total length of about 300 nm and a mass of 285 kDa, whereas the diameter ranges between 20 nm and 500 nm depending on the collagen type. The banding pattern of native collagen fibrils is between 64 nm and 67 nm. Fig. 8

schematically displays the assembly of single collagen helices into a native collagen type I fibril.

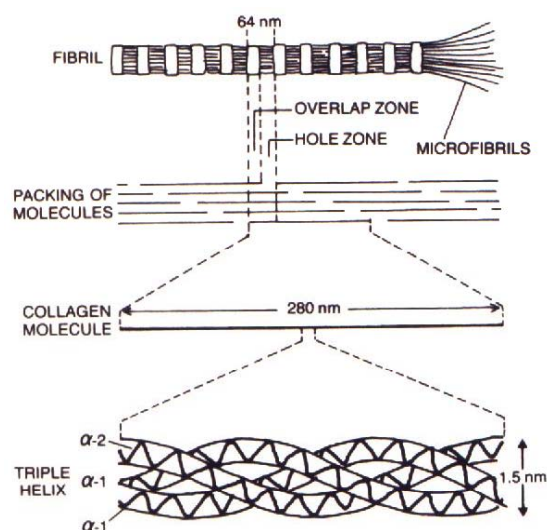


Fig. 8: Schematic drawing of the collagen fibril structure. Illustration of the molecular packing and origin of the banding pattern. (adapted from <http://ntri.tamuk.edu>)

Collagens are very widespread in mammals and occur in different tissues. The most common form is collagen type I. Up to now about 20 different collagen types have been investigated. Collagens can be classified in fibrillar collagens, fibril associated, network forming, and filamentous anchoring collagens. Collagens are a component in tendons, skin, cartilage, vessels, cornea, membranes and so on.

During the formation of the collagen fibrils, $\alpha 1$ -glycoprotein is proposed to play a very important role. It is also known as orosomucoid and is a 41kDa single polypeptide, which occurs in blood plasma. Up to now the exact biological function remains unknown, whereas the structure has been investigated by Kopecky et al. [30] and the influence on the synthesis of FLS fibrils was first shown by Franzblau et al. [31].

3.2.1.1 *In vivo* Self-Assembly of Collagen

Collagen biosynthesis consists of many steps, divided into intracellular (cf. Fig. 9) and extracellular (cf. Fig. 10) synthesis. Fibroblasts are responsible for the intracellular transformations. A polypeptide precursor emerges at the polyribosomes and after cleavage of the signal peptides, procollagen is formed. Pro- $\alpha 1$ and $\alpha 2$ are synthesised simultaneously. During the synthesis left handed helices are formed which exhibit non helical sections at the C- and N-terminal ends with a length of 16 and 25 amino acids respectively, the so called telopeptides. Hydrogen bonds at the center of the triple helix are responsible for the cohesion. After the hydroxylation of proline and lysine residues, the collagen chains wind together to the triple helical structure. The hydroxylation of proline is not merely a prerequisite, but is also responsible for the temperature stability of the collagen helix. Only hydroxylized procollagen molecules are secreted from the

cell. Subsequent steps after the hydroxylation are a glycolisation of single hydroxyl residues, where one or two sugar groups (galactose or glucose) bind, and the creation of disulfide bridges at the C-terminal. The degree of glycolisation is dependent on the type of collagen. After the intracellular triple helical assembly has been finished the molecules are secreted from the cell into the extracellular space [27].

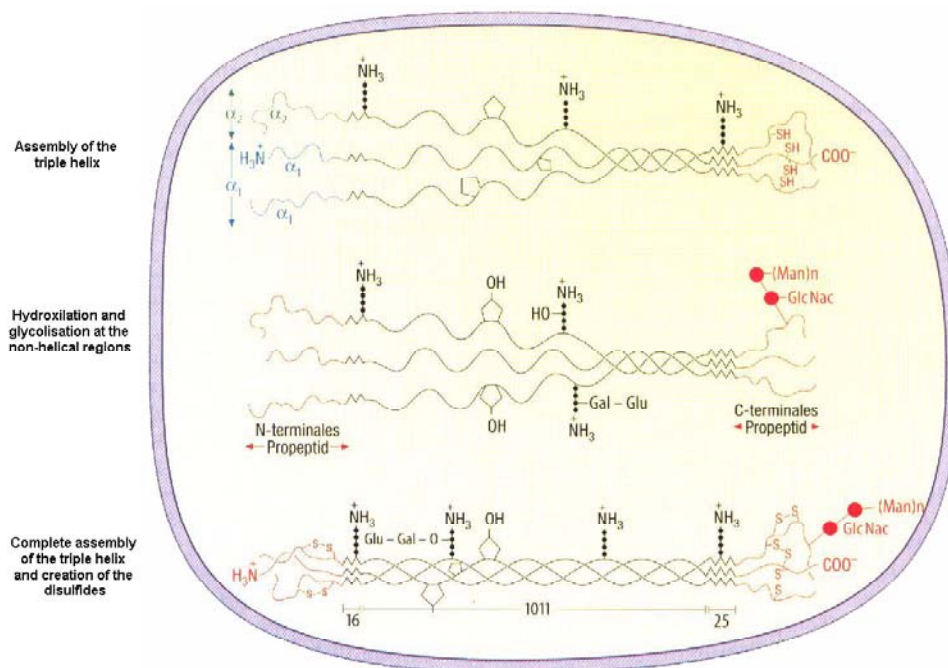


Fig. 9: Intracellular transformations of collagen chains. (adapted from [27])

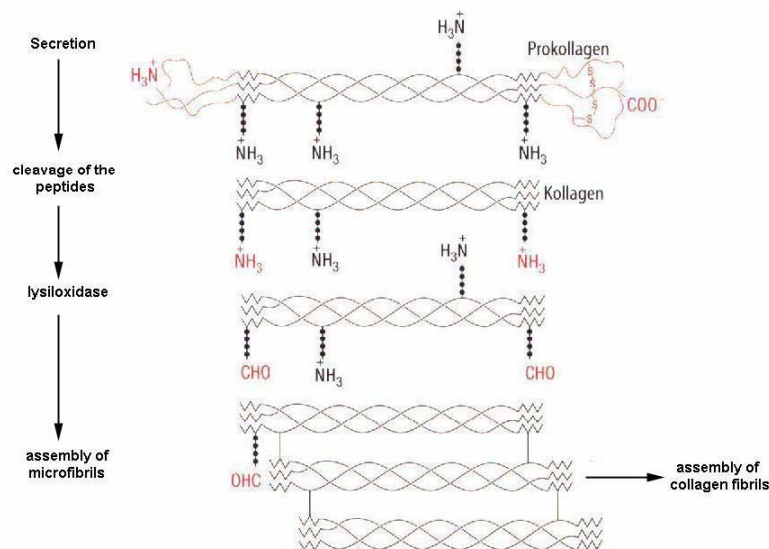


Fig. 10: Extracellular modifications of collagen helices. (adapted from [27])

Two specialized procollagen proteinases cleave both peptides at the C-terminal and the N-terminal ends. In the regions of the non-helical sites of the collagens, the telopeptides - lysyl and hydroxyllysyl residues - are desaminated. The resulting aldehydes form bifunctional crosslinkings which play an important role for the elasticity

of collagen. Due to these crosslinkings insoluble collagen microfibrils emerge in salt solutions and the melting point of the microfibrils increases to 67°C [27].

Collagen molecules align parallel to each other. Due to hydrophilic and hydrophobic sequences the collagen molecules have a characteristic charge distribution. During the agglomeration the positive and negative charge centers neutralize each other. The growth mechanism of microfibrils to collagen fibrils is characterized by an increase in diameter and is up to now not completely understood. The final diameter of the collagen fibril depends on the collagen type, but also on the interaction with other proteins in the extracellular matrix.

The half life of collagen depends on the adjacent connective tissue and several other factors, such as inflammations, arthritis or wound healing. Collagenases are responsible for the decomposition of collagen. These enzymes originate from endothelium cells, fibroblasts and other cells. Under normal conditions a subtle regulated balance exists. When it is disturbed the collagen decomposition might increase [27].

3.2.1.2 *In vitro* Self-Assembly of Collagen

A widespread method to obtain single collagen fibrils is the *in vitro* preparation from purified collagen. Collagens are often extracted in monomeric form with diluted acid solutions. The assembly process is mainly entropy driven, hence temperature dependent. Due to a loss of solvent molecules the collagen molecules self-assemble into fibrils. These fibrils are unipolar and have small tapered ends [32]. The specific self-assembly conditions like temperature, ionic strength, pH-value are very important during collagen morphogenesis. Fundamental work for the understanding of these determining factors was published by Gross, Wood, Keech et al. [33-39] and Bard and Chapman [40, 41]. The preparation of collagen fibrils by dialysis was introduced by Orekhovich, who could prove the existence of procollagen by dialysing mammalian skin against water [42]. Further dialysis experiments were done by Highberger [43], who developed a procedure to assemble LS fibrils (Long-Spacing) against water. In absence of salt from neutralizing processes it was possible to investigate the influence of mucoprotein [43]. The interaction of collagen with α 1-acid glycoprotein during the formation of fibrous long spacing fibers was investigated for the first time by Franzblau et al. [31].

For the *in vitro* preparation of collagen fibrils several factors and conditions have to be controlled during self-assembly. The initially introduced diluted acid, for example acetic acid or hydrochloric acid, has to be removed from the solution. This can be accomplished either by neutralization or removal during a dialysis process. Viscosity measurements during *in vitro* self-assembly show an increasing viscosity upon removal of the acid from solution. This viscosity change is time independent, but directly related to the concentration of the acetic acid [31, 44], which diffuses through the membrane of a dialysis tubing [45].

During the dialysis process the membrane of the dialysis tubing acts as a molecular sieve and separates macromolecules from low-molecular-mass substances like acid molecules. Single step processes are primarily determined by the equilibrium of the concentrations between both sides of the membrane. An enhancement of the separation efficiency can be attained by continuously rinsing one side of the membrane. When doing so, the continuous diffusion of molecules smaller than the pit diameter of the membrane can be maintained. In order to establish such multistage processes with a dialysis tubing the external side needs to be purged with DI-water. This is an efficient measure to decrease the process time and increase the yield of the target molecule.

For the preparation of collagen fibrils the dialysis method seems to be preferable, particularly when the influence of other molecules (from neutralisation) should be excluded and/or the influence of a certain substance should be studied. For the investigation of *in vitro* self-assembly of collagen it is indispensable to control or regulate the dialysing conditions. The most important aspect is the separation of the acid molecules from the collagen molecules. The separation process in particular the diffusion of the acid molecules is determined by the pH-value which can be controlled by an automated dialysis system [45], (cf. publication P1, Controlled Self-Assembly of Collagen Fibrils by an Automated Dialysis System, chapter (5.1)). The output signal of the pH-meter is read out by an 8-bit analog digital converter (Velleman) and then processed as described in the following (Fig. 11). A Visual Basic program controls the actual pH-value and compares it with the setpoint value. If the actual value is lower than the setpoint value, valve X1 will be opened and dialysis buffer is added to the external side and vice versa. The digital output (open collector) of the interface card switches a relay, which opens the valve.

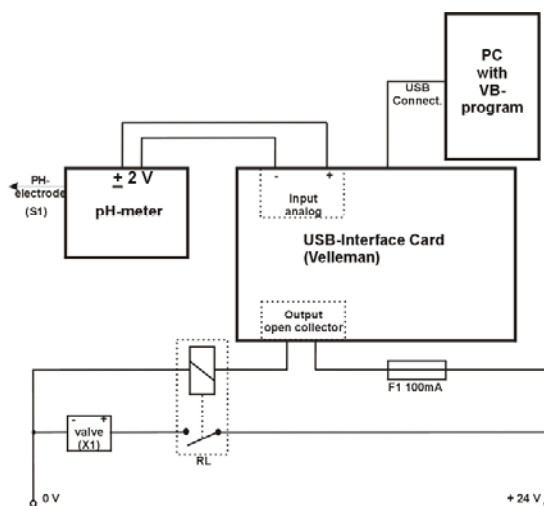


Fig. 11: Schematic diagram of the pH-control system

The pH-value is measured with a pH-meter and read into the USB AD/DA card with its analog input channel and a 15x amplification. The system is controlled by a Visual Basic program. An open collector output controls a relais which opens and closes a valve, thereby controlling the flow of dialysis buffer.

3.2.2 Structural Properties of Single Collagen Fibrils

Collagen molecules are axially staggered and shifted by multiples of the banding pattern. When charged the banding pattern gives rise to contrast in SEM topographs. Based on AFM topographical investigations complemented by density values obtained from SEM measurements, a staggered arrangement of collagen molecules with gap and overlap zones was proposed. Native fibrils and fibrous long spacing fibrils (FLS-fibrils) were prepared and imaged with the AFM by Paige et al. [46, 47]. Native, intermediate and mature FLS collagen type I as well as native type II fibrils are depicted in Fig. 12 and described in chapter (5.1), publication P1 [45].

Cocoon-like fibrils with a size of hundreds of nanometers in diameter and a length of (10-20) μm were observed as a byproduct of FLS-fibrils preparation. For the formation of FLS- and cocoon-like fibrils a stepwise process is postulated [48].

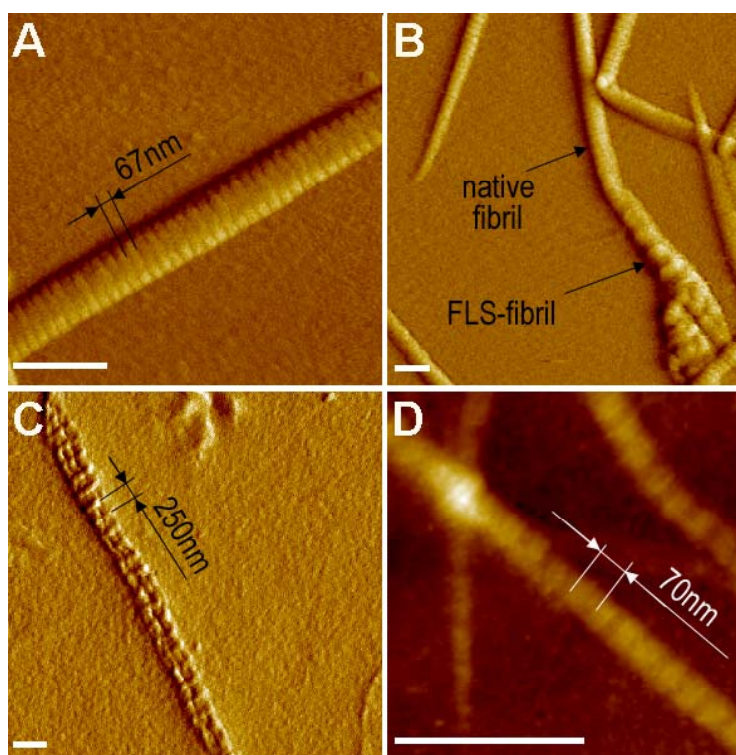


Figure 12: AFM images of **(A)** a native collagen type I fibril. (scalebar corresponds to 500nm, error signal, contact mode, in decanol) **(B)** native and FLS collagen type I fibrils. The formation is changing along the axis of the fibril. (scalebar corresponds to 500nm, error signal, contact mode, in decanol) **(C)** an intermediate FLS-fibril, assembled with increased $\alpha 1$ -acid glycoprotein concentration. (scalebar corresponds to 500nm, error signal, contact mode, in air) **(D)** native collagen type II fibrils. The banding is clearly visible and the repeating distance amounts to 70 nm. The diameter of collagen II (110 nm in width and 13 nm height) is much smaller than the diameter of collagen I. (scalebar corresponds to 500nm, topography signal, non-contact mode, in air)

The presence of collagen type I with kinks, caused by mechanical deformation leads to the hypothesis that collagen fibrils could mechanically behave like tubes as also

observed by Gutschmann et al. [49]. They suggest that collagen molecules exhibit a higher degree of crosslinking near the fibril surface and are more disordered or softer at the center. A collagen type I fibril with a kink is depicted in the inset of Fig. 13, see also chapter [\(5.2\)](#), publication P2, Structural Investigations on Native Collagen Type I Fibrils and reference [50]. Due to the proposed inhomogeneous structure collagen fibrils are expected to exhibit an extraordinary reparation mechanism. The stiff outer shell breaks, whereas the fluid core remains intact and is able to heal defects in the outer shell.

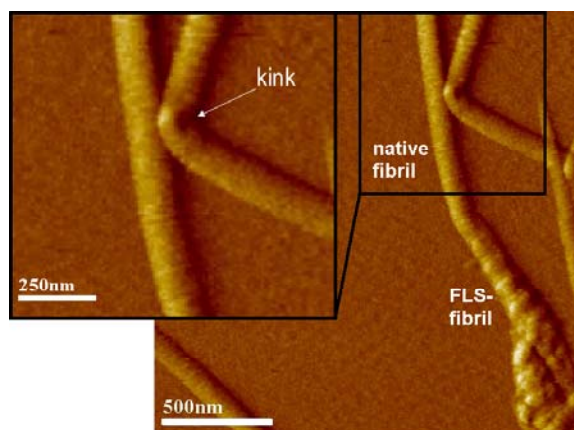


Fig. 13. High resolution AFM image showing a single collagen fibril with a kink. Because of such kinks collagen fibrils are compared to tubes. (error signal, scalebar corresponds to 500 nm).

Fratzl et al. observed a molecular gliding within the fibrils at high strain which finally leads to disruption of the structure [51]. Scanning electron tomographs of corneal fibrils showed the organisation of approximately 15° tilted microfibrils (~4 nm in diameter) in a 36 nm thick collagen fibril. Further structural investigations revealed that microfibrils exhibit ordered and disordered regions within the 67 nm banding pattern [52].

3.2.2.1 Microdissection of Single Collagen Fibrils

Microdissection using AFM was performed on FLS-fibrils (1.7 μm width, 270 nm banding pattern) in order to gain access to the FLS banding pattern also in the middle of the fibril [53]. As proposed by Rainey et al. the characteristic banding originates from the attachment of α 1-acid glycoprotein at specific distances [48]. On the contrary the banding structure of native collagen fibrils is defined by the repetition of overlap and gap zones [54]. Structural investigations subsequent to a dissection procedure on native collagen fibrils have never been published before. FLS fibrils are at least six times broader than native fibrils and in addition the proposed assembly is completely different from native ones.

In order to image the inner structure and to measure elastical properties in the center region of native collagen fibrils it is necessary to uncover the core of the collagen fibril. In our experiments we applied an AFM based microdissection to native collagen type I fibrils for further examination of the inner structure. Both the shell and upper parts of

the fibril were scratched away to obtain high resolution images of the core, a typical dataset is depicted in Fig. 14. To exclude artefacts caused by the scratching process it was performed under a defined angle with respect to the fibril axis. In conclusion, no structural differences between the banding pattern of the core and the outer shell were identified. Both banding patterns are identical in width as well as in the repeating distance. This fibril exhibits a banding pattern of 78 nm, a height of 30 nm, and a width of 270 nm. For the first time, this experiment utilized a dissection procedure applied to native collagens, in order to unambiguously prove that there are no morphological differences between core and shell. A more detailed representation can be found in reference [50], publication P2, and chapter [\(5.2\)](#).

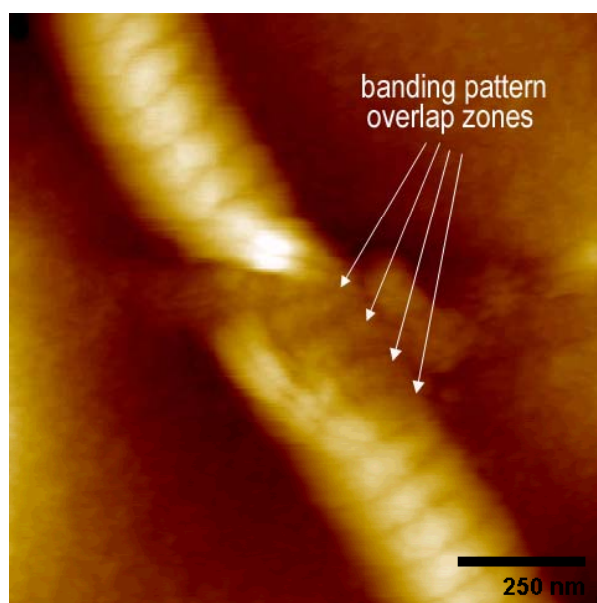


Fig. 14. High resolution AFM image of a microdissected collagen fibril. The core of the collagen fibril is uncovered and the banding pattern inside the fibril is visible. The arrows indicate the overlap zones of the collagen molecules that arise during the self-assembly process of the collagen fibril (non-contact mode, topography signal, scalebar corresponds to 250 nm, in air).

It seems very likely that during the microdissection process complete collagen layers are removed from the fibril, in particular when a structural model as described in chapter 3.2.1 *Formation of Collagen Fibrils*, where mature fibrils are comprised of tropocollagen crosslinked with their neighbours, is considered. However, it can not be completely excluded that molecules are ruptured and crosslinkings are destroyed upon scratching with the AFM tip.

3.2.2.2 Elasticity Measurements on Dissected Collagen Fibrils

The eligibility of the AFM as a tool for measuring elastic properties of collagen fibrils is well established [8, 55-58]. It is appropriate for pulling- and indentation experiments likewise. Pulling experiments were performed to examine crosslinking of substructures

and elongation properties of complete fibrils [55]. Two different series of rupture events were measured while probing the crosslinking of collagen subunits. Events with a periodicity of 78 nm and weaker ones with a periodicity of 22 nm were found. Similar results with multiple stretching peaks were obtained by Bozec and Horton on trimeric type I tropocollagen molecules [56]. Moreover, force spectroscopy on collagen fibrils which were adsorbed between the AFM cantilever and the substrate surface showed a large extensibility. In force-elongation and relaxation profiles several discontinuities and plateaus in the force curves indicate reorganisation events within the fibril [8]. The fibrillar structure and viscoelastic properties of collagen were measured by means of stress and strain curves, where several distinct regions could be distinguished [51], [59]. Initially crimps [60] and kinks [61] are removed, before a linear region arises due to the stretching of the molecular helices. Eventually, gap zones outnumber overlap zones. In case of cross-link deficient collagen first slippage can be seen [59] and higher strain results in disruption of the fibril.

By means of AFM based nanoindentation experiments, Xu et al. were able to show that the elastic modulus of thick lamellae is higher than that of thin lamellae of microtomed human lamellar bone samples [57]. This effect could not be observed with polished samples. Thick and thin lamellae differ in the density of collagen fibrils. Dense and thin lamellae have higher collagen fiber content whereas loose and thick lamellae have fewer fibrils and a higher mineral content. Wenger et al. proposed anisotropy of elastic properties of collagen fibrils taken from a rat tail due to alignment of molecules parallel to the fibril axis [58]. This conclusion was based on non-uniform AFM-tip imprints during elasticity measurements. However in the literature no spatially resolved elasticity measurements on different regions of the fibril as core and shell, which are proposed to behave mechanically different, can be found. The assumption of the structure and mechanical properties of core and shell was only derived from indirect measurements. In order to provide direct measurements, elastic properties were evaluated with a spatial resolution in the nanometer range, thus putative differences between core and shell can be identified.

Force spectroscopy experiments were performed on microdissected collagen fibrils as described before. For each point at least 100 spectra were recorded. In the experiments the maximal force was fixed, thereby limiting the maximal indentation depth in the linear elastical range. A maximum force of 6 nN was applied, which corresponds to a cantilever bending of 8.5 nm and an indentation of approximately 0.5 nm on the shell as well as in the core. Fig. 15(A) exemplarily depicts force distance curves, both for shell (black solid line) and core (grey dashed line). No major differences in the contact range are observable, which indicates similar elasticity of shell and core. The experimental data in the positive cantilever range above the zero line was used for the calculation of Youngs moduli as displayed in Fig. 15(B). Youngs moduli were obtained by fitting individual force–distance curves to the Hertzian model in the contact range. Details of the calculation procedure are elaborated in chapter 3.1.3.2. The proposed difference between a hard shell and a soft, less dense core could not be verified by our spatially resolved nanoindentation elasticity measurements. These results are consistent with our morphological investigations of the microdissected collagen type I fibril as displayed in Fig. 14. Core and shell were found

to be homogeneous and similar in structure. The average value accounts to 1.2 GPa, with the maximum of the histogram at 1 GPa [50].

As demonstrated by Domke et al. [25], an influence of the underlying hard substrate for indentation measurements of thin samples can not be completely excluded. From probing gels with different thickness he concluded that Young's modulus can be overestimated when thin samples are measured. In order to exclude this artefact, the displayed curves were measured with the same sample height for both core and shell.

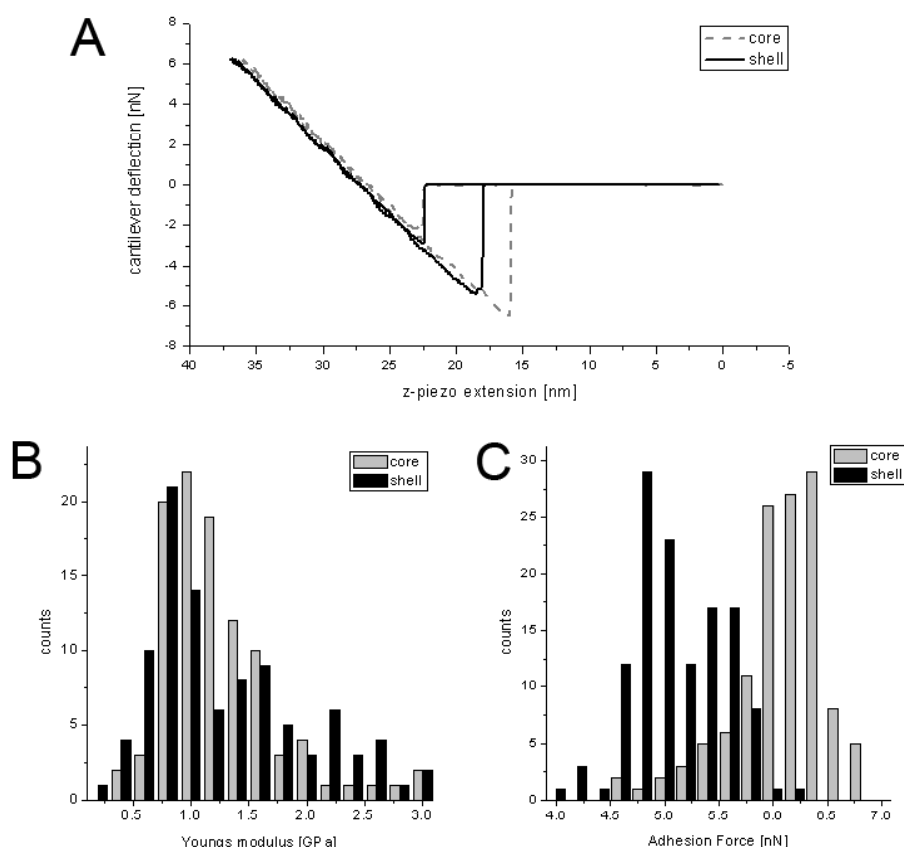


Fig. 15. **(A)** Typical example of a force–distance curve recorded on the shell and the core of a single collagen fibril respectively. The black solid line is a spectrum taken on the shell, whereas the grey dashed line was recorded in the core. **(B)** Elasticity measurement of a single collagen fibril. Force distance curves were recorded both on the shell and the uncovered core. The diagram is a histogram of Young's moduli as derived from the force distance curves **(C)** Adhesion measurement on a single collagen fibril. The data displays the evaluation of the adhesion forces as calculated from the height of the snap-out-of-contact region of the retraction curve. The values point to a higher adhesion on the core of the microdissected fibril.

The individual spectroscopy curves of core and shell as depicted in Fig. 15(A) indicate a higher adhesion on the core. The height of the snap-out-of-contact effect was calculated from the retraction curve. The statistical evaluation is displayed in Fig. 15(C) and clearly verifies the higher adhesion on the core. Average values account to 5 nN for the shell and 6 nN for the core of the fibril. This was already suggested by

Gutsmann et al. [49] and interpreted with a higher degree of crosslinking of collagen molecules near the fibril surface as compared to the central region. This would result in more possibilities for bond formation to the tip, thus a higher adhesion force. However the scratching process might have also influenced the outcome of the measurement due to rupture events on the molecular level and destroyed crosslinks. This is a major problem when probing inhomogeneous samples. Destroyed crosslinks and ruptured molecules might be responsible for higher adhesion forces between sample and tip as measured in our experiments. The mechanical properties could also be modified since the collagen fibrils were imaged in a dried state rather than preserved under physiological conditions [50], cf. chapter [\(5.2\)](#), publication P2, Structural Investigations of Native Collagen Type I Fibrils.

Our results contribute to the clarification of the spatial dependence of elastical properties in native collagen. Mechanical properties of core and shell regions were found to be similar, thereby proving the applicability of the method for the characterisation of elastic properties in inhomogeneous samples.

3.2.3 *In situ* Collagen Applications and Properties of Bone Tissue

3.2.3.1 Interface between Biomaterials and Biological Systems

The function of biomaterials at the interface with biological systems is extremely versatile. In most cases the success of a clinical treatment strongly depends on biological reactions at the interface between implants and tissue. The treatment of bone, body or joint defects requires optimized materials in order to enhance bone formation and improve the attachment to for instance implants [62]. In former studies type I collagen, fibronectin and vitronectin were studied with respect to their properties of intermediate adhesion between osteoblasts and implants [63]. The adhesion was found to be strongly dependent on the concentration of the mediator, whereas at low concentrations best results were obtained with collagen followed by fibronectin and vitronectin after 24 hours. For the stabilization of implants and improvement of skeletal fixations, implants were coated with porous layers in order to increase the surface area. Chemical and physical properties of bone and implants are responsible for the attachment [62]. However, the initial healing process was slowed down by rough surfaces and only after a certain period of cell growth the advantages of the larger surface area led to a prolonged cell spreading [64, 65].

In order to promote the initial healing process and to achieve an improved skeletal fixation both surface properties have to be combined. First the surface has to be coated with appropriate biomaterials, while the topography must exhibit a relatively high roughness. Collagen and fibronectin are commonly used for pre-coating cell culture slides. However bone sialoprotein (BSP) has been found to enhance the growth of osteoblasts.

We investigated the uniformity of different substrate coatings and the cell growth on mica using an AFM. In addition the dental implant material titanium-hydroxyapatite (TICER) was investigated. The influence of collagen (in non-crystalline state), BSP and fibronectin on the evolution of adult human maxillar bone cells was studied *in vitro* and

compared. The AFM measurements reveal huge differences in morphological properties, typical results are shown in Fig. 16. Collagen wets the surface and covers it very homogeneously, whereas BSP coatings are not fully closed. Only single drops are dispersed across the surface. Similar properties were found for fibronectin, but the area density of droplets was considerably higher. The morphology of the cells on pretreated surfaces exhibited no significant differences for the coatings investigated here as demonstrated in Fig. 16.

For the evaluation of the influence of specific surface coatings, the area density of cells adhering to the substrate was determined. BSP yielded the highest number of living cells on mica, followed by collagen [66], (cf. Fig. 17, adapted form [66]). An untreated TICER control sample promoted the cell growth much better than mica, especially after 25 days.

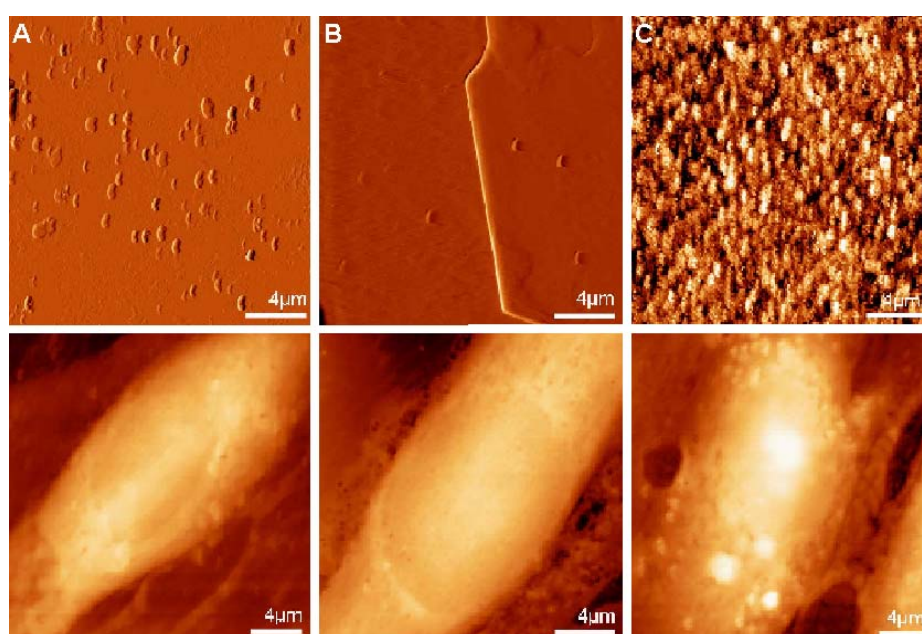


Fig. 16 Different surface functionalizations and their influence on cell growth **(A)** Fibronectin on mica; many droplets cover the surface. **(B)** BSP on mica; only a few droplets cover the surface, much less than with fibronectin. **(C)** Collagen on mica; a very homogeneous layer is formed. The lower row depicts AFM images of the corresponding cell growth experiments.

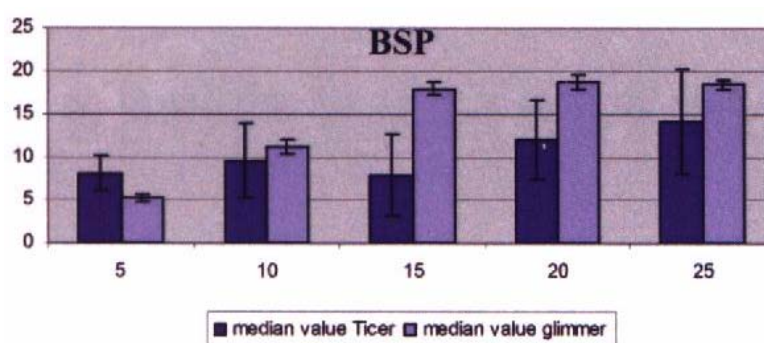


Fig. 17: Number of *in vitro* grown cells on BSP coated mica (glimmer) and Ticer after 5, 10, 15, 20 and 25 days. Average values with the corresponding standard deviation are shown. BSP on mica exhibited enhanced cell growth after 15 days. Adapted from [66], see also chapter 5.3.

Comparing both substrate materials without coating, Ticer showed the highest growth rates. On mica, the fastest cell growth was observed with BSP coating followed by collagen, although the coating of collagen was found to be more homogeneous. This means the cell growth enhancement mediated by dispersed droplets of BSP is equally efficient as a closed collagen layer. These results indicate that cell growth is strongly dependent on the implant material, however the properties of the implant surfaces can possibly be altered by surface coatings, thereby shortening the healing time through promoted cell proliferation especially for the first days.

Surface properties of the substrate and coating layers can be easily characterized by means of nanotechnological methods like AFM. In combination with other analytical methods suitable solutions for medical applications can be developed more efficiently.

3.2.3.2 Properties of Complex Organic and Anorganic Biomaterials

Mechanical properties of composite materials are strongly influenced by the single constituents and their mutual interaction. Characterisation of the composition and identification of important interactions among the substructures is therefore of substantial interest, especially for highly complex biological tissues like bones. It is well known that bone consists mainly of a collagen type I matrix and calcium phosphate supplied as hydroxyapatite. Apatites are complex salts with Ca^{2+} as center atom and $\text{Ca}_3(\text{PO}_4)_2$ – molecules as ligands. The formation of apatite occurs near osteoblasts and collagen fibrils act as crystalization seeds. Due to their high calcium content, bones serve as a reservoir for this cation and supply it to the blood circulation of the body upon demand [67].

A basic component of bones is the cortical bone (compact bone) which forms a strong hollow tube and features a high mineral content of about 70%. The trabecular bone (cancellous or spongy bone) consists of an open porous network. This network is filled with blood vessels, bone marrow, and fatty marrow particularly at higher ages. Microscopically the structure of the compact bone is built up by separate units, the so called osteons. They consist of Haversian canals, osteoblasts, arteries, capillaries and nerve fibers of up to 6 lamellar layers. In between are the osteocytes, osteoblasts which are completely surrounded by bone tissue and the osteoclasts which are responsible for bone resorption. The lamellar structure originates from the ordered arrangement of collagen fibrils. The compact bone makes up for ~80% of the bone mass, whereas the trabecular bone accounts to only 20% of the mass. The collagen content is only 23%, but represents approximately 90% of the organic matter [27]. Fig. 18 displays an AFM image recorded on human bone tissue. The collagen fibrils with their fibrillar structure and their banding pattern can be clearly recognized.

Imaging collagen fibrils in their natural environment, which plays a vital role for the interpretation of bone properties, could yield important insights in the understanding of mechanical properties of mammalian tissue. Nanoscale structural properties are very important for the mechanical behaviour of bones. Hansma et al. [68] proposed that

there is another substance beside the collagen fibrils with major impact on the mechanical properties of bone.

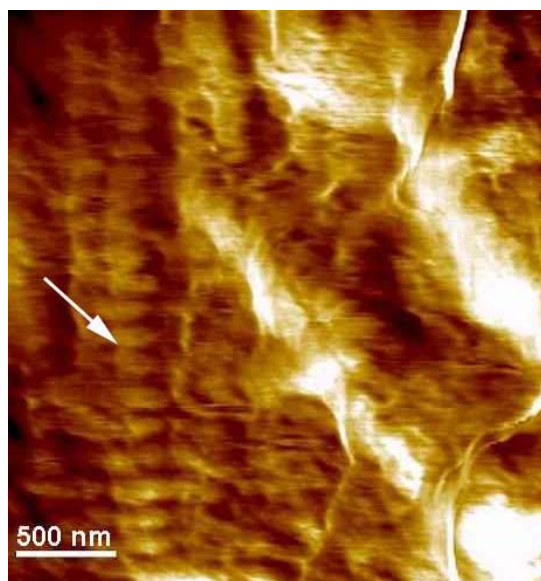


Fig. 18: AFM image of collagen from a bone sample; the fibrillar structure as marked by the white arrow is evident. Furthermore the banding pattern of collagen type I fibrils is clearly visible.

Abalone shells for example consist of 97% calcium carbonate, but are ~3000 times more fracture resistant than pure calcium carbonate. The remaining 3 % have to be an interstitial organic matrix with the ability to increase the resistance against mechanical deformation by dissipating the mechanical energy [69]. Fantner et al. [70] presented SEM topographs of collagen fibrils of fractured human bone. Collagen fibrils with cracks were identified, where individual fibrils were interconnected by small filaments. Besides that, an AFM based force spectroscopy was performed in aqueous buffer solutions. When Ca^{2+} -ions were present the rupture forces, as measured by pulling with the AFM tip, were higher than in the presence of Na^{+} -ions [68]. It was suggested that proteins such as osteopontin and bone sialoprotein with negatively charged functional groups, such as phosphate groups on phosphorylated amino acids are able to bind multivalent positive ions such as calcium. These pulling experiments were performed with a specialized force spectroscopy protocol with a functionalised tip. A small piece of bone was glued to a cantilever which was pressed against a bone specimen and subsequently separated [70]. The authors proposed the existence of sacrificial bonds in form of glue filaments which account for the rupture forces during the pulling experiments. These sacrificial bonds are assumed to be calcium mediated and interconnect adjacent filaments. Whereas filaments bond to collagen through mineral plates and possibly also to filaments. High stiffness and toughness of bone and other calcium containing materials can be explained by such glue filaments.

In order to investigate the lifetime and degradation of these bone-glue filaments, we prepared fresh porcine and ancient mammalian bone to compare morphological peculiarities. Samples were prepared according to the following procedure. Fresh porcine and ancient vertebrae were sawed into small pieces, $5 \times 5 \times 4 \text{ mm}^3$ in size. In

case of porcine vertebrae the bone marrow was rinsed out of the trabecular network with water pressurized through a homemade nozzle. The ancient vertebrae did not have bone marrow or other organic residues anymore, thus this preparation step could be omitted. Samples were stored in a physiological buffer, before compressing them with a small precision vise. The compression procedure introduces microcracks inside the bone, where the filamentous structures supposedly are. Without rehydrating the fully desiccated ancient bone sample in aqueous solutions, it just cracks into small pieces. After the formation of microcracks the samples were dried over night, before coating them with a thin gold film, a necessary pre-treatment for SEM based morphological investigations.

For the characterization of ancient bone, a sample was taken from the vertebrae of an Egyptian mummy. The sample originated from a grave complex in a burial ground for socially higher ranked people in Thebes West. The tomb was used during the period of the New Kingdom until the Late Period, from 1500 to 500 BC. Results from the morphological investigations are depicted in Fig. 19. The left column displays results from the ancient sample, whereas the right column shows results from the fresh porcine sample.

In both cases filamentous structures bridging microcracks were found, marked by the red arrows in Fig. 19. The diameter of these structures was determined to be in the range of (20 – 40) nm. These diameter values are consistent with results of Hassenkam et al. [71], who published a diameter of ~20 nm. By means of a morphological investigation of an ancient Egyptian mummy specimen we were able to show that the filaments, commonly referred to as bone “glue”, survive timeframes of more than 2500 years. The first row of Fig. 19 depicts overall images of the trabecular bone. The trabecular sample of the ancient bone (image on the left hand side) appears rougher and more filigree than the fresh porcine bone (image on the right hand side). Fig. 20(A) and (B) present digital zooms of both images. It is evident that the surface structure of the mummy sample on the left hand side is much rougher than the fresh specimen. A fine filamentous structure runs through the trabecular. This distinct morphological difference is probably caused by degradation processes of organic and anorganic material over time.

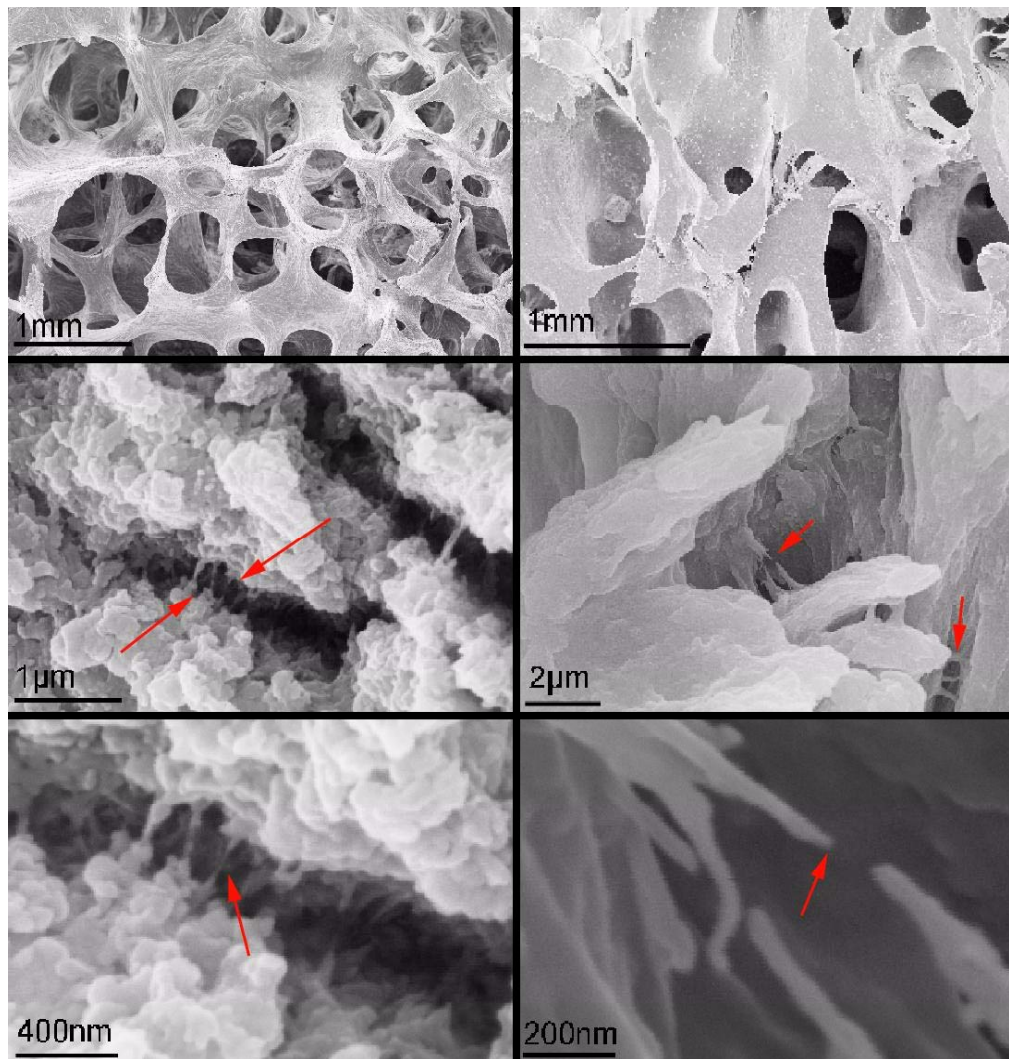


Fig. 19: Scanning electron topographs of ancient human (left column) and fresh porcine vertebrae (right column) bone. The specimens were mechanically deformed in order to create microcracks. Images in the same row were taken at nearly the same magnification. Red arrows mark „glue“-filaments spanning the cracks.

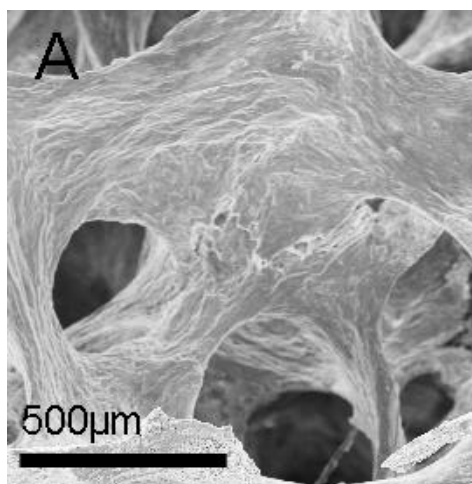
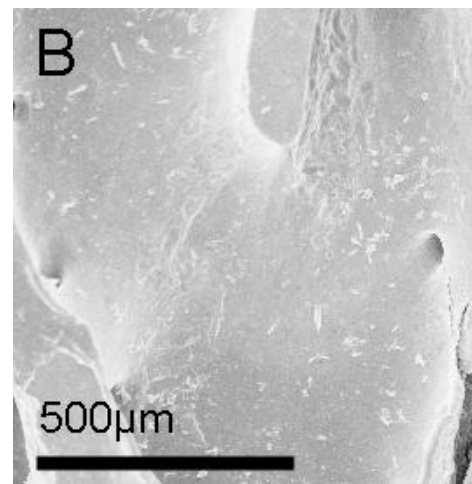


Fig. 20: (A) Trabecular of mummy vertebrae.



(B) Trabecular of porcine vertebrae.

3.3 Nanotechnology in the Forensic Science

Today forensic scientists review the anamnesis, interview witnesses, examine the potential crime scene, perform autopsies and investigate appropriate specimens for toxicological residues, and carry out microscopic examinations and DNA analysis.

3.3.1 Chronological Reconstruction of Crimes

The chronological reconstruction of crimes is highly important for the forensic science especially in homicide cases. Several methods have been evaluated with respect to the reliability of data and have been partly established in routine forensic medicine.

In the early post mortem period the rectal temperature is evaluated in order to determine the cooling rate by means of an established algorithm [72-75]. The assessment of the cooling curve is not trivial due to the heat production of many ongoing aerobic and anaerobic metabolic processes and muscular contractions [75]. Nevertheless the measurement is straightforward, non invasive and reproducible. Yet it only provides a reliable estimate when a high gradient between body- and ambient temperature is present.

Other methods are based on the increase of the potassium concentration in the vitreous humour (KV) [76-78]. However several studies found out that the scattering of potassium levels in KV with regard to the post mortem interval (PMI) is very high. The evolution of the KV value after death is assumed to be dependent on extrinsic and intrinsic factors which can not be measured directly.

Changes of the extracellular electrical impedance of the abdomen of rats were reported by Querido [79] and Querido and Philips [80] as an approach to estimate the time since death. Those groups found out that within the first 3 days the impedance increases and then decreases with time since death. A possible explanation for the initial increase of the resistivity is the transfer of sodium and chloride from the extracellular to the intracellular compartment and a smaller potassium current from inside to outside the cell [81]. This method is severely limited by the fact that the resistivity strongly depends on the effective cross sectional area between the electrodes, which is a priori not known for a specific abdomen. Straton et al. [82] investigated nerve conduction properties and found a relation between several aspects of nerve function and PMI. But the relationship can not be easily calculated and the method is only applicable under laboratory conditions so far.

A huge amount of arthropod species lives in our environment and is attracted by human remains. So, forensic informations about the PMI can also be provided by entomological investigations of bodies [83].

Another challenge in the forensic science is the PMI determination of skeletal remains. Depending on the ambient conditions (climate, nature of soils, effects of animals and insects and so on), the decomposition of a human body advances at a different rate. One of the first papers with morphological, histological, chemical and physical investigations was published by Berg and Specht [84]. Different authors applied various techniques for dating skeletal remains such as optical-morphological procedures [85, 86], studies of the nitrogen and amino acid contents, anti-human serum and benzidine reaction [87-89], microradiography and electron microscopical studies [90]. In order to date skeletal remains with an anticipated age of several tens of years. Swift et al. could

demonstrate the existence of a relation between distinct radionuclides and the PMI for the first time [91]. For these experiments uranium, lead, polonium and caesium were evaluated and a correlation between the radionuclide concentration and the time of death could be shown.

3.3.2 Age Determination of Blood Spots

Blood is one of the most important fluids in the mammalian body. Our blood circulation transports oxygen and carbon dioxide, nutrients, vitamins, electrolytes and waste products. It regulates hormones and contributes to the body temperature regulation. In addition, sophisticated mechanisms protect us from excessive blood loss at wounds and leucocytes protect us from diseases. The body of a human adult holds approximately 5 liters of blood. Blood is a suspension and contains erythrocytes (red blood cells), leucocytes (white blood cells), thrombocytes and plasma (water and dry matter). About 99% of the cells in blood are erythrocytes and the plasma contains 90% water. Modern medicine heavily relies on blood analysis for disease diagnostics and treatment. The single blood components themselves are tested as well as various substances which can indicate diseases and abnormal functions of organs.

During crime scene investigations in forensic medicine the examination of blood and bloodstains is a major source of information. Blood is used for the identification of people by means of chemical and molecular genetical tests (genetical fingerprint). Blood stain patterns are evaluated in order to reconstruct the crime. The information obtained may assist in identifying suspect and allows the reconstruction of the course of events. Many established methods for the detection and identification of blood spots exist, yet the age determination of blood in forensic medicine is still an unsolved issue. Several different approaches were proposed, but none was appropriate for routine forensic work.

The solubility of old blood samples was studied as a function of time since blood loss by Schwarzsacher [92]. However, from experiments with aged blood samples it was not possible to correctly predict the age. Methods such as remission photospectrometry [93] or electron-spin-resonance [94], which are able to detect age-dependent increase of signal intensity of meth-hemoglobin, non-hem-iron molecules, and organic radicals were introduced in the eighties of the last century. These measurements were found to be very prone to errors and allow only for a rough estimation of the bloodstain age. High performance liquid chromatography (HPLC) was used to measure the amount of globin chains hemoglobin [95]. With increasing age of the blood, a decreasing number of the heme related α -chains was measured. Heme is the subunit of haemoglobin which is also responsible for the red color. Also this method is inappropriate for routine forensic work, because of high deviations among standardized blood samples. Nearly all described methods suffer from a large error margin in the age determination of the blood samples and yielded reasonable accuracy only under laboratory conditions. It is unlikely that those methods will ever be applied directly at the crime scene. Besides that, the required amount of blood is quite high, and samples will rather be used for more conclusive analysis as for instance genetic tests.

3.3.2.1 Morphology of Aged Blood

Many morphological and surface interaction studies have been done on human erythrocytes with the AFM. Nowakowski and Luckham showed that it is possible to image the cytoskeleton of red blood cells in liquid with the AFM [96]. Different compressibilities of the cell surface depending on the position of the underlying cytoskeleton resulted in higher indentations for distinct areas. A specialized preparation procedure allowed Swihart et al. to image the inner surface of the erythrocyte membrane in aqueous solutions [97]. Irregular meshworks of triangular and rectangular openings with mesh sizes from 35 to 100 nm were found.

By measuring adhesion forces between a functionalized tip and a mixture of two different populations of group A and O red blood cells, both cell types could be distinguished by the affinity to the receptor covering the AFM tip [98]. The resistance against mechanical deformations during circulation in the mammalian body is characterized by biomechanical and biophysical studies. Ohta et al. [99] demonstrated that fine artificial structural changes on the surface of red blood cells induced shear stress.

The first attempt to investigate the relation between the age of dried blood cells and their morphology was carried out by Chen and Cai [100]. Cell shrinking, nanometer scaled protuberances and fissures occurred after 0.5 days and increased in number with time until 2.5 days. The authors proposed a distinct relation between the alteration of the cells and the PMI. Because those cells have been prepared specifically for the experiment, it is difficult to utilize these results under realistic conditions, where blood stains have dried over periods of several days or weeks under ambient conditions.

We characterized the morphological and elastic properties of blood stains, prepared on glass slides without any kind of pre-treatment or modifications, by means of AFM imaging and force spectroscopy. The AFM topographs of the bloodstain did not show any morphological alterations caused by drying throughout the evaluation period of 31 days [101], see also publication P4, Age Determination of Blood Spots in Forensic Medicine by Force Spectroscopy, (5.4). Fig. 21 depicts AFM images of the same region of the fresh and dried blood spot, taken after two weeks. In the overview image small cracks can be identified both after drying as well as after waiting for a period of 2 weeks. In higher resolution images donut-like shaped red blood cells can be easily recognized. Most interestingly, both the erythrocytes and the cracks of the investigated bloodstain did not exhibit any morphological alterations during the observation time. Several blood samples were imaged, but no morphological alterations were recognized, even for bloodstain samples, which were preserved for more than 6 months under ambient laboratory conditions, results are not shown here.

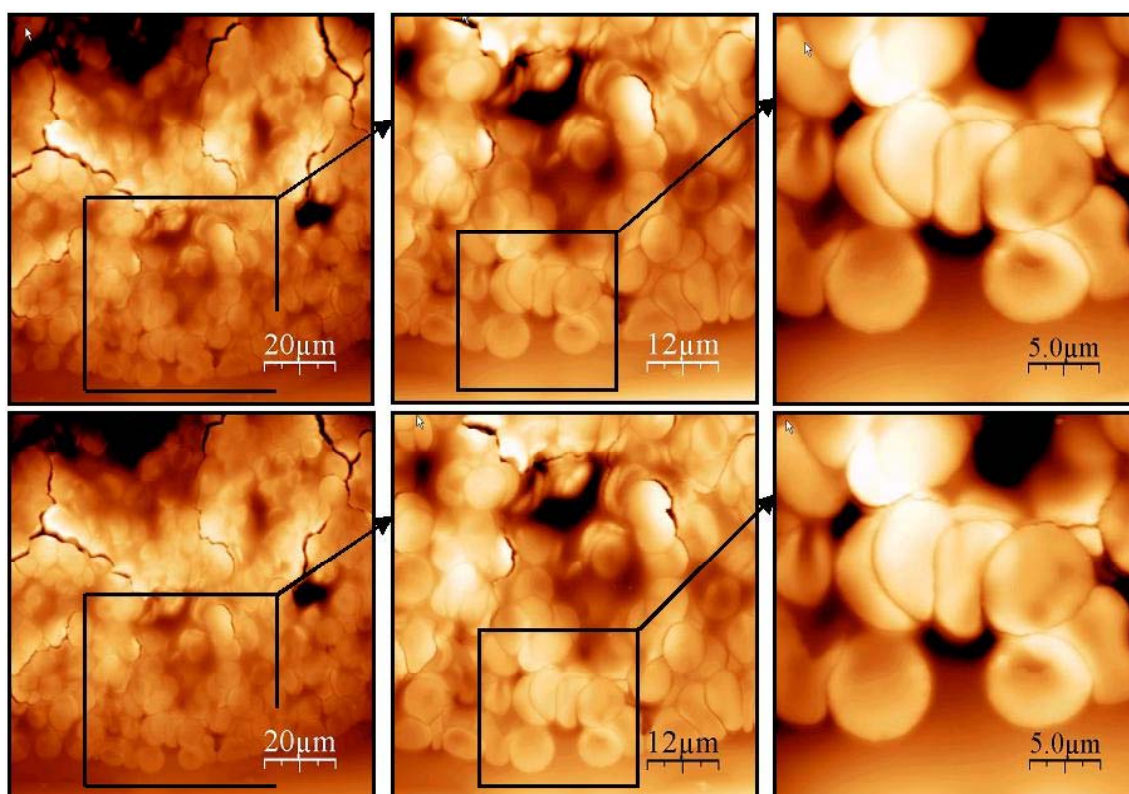


Fig. 21: Results of the morphological investigations on dried blood with the AFM. The first row depicts images, obtained directly after drying with decreasing scan area and increasing resolution respectively from left to right. The second row depicts the same region of the identical sample after a waiting period of two weeks.

3.3.2.2 Elasticity of Aged Blood

In order to measure elastical properties as described in chapter 3.1.2, force distance curves were recorded. The measurements were conducted on three differently aged blood samples by using the tip as a nanoindenter.

Force spectroscopy was performed on different areas of the sample, mainly at the relatively thick center of the spot in order to exclude overestimation of the elastic modulus due to compression of the sample between tip and substrate. Fig. 22 displays the fitted slopes of the force distance curves versus the drying time of the blood spots. The elastic modulus increases significantly with drying time. The displayed data represents average values of the slopes of the force distance curves. For a direct comparison it is sufficient to calculate only the slopes of the curves. Calculated Youngs moduli amounted to average values of 0.3 GPa for the 1.5h old sample, 0.6 GPa for the 30h old sample and about 2.5GPa for the 31d old sample, see also chapter [\(5.4\)](#) and reference [101], publication P4.

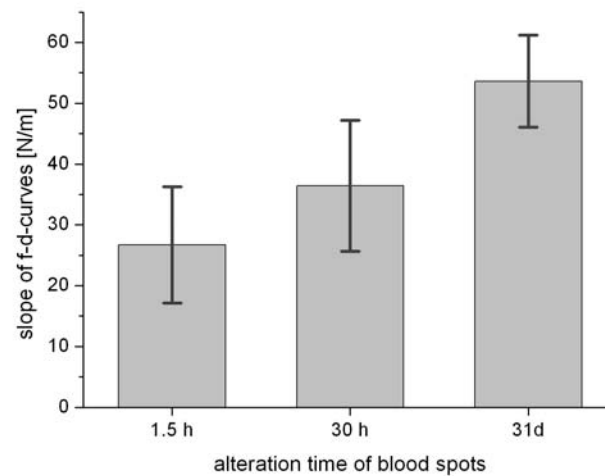


Fig. 22: Slope of force distance curves versus aging time. Alterations of the elasticity upon aging are clearly visible. Measurements were performed 1.5 h, 30 h and 31d after drying and the average of ~100 measurements is presented.

However the standard deviation as calculated from ~ 100 measurements is rather high. The histogram in Fig. 23 gives an impression of the huge scattering of individual measurements. This might result from inhomogeneous assembly within the blood spot, which could lead to a spatial variation of the elasticity.

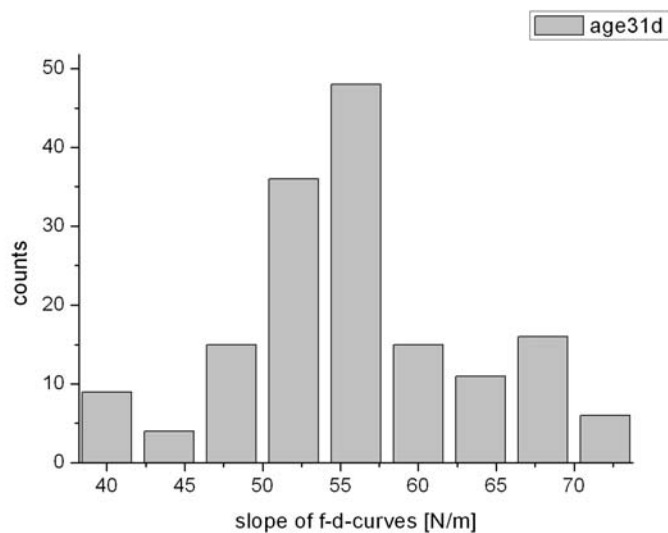


Fig. 23: Histogram of the slopes of force distance curves acquired on a blood sample after 31 days aging time. The huge scattering of the data can be attributed to the inhomogeneous structure of the blood spot. Furthermore, an influence of the bulk below the surface of the sample can not be fully excluded.

These results represent the first utilization of AFM based force measurements in order to estimate the age of blood stains by examining the elastic properties. This novel method might contribute to the so far unsolved problem in forensic medicine of

precisely determining the age of blood traces. The measurement does not require large sample areas or large volumes of blood. Also it is non-destructive, i.e. the blood can still be used for supplementary measurements as genetical fingerprinting. Nevertheless the data exhibited a rather high standard variation and indicates a few limitations, which can probably be explained by the inhomogeneous composition. When the coagulation sets in the fibrin network is generated in which platelets, red and white blood cells and other blood components are trapped. Despite the fact that the blood spot appears macroscopically homogeneous, the distinct influence of each single component on the observed increase in elasticity might be very different. In fact, there is evidence that at least the erythrocytes change their properties during *in vivo* aging within their lifetime of 120 days [102]. However, it is certain that this alteration does not play a major role for the elasticity changes observed during the aging of the blood. Also we did not conduct our experiments on single components. Thus, the next steps are elasticity and stiffness measurements of each single blood component. This should clarify the reason for the high deviations and help to pave the road for a novel tool in forensic casework for age determination of blood stains.

4. References

- [1] S. J. Eppel, B.N. Smith, H. Kahn, and R. Ballarini, Nano measurements with micro devices: mechanical properties of hydrated collagen fibrils, *J. R. Soc. Interface* 3 (2006) 117-121.
- [2] S. Kamat, X. Su, R. Ballarini, and A. H. Heuer, Structural basis for the fracture toughness of the shell of the conch *Strombus gigas*, *Nature* 405 (2000) 1036-1040.
- [3] J. Y. Rho, L. Kuhn-Spearing, and P. Zioupos, Mechanical properties and the hierarchical structure of bone, *Med. Eng. Phys.* 20 (1998) 92-102.
- [4] N. Nassif, N. Pinna, N. Gehrke, M. Antonietti, C. Jäger, and H. Cölfen, Amorphous layer around aragonite platelets in nacre, *Proceedings of the National Academy of Sciences* 102 (2005) 12653-12655.
- [5] C. Merkel, E. Griesshaber, K. Kelm, R. Neuser, G. Jordan, A. Logan, W. Mader, and W. W. Schmahl, Micromechanical properties and structural characterization of modern inarticulated brachiopod shells, *Journal of Geophysical Research* 112 (2007) 1-12.
- [6] H. G. Hansma, J. Vesenska, C. Siegerist, G. Kelderman, H. Morrett, R. L. Sinsheimer, V. Elings, C. Bustamante, and P. K. Hansma, Reproducible Imaging and Dissection of Plasmid DNA under Liquid with the Atomic Force Microscope, *Science* 256 (1992) 1180-1184.
- [7] S. Thalhammer, R. W. Stark, S. Muller, J. Wienberg, and W. M. Heckl, The atomic force microscope as a new microdissecting tool for the generation of genetic probes, *J Struct Biol* 119 (1997) 232-237.
- [8] J. S. Graham, A. N. Vomund, C. L. Phillips, and M. Grandbois, Structural changes in human type I collagen fibrils investigated by force spectroscopy, *Exp Cell Res* 299 (2004) 335-342.
- [9] G. Binnig, H. Rohrer, C. Gerber, and E. Weibl, Surface studies by scanning tunneling microscopy, *Phys Rev Lett* 49 (1982) 57-61.
- [10] G. Binnig, C. F. Quate, and C. Gerber, Atomic Force Microscope, *Phys Rev Lett* 56 (1986) 930-933.
- [11] D. Meschede, *Gerthsen Physik*, ed., Berlin, Heidelberg, New York 2002.
- [12] W. M. Heckl, *Scanning the thread of life*, ed., Piper Verlag, München, Zürich 1995.
- [13] B. Cappella, and G. Dietler, Force-distance curves by atomic force microscopy, *Surface Science Reports* 34 (1999) 1-104.
- [14] H. Hertz, Über die Berührung fester elastischer Körper, *J. Reine angewandte Mathematik* 92 (1882) 156-171.
- [15] I. N. Sneddon, The relation between load and penetration in the axisymmetric Boussinesq problem for a punch of arbitrary profile, *Int. J. Eng. Sci.* 3 (1965) 47-57.
- [16] K. L. Johnson, *Contact Mechanics*, ed., Cambridge University Press, Cambridge 2003.
- [17] W. C. Oliver, and G. M. Pharr, Measurement of hardness and elastic modulus by instrumented indentation: Advances in understanding and refinements to methodology, *Journal of Materials Research* 19 (2004) 3-20.
- [18] B. V. DeJaguin, V. M. Müller, and Y. P. Toporov, Effect of Contact Deformations on the Adhesion of Particles, *J. Colloid Interface Sci.* 53 (1975) 314-326.

- [19] A. Gigler, in Fakultät für Naturwissenschaften, Abteilung für experimentelle Physik, 2006 p. 159 Universität Ulm, Ulm.
- [20] K. L. Johnson, K. Kendall, and A. D. Roberts, Surface energy and the contact of elastic bodies, *Proc. Roy. Soc. London A* 324 (1971) 301-313.
- [21] M. D. Pashley, J. B. Pethica, and D. Tabor, Adhesion and micromechanical properties of metal surfaces, *Wear* 100 (1984) 7-31.
- [22] V. M. Müller, V. S. Yushchenko, and B. V. Dejarguin, On the influence of molecular forces on the deformation of an elastic sphere and its sticking to a rigid plane, *J. Colloid Interface Sci.* 77 (1980) 91-101.
- [23] D. Maugis, Adhesion of spheres: The JKR-DMT transition using a dugdale model, *J. Colloid Interface Sci.* 150 (1992) 243-269.
- [24] K. L. Johnson, *Contact Mechanics*, ed., Cambridge University Press, Cambridge 1994.
- [25] J. Domke, and M. Radmacher, Measuring the Elastic Properties of Thin Polymer Films with the Atomic Force Microscope, *Langmuir* 14 (1998) 3320-3325.
- [26] J. Koolman, and K.-H. Röhm, *Taschenatlas der Biochemie*, ed., Stuttgart, New York 1998.
- [27] G. Löffler, and P. E. Petrides, *Biochemie und Pathobiochemie*, 5th. ed., Berlin, Heidelberg, New York 1997.
- [28] F. Rauch, and F. H. Glorieux, Osteogenesis imperfecta, *The Lancet* 363 (2004) 1377-1385.
- [29] M. B. Shattuck, M. G. L. Gustafsson, K. A. Fisher, K. C. Yanagimoto, A. Veis, R. S. Bhatnagar, and J. Clarke, Monomeric Collagen Imaged by Cryogenic Force Microscopy, *J Microsc-Oxford* 174 (1994) Rp1-Rp2.
- [30] V. J. Kopecky, R. Ettrich, K. Hofbeuerova, and V. Baumruck, Structure of human α 1-acid glycoprotein and its affinity binding site, *Biomechanical and Biophysical research Communications* 300 (2003) 41-46.
- [31] C. Franzblau, K. Schmid, B. Faris, J. Beldekas, P. Garvin, H. M. Kagan, and B. J. Baum, Interaction of Collagen with Alpha-1-Acid Glycoprotein, *Biochim Biophys Acta* 427 (1976) 302-314.
- [32] K. E. Kadler, D. F. Holmes, J. A. Trotter, and J. A. Chapman, Collagen fibril formation, *Biochem J* 316 (1996) 1-11.
- [33] J. Gross, The Behaviour of Collagen Units as a Model in Morphogenesis, *Journal of Cell Biology* 2 (1956) 261-279.
- [34] J. Gross, J. H. Highberger, and F. O. Schmitt, A New Fibrous Structure Obtained from Extracts of Collagenous Connective Tissue, *J Appl Phys* 22 (1951) 112-112.
- [35] J. Gross, J. H. Highberger, and F. O. Schmitt, Some Factors Involved in the Fibrogenesis of Collagen Invitro, *P Soc Exp Biol Med* 80 (1952) 462-465.
- [36] J. Gross, J. H. Highberger, and F. O. Schmitt, Collagen Structures Considered as States of Aggregation of a Kinetic Unit - the Tropocollagen Particle, *P Natl Acad Sci USA* 40 (1954) 679-&.
- [37] J. Gross, and D. Kirk, Heat Precipitation of Collagen from Neutral Salt Solutions - Some Rate-Regulating Factors, *J Biol Chem* 233 (1958) 355-360.
- [38] G. C. Wood, Formation of Fibrils from Collagen Solutions.2. Mechanism of Collagen-Fibril Formation, *Biochem J* 75 (1960) 598-605.

- [39] G. C. Wood, and M. K. Keech, Formation of Fibrils from Collagen Solutions. I. Effect of Experimental Conditions - Kinetic and Electron-Microscope Studies, *Biochem J* 75 (1960) 588-&.
- [40] J. B. L. Bard, and J. A. Chapman, Polymorphism in Collagen Fibrils Precipitated at Low Ph, *Nature* 219 (1968) 1279-&.
- [41] J. B. L. Bard, and J. A. Chapman, Diameters of Collagen Fibrils Grown in-Vitro, *Nature-New Biol* 246 (1973) 83-84.
- [42] V. N. Orekhovich, A. A. Tustanovskii, K. D. Orekhovich, and N. E. Plotnikova, O Prokollagene Kozhi, *Biochemistry-Ussr+* 13 (1948) 55-&.
- [43] J. H. Highberger, J. Gross, and F. O. Schmitt, The Interaction of Mucoprotein with Soluble Collagen - an Electron Microscope Study, *P Natl Acad Sci USA* 37 (1951) 286-291.
- [44] S. Newman, M. Cloitre, C. Allain, G. Forgacs, and D. Beysens, Viscosity and elasticity during collagen assembly in vitro: Relevance to matrix-driven translocation, *Biopolymers* 41 (1997) 337-347.
- [45] S. Strasser, A. Zink, W. M. Heckl, and S. Thalhammer, Controlled self-assembly of collagen fibrils by an automated dialysis system, *Journal of Biomechanical Engineering* 128 (2006) 792-796.
- [46] M. F. Paige, J. K. Rainey, and M. C. Goh, Fibrous long spacing collagen ultrastructure elucidated by atomic force microscopy, *Biophys J* 74 (1998) 3211-3216.
- [47] M. F. Paige, J. Strzelczyk, J. Rainey, and M. C. Goh, Type I collagen fibril formation: A colloidal approach, *Abstr Pap Am Chem S* 216 (1998) U624-U624.
- [48] J. K. Rainey, C. K. Wen, and M. C. Goh, Hierarchical assembly and the onset of banding in fibrous long spacing collagen revealed by atomic force microscopy, *Matrix Biol* 21 (2002) 647-660.
- [49] T. Gutsmann, G. E. Fantner, M. Venturoni, A. Ekani-Nkodo, J. B. Thompson, J. H. Kindt, D. E. Morse, D. K. Fygenson, and P. K. Hansma, Evidence that collagen fibrils in tendons are inhomogeneously structured in a tubelike manner, *Biophys J* 84 (2003) 2593-2598.
- [50] S. Strasser, A. Zink, M. Janko, W. M. Heckl, and S. Thalhammer, Structural investigations on native collagen type I fibrils using AFM, *Biochem Bioph Res Co* 354(1) (2007) 27-32.
- [51] P. Fratzl, K. Misof, I. Zizak, G. Rapp, H. Amenitsch, and S. Bernstorff, Fibrillar structure and mechanical properties of collagen, *J Struct Biol* 122 (1998) 119-122.
- [52] D. F. Holmes, C. J. Gilpin, C. Baldock, U. Ziese, A. J. Koster, and K. E. Kadler, Corneal collagen fibril structure in three dimensions: Structural insights into fibril assembly, mechanical properties, and tissue organization, *P Natl Acad Sci USA* 98 (2001) 7307-7312.
- [53] C. K. Wen, and M. C. Goh, AFM nanodissection reveals internal structural details of single collagen fibrils, *Nano Lett* 4 (2004) 129-132.
- [54] J. A. Petruska, and A. J. Hodge, Subunit Model for Tropocollagen Macromolecule, *P Natl Acad Sci USA* 51 (1964) 871-&.
- [55] T. Gutsmann, G. E. Fantner, J. H. Kindt, M. Venturoni, S. Danielsen, and P. K. Hansma, Force spectroscopy of collagen fibers to investigate their mechanical properties and structural organization, *Biophys J* 86 (2004) 3186-3193.

-
- [56] L. Bozec, and M. Horton, Topography and mechanical properties of single molecules of type I collagen using atomic force microscopy, *Biophys J* 88 (2005) 4223-4231.
- [57] J. Xu, J. Y. Rho, S. R. Mishra, and Z. Fan, Atomic force microscopy and nanoindentation characterization of human lamellar bone prepared by microtome sectioning and mechanical polishing technique, *J Biomed Mater Res* 67A (2003) 719-726.
- [58] M. P. E. Wenger, L. Bozec, M. A. Horton, and P. Mesquida, Mechanical properties of collagen fibrils, *Biophys J* e-published ahead of print (2007) doi:10.1529/biophysj.1106.103192.
- [59] R. Puxkandl, I. Zizak, O. Paris, J. Keckes, W. Tesch, S. Bernstorff, P. Purslow, and P. Fratzl, Viscoelastic properties of collagen: synchrotron radiation investigations and structural model, *Philos T Roy Soc B* 357 (2002) 191-197.
- [60] J. Diamant, R. G. C. Arridge, E. Baer, M. Litt, and A. Keller, Collagen - Ultrastructure and Its Relation to Mechanical Properties as a Function of Aging, *P Roy Soc Lond B Bio* 180 (1972) 293-&.
- [61] P. Fratzl, N. Fratzlzelman, and K. Klaushofer, Collagen Packing and Mineralization - an X-Ray-Scattering Investigation of Turkey Leg Tendon, *Biophys J* 64 (1993) 260-266.
- [62] A. Bernstein, S. Henning, R. Hube, U. Schietsch, and W. Hein, in *Micro- and Nanostructures of Biological Systems* (Hein, G. B. a. H.-J., Ed.), 2000 pp. 93-108 Shaker, Halle.
- [63] M. E. Lacouture, J. L. Schaffer, and L. B. Klickstein, A comparison of type I collagen, fibronectin and vitronectin in supporting adhesion of mechanically strained osteoplasts, *J. Bone Miner. Res.* 17 (2002) 481-492.
- [64] S. D. Cook, K. A. Walsch, and R. J. J. Haddad, Interface mechanics in bone growth into porous Co-Cr-Mo alloy implants, *Clin Orthop* 193 (1985) 271-280.
- [65] E. M. Leiz, J. Hemmerle, and M. Leize, Characterization at the bone crystal level or the titanium-coating/bone interfacial zone, *Clin. Oral Res.* 11 (2000) 279-288.
- [66] H. Hilbig, M. Kirsten, R. Rupietta, H.-L. Graf, S. Thalhammer, S. Strasser, and F. P. Armbruster, Implant surface coatings with bone sialoprotein, collagen, and fibronectin and their effects on cells derived from human maxillar bone, *European Journal of Medical Research* 12 (2007) 6-12.
- [67] P. Karlson, *Kurzes Lehrbuch der Biochemie für Mediziner und Naturwissenschaftler*, 13 ed., Georg Thieme Verlag, Stuttgart, New York 1988.
- [68] P.K. Hansma, G.E. Fantner, J.H. Kindt, P.J. Thurner, G. Schitter, P.J. Turner, S.F. Udwin, and M. M. Finch, Sacrificial bonds in the interfibrillar matrix of bone, *J Musculoskelet Neuronal Interact* 5 (2005) 313-315.
- [69] J. D. Currey, Mechanical-Properties of Mother of Pearl in Tension, *P Roy Soc Lond B Bio* 196 (1977) 443.
- [70] G. E. Fantner, T. Hassenkam, J. H. Kindt, J. C. Weaver, H. Birkedal, L. Pechenik, J. C. Cutroni, G. A. G. Cidade, G. D. Stucky, D. E. Morse, and P. K. Hansma, Sacrificial bonds and hidden length dissipate energy as mineralized fibrils separate during bone fracture, *Nature Materials* 4 (2005) 612-616.
- [71] T. Hassenkam, G. E. Fantner, J. C. Cutroni, J. C. Weaver, D. E. Morse, and P. K. Hansma, High-resolution AFM imaging of intact and fractured trabecular bone, *Bone* 35 (2004) 4-10.
-

- [72] J. Davy, Observations on the temperature of the human body after death, *Res. Physiol. Anatom London* 1 (1839) 228.
- [73] J. W. Burnham, On the rate of cooling of the human body after death, *Edin. Med. J.* 25 (1880) 993.
- [74] A. Brown, and T. K. Marshall, Body temperature as a means of estimating the time of death, *J. Forensic Sci.* 4 (1974) 125-133.
- [75] L. M. Al-Alousi, A study of the shape of the post-mortem cooling curve in 117 forensic cases, *Forensic Science International* 125 (2002) 237-244.
- [76] W. O. Sturner, and G. E. Gantner, The post-mortem interval; a study of potassium in the vitreous humour, *Am. J. Clin. Pathol.* 42 (1964) 134-144.
- [77] N. Lange, S. Swearer, and W. Q. Sturner, Human postmortem interval estimation from vitreous potassium: an analysis of original data from six different studies, *Forensic Science International* 66 (1994) 159-174.
- [78] H. N. Naumann, Postmortem chemistry of the vitreous body in man, *Arch. Ophthalmol.* 62 (1959) 356-363.
- [79] D. Querido, Time dependent changes in electrical resistance of the intact abdomen during the 1-504 postmortem period in rats, *Forensic Science International* 67 (1994) 17-25.
- [80] D. Querido, and M. R. B. Phillips, Changes in the resistivity and reactive components of abdominal impedance during the 1-21 day postmortem period in rats, *Forensic Science International* 85 (1997) 163-175.
- [81] D. Querido, and M. R. B. Phillips, Estimation of postmortem interval Temperature-correction of extracellular abdominal impedance during the first 21 days of death, *Forensic Science International* 116 (2001) 133-138.
- [82] K. J. Straton, A. Busuttil, and M. A. Glasby, Nerve conduction as a means of estimating early post-mortem interval, *Int. J. Legal Med.* 105 (1992) 69-74.
- [83] M. Benecke, A brief history of forensic entomology, *Forensic Science International* 120 (2001) 2-14.
- [84] S. Berg, and W. Specht, Die Altersbestimmung von Skelettfunden als forensische und archäologische Aufgabe, *Dtsch. Z. gerichtl. Med.* 47 (1958) 209-241.
- [85] S. Berg, The determination of bone age, In F. Lundquest (ed.) ed., New York 1963.
- [86] S. Berg, Die Altersbestimmung von Skelettfunden als Forensisch und archäologische Aufgabe, *Münch. Med. Wschr* 47 (1964) 989-995.
- [87] B. Knight, and L. Lauder, Practical methods of dating skeletal remains: a preliminary study, *Med. Sci. Law* 7 (1967) 205-208.
- [88] B. Knight, Methods of dating skeletal remains, *Med. Sci. Law* 9 (1969) 247-252.
- [89] B. Knight, and L. Lauder, Methods of dating skeletal remains, *Hum. Biol.* 41 (1969) 322-341.
- [90] M. Yoshino, T. Kimijima, S. Miyasaka, H. Sato, and S. Seta, Microscopical study on estimation of time since death in skeletal remains, *Forensic Science International* 49 (1991) 143-158.
- [91] B. Swift, I. Lauder, S. Black, and J. Norris, An estimation of post-mortem interval in human skeletal remains: a radionuclide and trace element approach, *Forensic Science International* 117 (2001) 73-87.
- [92] W. Schwarzacher, Altersbestimmung von Blutspuren, *Z. Ges. Gerichtliche Med.* 15 (1930) 119-124.

- [93] G. Lins, and V. Blazek, The use of remission analysis for direct colorimetric determination of age of blood stains, *J. Legal Med.* 88 (1982) 13-22.
- [94] T. Mikki, A. Kai, and M. Ikeya, Electron-spin resonance of bloodstains and its application to the estimation of time after bleeding, *Forensic Science International* 35 (1987) 149-158.
- [95] H. Inoue, F. Takabe, M. Iwasa, Y. Maeno, and Y. Seko, A new marker for estimation of bloodstain age by high-performance liquid chromatography, *Forensic Science International* 57 (1992) 17-27.
- [96] R. Nowakowski, and P. Luckham, Imaging the surface details of red blood cells with atomic force microscopy, *Surface and Interface Analysis* 33 (2002) 118-121.
- [97] A. H. Swihart, J. M. Mikrut, J. B. Ketterson, and R. C. MacDonald, Atomic force microscopy of the erythrocyte membrane skeleton, *Journal of Microscopy* 204 (2001) 212-225.
- [98] M. Grandbois, W. Dettmann, M. Benoit, and H. E. Gaub, Affinity imaging of red blood cells using an atomic force microscope, *The Journal of Histochemistry and Cytochemistry* 48 (2000) 719-724.
- [99] Y. Otha, H. Okamoto, T. Kanno, and T. Okuda, Atomic force microscopic observation of mechanically traumatized erythrocytes, *Artif. Org.* 26 (2002) 10-17.
- [100] Y. Chen, and J. Cai, Membrane deformation of unfixed erythrocytes in air with time lapse investigated by tapping mode atomic force microscopy, *Micron* 37 (2006) 339-346.
- [101] S. Strasser, A. Zink, G. Kada, P. Hinterdorfer, O. Peschel, W. M. Heckl, A. G. Nerlich, and S. Thalhammer, Age determination of blood spots in forensic medicine by force spectroscopy, *Forensic Science International* 170 (2007) 8-14.
- [102] M. Baumann, Cell ageing for 1 day alters both membrane elasticity and viscosity, *Pflug Arch Eur J Phy* 445 (2003) 551-555.

5. Publications

Publication 1:

Controlled Self-Assembly of Collagen Fibrils by an Automated Dialysis System

Stefan Strasser, Albert Zink, Wolfgang M. Heckl, Stefan Thalhammer

Journal of Biomechanical Engineering (2006), 128, 792-796

Publication 2:

Structural Investigations on Native Collagen Type I Fibrils

Stefan Strasser, Albert Zink, Marek Janko, Wolfgang M. Heckl, Stefan Thalhammer

Biochemical and Biophysical Research Communications (2007), 354(1), 27-32

Publication 3:

Implant Surface Coatings with Bone Sialoprotein, Collagen and Fibronectin and their Effects on Cells derived from Human Maxillar Bone

H. Hilbig, M. Kirsten, R. Rupietta, H. L. Graf, S. Thalhammer, S. Strasser, F. P. Armbruster

European Journal of Medical Research (2007), 12, 6-12

Publication 4:

Age Determination of Blood Spots in Forensic Medicine by Force Spectroscopy

Stefan Strasser, Albert Zink, Gerald Kada, Peter Hinterdorfer, Oliver Peschel, Wolfgang M. Heckl, Andreas G. Nerlich, Stefan Thalhammer

Forensic Science International (2007), 170, 8-14

5.1 Controlled Self-Assembly of Collagen Fibrils by an Automated Dialysis System

Stefan Strasser, Albert Zink, Wolfgang M. Heckl, Stefan Thalhammer

Journal of Biomechanical Engineering (2006), 128, 792-796

Controlled Self-Assembly of Collagen Fibrils by an Automated Dialysis System

Stefan Strasser

Albert Zink

Department für Geo- und Umweltwissenschaften,
Ludwig-Maximilians-Universität,
80333 Munich, Germany

Wolfgang M. Heckl

Department für Geo- und Umweltwissenschaften,
Ludwig-Maximilians-Universität,
80333 Munich, Germany and
Deutsches Museum,
Museumsinsel 1, 80538 Munich, Germany

Stefan Thalhammer¹

Department für Geo- und Umweltwissenschaften,
Ludwig-Maximilians-Universität,
80333 Munich, Germany and
GSF-Forschungszentrum für Umwelt und Gesundheit
GmbH,
Ingolstädter Landstrasse 1, 85764 Oberschleissheim,
Germany
e-mail: s.t@lmu.de

In vitro self-assembled collagen fibrils form a variety of different structures during dialysis. The self-assembly is dependent on several parameters, such as concentrations of collagen and α 1-acid glycoprotein, temperature, dialysis time, and the acid concentration. For a detailed understanding of the assembly pathway and structural features like banding pattern or mechanical properties it is necessary to study single collagen fibrils. In this work we present a fully automated system to control the permeation of molecules through a membrane like a dialysis tubing. This allows us to ramp arbitrary diffusion rate profiles during the self-assembly process of macromolecules, such as collagen. The system combines a molecular sieving method with a computer assisted control system for measuring process variables. With the regulation of the diffusion rate it is possible to control and manipulate the collagen self-assembly process during the whole process time. Its performance is demonstrated by the preparation of various collagen type I fibrils and native collagen type II fibrils. The combination with the atomic force microscope (AFM) allows a high resolution characterization of the self-assembled fibrils. In principle, the represented system can be also applied for the production of other biomolecules, where a dialysis enhanced self-assembly process is used. [DOI: 10.1115/1.2264392]

Keywords: AFM, dialysis system, self-assembly, collagen

¹Corresponding author.

Contributed by the Bioengineering Division of ASME for publication in the JOURNAL OF BIOMECHANICAL ENGINEERING. Manuscript received August 25, 2005; final manuscript received March 12, 2006. Review conducted by Ellen M. Arruda.

1 Introduction

Collagen molecules consist of three polypeptide chains (α -chains) which form a unique triple-helical structure. More than 20 genetically distinct collagens exist in mammalian tissue, where collagen types I, II, III, V, and XI self-assemble into D-periodic cross-striated fibrils. Collagen molecules, forming the fibril, consist of an uninterrupted triple helix, approximately 300 nm in length and 1.5 nm in diameter. The collagen self-assembles in cross-striated fibrils, that normally occur in the extracellular matrix of connective tissues. These fibrils are stabilized by covalent cross linking of specific lysines and hydroxylsines [1]. Fundamental experiments for the understanding of the morphogenesis of collagen units and fibrils in vitro and influencing factors e.g., temperature, ionic strength, pH value, and so on, were performed by Gross, Wood, Keech et al. [2–8] and continued work was done by Bard and Chapman [9,10]. Orekhovich [11] dialyzed for the first time a mammalian skin extract against water and showed with the process the existence of procollagen. Based on this work, Highberger [12] developed a procedure to obtain LS fibrils (long-spacing) by a dialysis process against water. While no neutralizing process or salt concentrations were influencing the fibril synthesis, other factors like the presence of mucoprotein could be investigated [12]. The resulting fibrils could be visualized by several methods like scanning electron microscopy (SEM) with adequate resolution. However an improvement in the field of imaging molecular structures was accomplished by the invention of the atomic force microscope (AFM) by Binnig et al. [13] to get real three-dimensional profiles. Studies on collagen molecules by cryo-AFM [14] and normal AFM studies of segment-long spacing (SLS) crystals of collagen [15] have revealed variations in the structure. AFM investigations carried out by Paige et al. [16] show native fibrils and fibrous long spacing fibrils (FLS-fibrils) [17]. Cocoonlike fibrils, which are hundreds of nanometers in diameter and 10–20 mm in length, were found to coexist with mature FLS fibrils. On the basis of detailed AFM studies a stepwise process in the formation of FLS collagen was proposed. Different pH ranges in the in vitro fibrillogenesis and the influence of α 1-acid glycoprotein were investigated to clarify the various stages in the self-assembly process of the fibrils. In the early stages below pH 4 thin nonbanded fibrils were formed. Filamentous structures showed protrusions at pH ~4 and at pH >4.6 mature fibers emerged [18]. Gutsmann et al. observed that collagen fibrils from tendons behave mechanically like tubes and concluded that the collagen fibril is an inhomogeneous structure composed of a relatively hard shell and a softer, less dense core [19]. For investigation of single collagen fibrils by AFM, collagen fibrils have to be prepared in vitro. In order to start the self-assembly of collagen fibrils, it is necessary to remove or neutralize the diluted acetic acid, hydrochloric acid or other acids from the solution, which were initially used to dissolve the collagen tissue. Viscosity measurements during in vitro self-assembling show an increasing viscosity upon removal of the acid from the solution. The viscosity change is time independent, but directly related to the concentration of the acetic acid [20,21], which diffuses through the membrane of a dialysis tubing. The membrane of the dialysis tubing acts as a molecular filter. The theory of restricted diffusion and molecular sieving through the walls of living capillaries was first described by Pappenheimer et al. [22,23]. Renkin extended this theory through the characterization of artificial cellulose membranes [24]. Today ultrafiltration and separation are often carried out using regenerated cellulose [25,26]. The different membranes have a defined porosity (pore diameter) and varying solvent compatibility. In the least complicated case, only the pore diameter of the membrane and the size of the molecule are decisive for the separation of certain substances. The efficiency of the transport process is dependent on the concentration gradient between both sides of the membrane. This technique can be used for purification and separation of DNA [26] and other biomolecules [27], desalination [28] or to control self-assembly processes of macromol-

ecules, such as collagen [16,20]. Bosch et al. developed an Advanced Protein Crystallisation Facility (APCF) for protein crystallisation according to the methods liquid-liquid diffusion, dialysis and vapour diffusion (hanging drop) [29]. Vergara, Berisio, and Zagari et al. used this equipment for crystallization of collagen-like polypeptides in microgravity [30,31]. In general, dialysis is used to separate macromolecules from low-molecular substances. In the most basic setup it is a single stage process which is terminated by the equilibrium of the concentrations. The exchange of the external medium implies an effectivity improvement of the dialysis and leads to a multistage process. This can be done by continuously purging the external side (dialysis liquid) with DI water (deionized water) in order to shorten the process time and increase the yield of the targeted protein/macromolecule. The transport through a membrane in a single stage process was described by Renkin [24], see Eq. (1),

$$\frac{dn}{dt} = D \cdot \frac{A}{\Delta x} \Delta c \quad (1)$$

where dn/dt is diffusion rate, Δc is the concentration difference across the membrane, $A/\Delta x$ is the diffusion area per unit path length, D is the free diffusion coefficient of the solute which fills the pores. The dialysis is not only used for separation purposes, but it also can be applied to control the self-assembly of collagen fibrils by changing the acetic acid concentration of the collagen solution. In contrast to simple acid base titration systems or pH-stat methods where the pH value is held constant, herein we present a novel, fully automated dialysis system. It allows a highly efficient control of the diffusion rate of acetic acid molecules through a membrane like a dialysis tubing by means of feedback control. Obviously, this improves the preparation of collagen fibrils and is an appropriate prerequisite for unique experiments on collagen assembly for structural high resolution imaging and the investigation of mechanical properties of distinct assembled collagen fibrils. The represented system can, in principle, also be applied to the production of other biomolecules, where a dialysis enhanced self-assembly process with a stable and controllable permeation of molecules through a membrane is used.

2 Materials and Methods

2.1 Preparation of the Collagen Solution. The solution for assembling collagen fibrils was prepared from calf skin (Sigma). Approximately 1 mg of the compound was dissolved in 1 ml of 0.5% acetic acid overnight at 4°C. The solution was sonicated for 1 h at 0°C to detach any collagen aggregates. Finally, the mixture was centrifuged at 4000 rpm for 90 min at 4°C and the supernatant was filtered through a 0.2 µm filter unit (Sigma) (modified protocol of Paige et al. [16]). In order to initiate the self-assembly process of FLS fibrils during the dialysis α1-acid glycoprotein is added. For preparing native fibrils this is not necessary. By utilizing an increased amount of α1-acid glycoprotein, the yield of FLS fibrils becomes higher. In this case assembly of native fibrils is reduced and vice versa. The α1-acid glycoprotein is incorporated into the fibril during the dialysis [18]. The final mixture as taken for dialysis is comprised of 0.5 mg/ml collagen, and 0.2 mg/ml α1-acid glycoprotein. The pH value of the solution is at pH 3.3.

2.2 Dialysis of the Collagen Solution and Preparation for AFM Imaging. For the experiments a dialysis tubing (Serva, visking® 8/32) with a molecular weight cutoff (MWCO) of 12 kDa–14 kDa and a tube diameter of 6 mm was used. The external side was rinsed with DI water to adjust the end pH in the dialysis vessel (liquid level about 300 ml) to pH 5.5 or higher (see Rainey et al. [18]). The dialysis took about 17 h (following the protocol of Paige et al. [14]) and at the beginning the pH value of the dialysis liquid was adjusted to pH 3.3. At the beginning there is no concentration gradient of the acetic acid molecules between

the collagen solution inside the dialysis tubing and the dialysis liquid in the beaker. Not until the dialysis liquid is slowly rinsed out, does the acetic acid diffuse through the membrane. With the regulation system the concentration outside the beaker is controlled and due to diffusion the concentration inside will become equal. The reservoir contains 2 l neutral distilled water (pH7). As described previously, for self-assembly of the dissolved collagen fibers it is very important to finally obtain a pH > 5.5 [18]. The importance of a precise pH value required a totally closed system to avoid dissolution of ambient carbon dioxide. To exclude such effects the whole system is hermetically closed and connected to a bag filled with nitrogen for volume compensation. Nitrogen was chosen instead of air due to the pH-lowering effect of CO₂ (carbonic acid) in ambient air. A magnetic stirrer in the reaction chamber homogenizes the solution. The DI water from the reservoir is added in a defined manner by a two-step feedback controller (Fig. 1(A)).

The output of the pH meter is read out by a 8-bit-USB-interface-card (Velleman) programmed in Visual Basic. If the actual value is lower than the setpoint value the valve X1 will be opened and the DI water is added to the external side. Thereby, a setpoint curve for the pH value will be retraced. The acetic acid molecules are rinsed out of the beaker. The permeation through the dialysis tubing goes on until the concentration gradient is zero. If the valve can be opened the diffusion starts again. The digital output (open collector) of the interface card switches a relay which opens the valve. The input signal of the interface card is amplified by a factor of 15 resulting in a resolution of ΔpH = 0.05. For a sufficient control the valve is checked every 5 s. If necessary, the flow through the valve can be reduced with a flow limiter. The freely programmable card is equipped with several digital and analog in- and outputs. This allows the measurement and control of various parameters like temperature, ionic strength, concentrations or several other gaugable parameters. After finishing the dialyzing process, 10 µl of the collagen solution is dropped on freshly cleaved mica and dried for 1 h at room temperature.

2.3 AFM Microscopy. For characterization an AFM Topometrix Explorer (Atos, Germany) was used. It was operated both in noncontact mode and contact mode under ambient conditions, with 35% relative humidity, using NSC11A/B (noncontact silicon cantilever) cantilevers (Mikromasch, Estonia). For experiments in liquid (decanol) CSC21A (contact silicon cantilever, Mikromasch, Estonia) cantilevers were used. The spring constants of the non-contact probes (NSC) were 3 N m⁻¹ (a) and 48 N m⁻¹ (b). The spring constant of the contact mode cantilever was 0.3 N m⁻¹. The resonant frequencies of the NSC cantilevers were 60 kHz (a) and 330 kHz (b). The nominal tip radius was specified as <10.0 nm. Image analysis was performed using SPIP software (Image Metrology, Denmark).

3 Results

At first the properties of the dialysis tubing were tested, in order to check the performance of the system. 1 ml of 0.5% acetic acid, which equals the volume and concentration of the collagen/α1-acid glycoprotein solution at the beginning of the dialysis, was pipetted into 300 ml DI water (equals the volume of the dialysis chamber) and the changes of the pH value were recorded. The pH value was expected to be approximately pH 4.15. The bright curve in Fig. 2 indicates a dispersion time of approximately 2–3 min for acetic acid in the beaker.

In a second experiment the dialysis tubing was filled with 1 ml of 0.5% acetic acid and positioned into the beaker filled with 300 ml DI water. In both cases the liquid in the beaker was stirred moderately. Immediately after the addition of the acetic acid the minimal pH value was reached, whereas it took about 30 min with the dialysis tubing until 90% of the pH value alteration was reached (see Fig. 2). In comparison to the total time of the dialysis

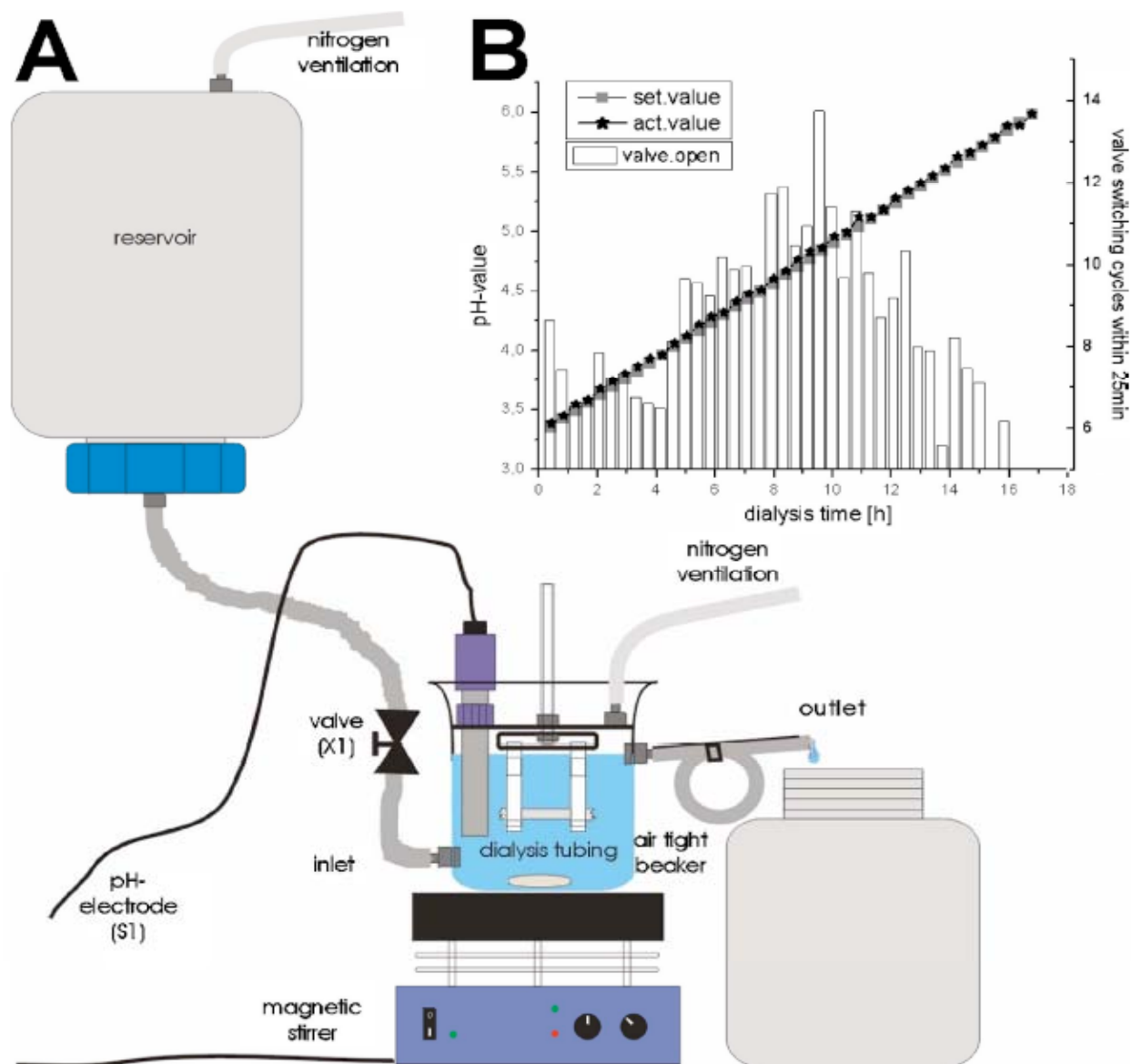


Fig. 1 (A) Sketch of the dialysis system, with the following workflow: The rinsing medium flows through the valve X1 into the beaker (via the inlet (air tight lid, with O-ring)). The outlet is fixed at a predetermined height, therefore a constant level of the dialysis liquid is guaranteed. The dialysis liquid in the beaker is stirred and the pH value is measured online. With a holding fixture the dialysis tubing is fastened in the medium. To achieve a volume compensation, mainly in the reservoir, the reservoir and the beaker are connected to a bag filled with nitrogen. The valve X1 is controlled by a USB interface card and dialysis rate in the system can be controlled online. (B) pH control curve during dialysis. Depicted are the setpoint value (set.value) and the actual pH value (act.value). The columns display the switching state of the valve within every 25 min. One valve-open-cycle lasts 5 s. The average variation can be calculated to $\Delta\text{pH}=0.033$ and the maximal variation to $\Delta\text{pH}=0.09$.

(17 h) the diffusion time was very short. An exponentially decreasing concentration gradient causes a slow down in permeation in the end of the dialysis. The final value of the dialysis compared to the curve without tubing ($\text{pH}=4.15$) was reached after ~ 1 h.

Figure 1(B) depicts the pH profile versus time of a typical dialysis with a total time of 17 h and a pH range between pH 3.3–6.0. The bright curve corresponds to the setpoint value, and the dark curve (in front of the set curve) to the actual value during the dialysis. The average variation can be calculated to $\Delta\text{pH}=0.033$ and the maximal variation to $\Delta\text{pH}=0.09$. In the lower part

of the diagram the switching state of the valve is recorded and displays that from $t=5$ h to $t=13$ h; the valve is opened for longer times than during the other intervals. To show the effectiveness of the system various collagen fibrils (collagen type I fibrils with different banding patterns and collagen type II fibrils) are displayed in Figs. 3(A)–3(D). Detailed structural properties can be recognized at the produced collagen fibrils and the capacity of the system is shown.

According to AFM measurements, the dimensions and banding pattern of native collagen I fibrils amount to 200–300 nm in

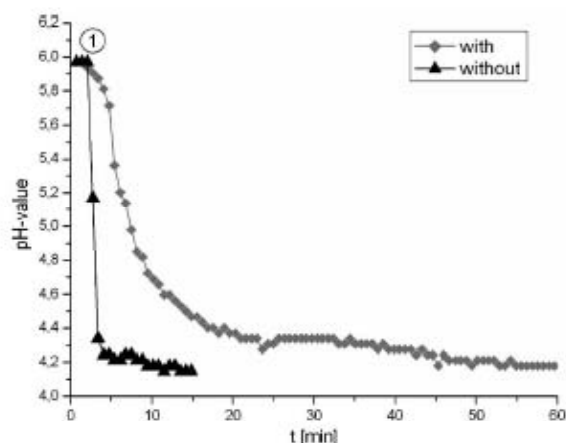


Fig. 2 Permeation time of the acetic acid. The bright (with) curve shows the pH change of the dialysis liquid during diffusion of acetic acid through the membrane of the dialysis tubing. The dark curve (without) shows the pH value of the dialysis liquid after addition of the same amount of acetic acid. ① marks the point in time when the acetic acid is added (pH value versus time (min)).

width, 20–30 nm in height, and in a banding distance of 64–70 nm. A typical collagen I fibril is shown in Fig. 3(A). Fibrils growing away from the cluster have a larger banding pattern at one end (near the cluster). However, this banding pattern disappears with increasing length of the fibril. The banding of these fibrils classifies one end as a FLS fibril with a banding pattern of 230 nm, the centerpiece, and the other end as a native fibril (see Fig. 3(B)). This partitioning is dependent on the $\alpha 1$ -acid glycoprotein distribution during the self-assembly process. Presumably, the single collagen fibril assembly starts at the cluster and grows in the opposite direction. The concentration of $\alpha 1$ -acid glycoprotein in the proximity of the fibril decreases, and only native fibrils can be assembled. With still higher $\alpha 1$ -acid glycoprotein concentration and at lower end-pH-values (see also Rainey et al. [18]), further formations of collagen type I can be found, like intermediate state FLS fibrils (Fig. 3(C)).

Native collagen type II fibrils were assembled using the same setup. The dimensions and banding pattern of native collagen II fibrils were measured to be 75–110 nm in width, 6–13 nm in height, and the banding distance is 67–75 nm. A typical collagen II fibril is shown in Fig. 3(D).

4 Discussion

The dialysis was already introduced for collagen fibrillogenesis by Orekhovich et al. [11] and Highberger et al. [12]. Orekhovich et al. dialyzed for the first time mammalian skin extracts against water and showed with this process the existence of procollagen. Based on this work, Highberger et al. showed in a further study a procedure to generate LS fibrils (long-spacing) with a dialysis process against water. In their work, the authors demonstrated that without a neutralizing process (no influences of salt concentrations) other factors like presence of mucoprotein could be investigated in more detail. In general, the dialysis method seems to be preferable if influences of other molecules (from neutralization) should be excluded and/or the influence of a certain substance should be tested.

To investigate the self-assembly pathway of collagen in vitro, it is necessary to control the conditions and in particular the permeation of the acid molecules in a dialyzing process. The described system allows an advanced control of the diffusion rate of the acetic acid or hydrochloric acid through the membrane of the

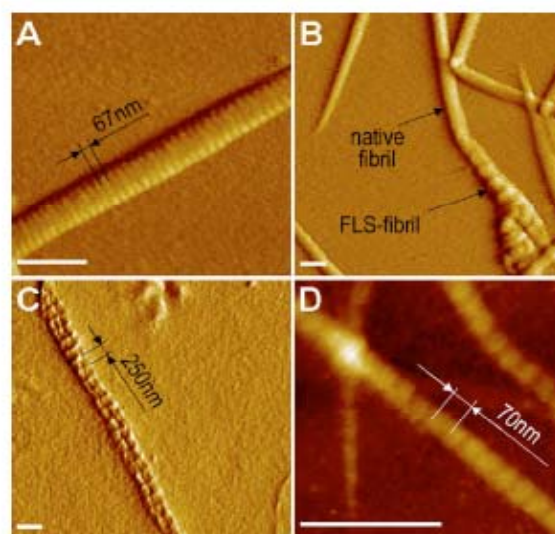


Fig. 3 AFM images of (A) a native collagen type I fibril. The banding is clearly visible and amounts to 67 nm, the width to 300 nm and the height to 20 nm (scale bar 500 nm, error signal, contact mode, decanol/end pH=6, $C_{\alpha 1\text{-acid glycoprotein}}=0.2$ mg/ml/dialysis time: 17 h). (B) Native and FLS collagen type I fibrils. The formation is changing along the axis of the fibril. This formation is typical for collagen clusters (scale bar 500 nm, error signal, contact mode, decanol/end pH=6, $C_{\alpha 1\text{-acid glycoprotein}}=0.3$ mg/ml/dialysis time: 17 h). (C) An intermediate FLS fibril, assembled with increased $\alpha 1$ -acid glycoprotein concentration (scale bar 500 nm, error signal, contact mode, ambient conditions/end pH=4.5, $C_{\alpha 1\text{-acid glycoprotein}}=0.5$ mg/ml/dialysis time: 10 h). (D) Native collagen type II fibrils. The banding is clearly visible and amounts to 70 nm. The diameter of collagen II (110 nm in width and 13 nm height) is much smaller than the diameter of collagen I (scale bar 500 nm, topography signal, noncontact mode, ambient conditions/end pH=6, $C_{\alpha 1\text{-acid glycoprotein}}=0.2$ mg/ml/dialysis time: 17 h).

dialysis tubing during the self-assembly process, including monitoring and recording of data. In this study, we demonstrated the performance of the system with the exemplary production of different collagen type I and type II fibrils in a self-assembly process in vitro. In principle, it is possible to synthesize all different acid soluble collagen types using this dialysis system.

The represented freely programmable dialysis system can be characterized and confined from other dialysis methods as follows. Figure 1(B) displays, that from $t=5$ h to $t=13$ h the valve is opened for longer times than during the other intervals. In the case of a noncontrolled system, e.g., a continuous flow, the permeation would not be linear over time and the reaction controlled from the self-assembly conditions.

As shown in Fig. 2 and in Sec. 3, the diffusion time during the dialysis using this tubing (MWCO of 12–14 kDa and pit diameter of 0.25 μm) is not the rate limiting process. Although, it described for these kinds of experiments in the literature [16], [18], the MWCO of the membrane is far too high to act as a barrier for the 60 Da acetic acid molecule. To regulate the self-assembly process it is necessary to control the permeation of the acetic acid. With the described experimental setup it is possible to control this during the whole process time.

A major advantage of this system is the high reproducibility of the dialysis and the possibility of controlling the permeation characteristics during dialysis. In contrast to simple acid base titration systems or pH-stat methods the diffusion of the acetic acid molecules through a membrane is the controlling parameter. The dif-

fusion depends on the the acid concentration of the dialysis buffer, which is controlled by the pH value of the dialysis buffer depending on time. Without such a control system it would be necessary to change the dialysis buffer several times [32]. As a consequence, this would result in an abrupt step in the dialysis immediately after the exchange of the external medium. The main advantage of the system is the exact control manner. It is possible to ramp every diffusion rate over time to every end concentration (here we applied a linear diffusion rate, but it would be possible to use any other mathematical equation). This enables experiments on the influence of determined acetic acid concentrations ramps on the self-assembly. For instance, elasticity measurements could be performed on collagen fibrils which were synthesized with distinct process parameters to check the consequences of different assembly conditions (e.g., more time for assembly of microfibrils at the beginning or for mature fibrils in the end of dialysis). It is also possible to use different dialyzing tubings to get higher diffusion rates. Higher pH values than pH 7 can be obtained by the accumulation of determined molecules and/or buffer solutions in a second reservoir. Only a second valve has to be controlled (with liquid from the second reservoir) after the acetic acid is rinsed out of the dialysis tubing with DI water and the pH value can be increased to every value with appropriate bases.

With the used dialysis tubing a Δ pH range of 3 could be exchanged within 1 h instead of 17 h as shown in Fig. 2. Dialysis tubings with bigger pore sizes are able to manage also higher exchange rates. The time limiting factor of the process is the molecule weight cut off of the membrane in combination with the difference of molecule size of single collagen molecules (should stay inside) and the solvent molecules (should go outside). A performance enhancement could be achieved by the choice of different dialysis tubings to let solvent molecules pass the membrane faster. The system allows every dialysis period which can be arranged with the diffusion time of the solvent molecules through the membrane. Different permeants with similar diffusion rates could be dialyzed simultaneously.

To investigate temperature effects on various processes a thermocouple heating element could be integrated easily into the system and controlled against the dialysis time. This allows investigations on the influence of the temperature during the different steps of collagen fibrillogenesis.

In general, the system allows the measurement and control of various parameters like temperature, ionic strength, concentrations, and several other gaugable parameters. Therefore, the represented system can be also used for the synthesis of other biomolecules, where a dialysis enhanced self-assembly process with a stable and controllable permeation of molecules through a membrane is necessary.

Acknowledgment

The authors would like to thank M. Lackinger for fruitful discussions and M. Bauer for technical support. This work was supported by a Deutsche Forschungsgemeinschaft (DFG) SFB 486 grant.

References

- [1] Kadler, K. E., Holmes, D. F., Trotter, J. A., and Chapman, J. A., 1996, "Collagen Fibril Formation," *Biochem. J.*, 316, pp. 1–11.
- [2] Gross, J., Hightberger, J. H., and Schmitt, F. O., 1951, "A New Fibrous Structure Obtained from Extracts of Collagenous Connective Tissue," *J. Appl. Phys.*, 22(1), pp. 112–112.
- [3] Gross, J., Hightberger, J. H., and Schmitt, F. O., 1952, "Some Factors Involved in the Fibrogenesis of Collagen In Vitro," in *Proceedings of the Society for Experimental Biology and Medicine*, Vol. 80(3), pp. 462–465.
- [4] Gross, J., Hightberger, J. H., and Schmitt, F. O., 1954, "Collagen Structures Considered as States of Aggregation of a Kinetic Unit—the Tropocollagen Particle," in *Proceedings of the National Academy of Sciences of the United States of America*, Vol. 40(8), pp. 679–688.
- [5] Gross, J., 1956, "The Behaviour of Collagen Units as a Model in Morphogenesis," *J. Biophys. Biochem. Cytol.*, 25(24, Suppl.), pp. 261–274.
- [6] Gross, J., and Kirk, D., 1958, "Heat Precipitation of Collagen from Neutral Salt Solutions—Some Rate-Regulating Factors," *J. Biol. Chem.*, 233(2), pp. 355–360.
- [7] Wood, G. C., and Keech, M. K., 1960, "Formation of Fibrils from Collagen Solutions. I. Effect of Experimental Conditions—Kinetic and Electron-Microscope Studies," *Biochem. J.*, 75, pp. 588–598.
- [8] Wood, G. C., 1960, "Formation of Fibrils from Collagen Solutions. 2. Mechanism of Collagen-Fibril Formation," *Biochem. J.*, 75, pp. 598–605.
- [9] Bard, J. B., and Chapman, J. A., 1968, "Polymorphism in Collagen Fibrils Precipitated at Low pH," *Nature (London)*, 219(160), pp. 1279–1280.
- [10] Bard, J. B. L., and Chapman, J. A., 1973, "Diameters of Collagen Fibrils Grown In Vitro," *Nature (London)*, 246(151), pp. 83–84.
- [11] Orekhovich, V. N., Tustanovskii, A. A., Orekhovich, K. D., and Plotnikova, N. E., 1948, "O Prokollagene Kozhi," *Biochemistry (Moscow)*, 13(1), pp. 55–60.
- [12] Hightberger, J. H., Gross, J., and Schmitt, F. O., 1951, "The Interaction of Microprotein with Soluble Collagen—An Electron Microscope Study," *Proc. Natl. Acad. Sci. U.S.A.*, 37(5), pp. 286–291.
- [13] Binnig, G., Quate, C. F., and Gerber, C., 1986, "Atomic Force Microscope," *Phys. Rev. Lett.*, 56(9), pp. 930–933.
- [14] Shattuck, M. B., Gustafsson, M. G. L., Fisher, K. A., Yanagimoto, K. C., Veis, A., Bhatnagar, R. S., and Clarke, J., 1994, "Monomeric Collagen Imaged by Cryogenic Force Microscopy," *J. Microsc.*, 174, pp. Rp1–Rp2.
- [15] Fujita, Y., Kobayashi, K., and Hoshino, T., 1997, "Atomic Force Microscopy of Collagen Molecules. Surface Morphology of Segment-Long-Spacing (SLS) Crystallites of Collagen," *J. Electron Microsc.*, 46(4), pp. 321–326.
- [16] Paige, M. F., Rainey, J. K., and Goh, M. C., 1998, "Fibrous Long Spacing Collagen Ultrastructure Elucidated by Atomic Force Microscopy," *Biophys. J.*, 74(6), pp. 3211–3216.
- [17] Morris, V. J., Kirby, A. R., and Gunning, A. P., 1999, *Atomic Force Microscopy for Biologists*, Imperial College Press, London.
- [18] Rainey, J. K., Wen, C. K., and Goh, M. C., 2002, "Hierarchical Assembly and the Onset of Banding in Fibrous Long Spacing Collagen Revealed by Atomic Force Microscopy," *Matrix Biol.*, 21(8), pp. 647–660.
- [19] Gutsman, T., Fantner, G. E., Venturini, M., Ikani-Nkodo, A., Thompson, J. B., Kindt, J. H., Morse, D. E., Fygeson, D. K., and Hansma, P. K., 2003, "Evidence that Collagen Fibrils in Tendons are Inhomogeneously Structured in a Tubelike Manner," *Biophys. J.*, 84(4), pp. 2593–2598.
- [20] Franzblau, C., Schmid, K., Paris, B., Beldekas, J., Garvin, P., Kagan, H. M., and Bamm, B. J., 1976, "Interaction of Collagen with Alpha-1-Acid Glycoprotein," *Biochim. Biophys. Acta*, 427(1), pp. 302–314.
- [21] Newman, S., Cloitre, M., Allain, C., Forgacs, G., and Beysens, D., 1997, "Viscosity and Elasticity During Collagen Assembly In Vitro: Relevance to Matrix-Driven Translocation," *Biopolymers*, 41(3), pp. 337–347.
- [22] Pappenheimer, J. R., Renkin, E. M., and Borrero, L. M., 1951, "Filtration, Diffusion and Molecular Sieving through Peripheral Capillary Membranes a Contribution to the Pore Theory of Capillary Permeability," *Am. J. Physiol.*, 167(1), pp. 13–46.
- [23] Pappenheimer, J. R., 1953, "Passage of Molecules Through Capillary Walls," *Physiol. Rev.*, 33(3), pp. 387–423.
- [24] Renkin, E. M., 1954, "Filtration, Diffusion, and Molecular Sieving through Porous Cellulose Membranes," *J. Gen. Physiol.*, 38(2), pp. 225–243.
- [25] Feins, M., and Sirkar, K. K., 2004, "Highly Selective Membranes in Protein Ultrafiltration," *Biotechnol. Bioeng.*, 86(6), pp. 603–611.
- [26] Kiesslich, J., Radacher, M., Neuhuber, F., Meyer, H. J., and Zeller, K. W., 2002, "On the Use of Nitrocellulose Membranes for Dialysis-Mediated Purification of Ancient DNA from Human Bone and Teeth Extracts," *Ancient Biomolecules*, 4(2), pp. 79–87.
- [27] Ruckenstein, E., and Zeng, X. F., 1997, "Macroporous Chitin Affinity Membranes for Lysozyme Separation," *Biotechnol. Bioeng.*, 56(6), pp. 610–617.
- [28] Atamanenko, I., Kryvoruchko, A., and Yurlova, L., 2004, "Study of the Scaling Process on Membranes," *Desalination*, 167(1–3), pp. 327–334.
- [29] Bosch, R., Lautenschlager, P., Potthast, L., and Stapelmann, J., 1992, "Experiment Equipment for Protein Crystallization in Mu-G Facilities," *J. Cryst. Growth*, 122(1–4), pp. 310–316.
- [30] Vergara, A., Corvino, E., Sorrentino, G., Piccolo, C., Tortora, A., Carotenuto, L., Mazzarella, L., and Zagari, A., 2002, "Crystallization of the Collagen-Like Polypeptide (PPG)(10) Aboard the International Space Station. I. Video Observation," *Acta Crystallogr., Sect. D: Biol. Crystallogr.*, 58, pp. 1690–1694.
- [31] Berisio, R., Vitagliano, L., Sorrentino, G., Carotenuto, L., Piccolo, C., Mazzarella, L., and Zagari, A., 2000, "Effects of Microgravity on the Crystal Quality of a Collagen-Like Polypeptide," *Acta Crystallogr., Sect. D: Biol. Crystallogr.*, 56, pp. 55–61.
- [32] Graham, J. S., Vomund, A. N., Phillips, C. L., and Grandbois, M., 2004, "Structural Changes in Human Type I Collagen Fibrils Investigated by Force Spectroscopy," *Exp. Cell Res.*, 299(2), pp. 335–342.

5.2 Structural Investigations on Native Collagen Type I Fibrils

Stefan Strasser, Albert Zink, Marek Janko, Wolfgang M. Heckl, Stefan Thalhammer

Biochemical and Biophysical Research Communications (2007), 354(1), 27-32

Available online at www.sciencedirect.com

ScienceDirect

Biochemical and Biophysical Research Communications 354 (2007) 27–32

BBRC

www.elsevier.com/locate/ybbrc

Structural investigations on native collagen type I fibrils using AFM

Stefan Strasser ^{a,c}, Albert Zink ^{a,c}, Marek Janko ^{a,c},
Wolfgang M. Heckl ^{a,b}, Stefan Thalhammer ^{c,*}

^a Department of Geo- and Environmental Sciences, Ludwig-Maximilians-Universität, 80333 Munich, Germany

^b Deutsches Museum, Museumsinsel 1, 80538 Munich, Germany

^c GSF-National Research Center for Environment and Health, Institute of Radiation Protection, AG Nanoanalytics, 85764 Neuherberg, Germany

Received 4 December 2006

Available online 22 December 2006

Abstract

This study was carried out to determine the elastic properties of single collagen type I fibrils with the use of atomic force microscopy (AFM). Native collagen fibrils were formed by self-assembly in vitro characterized with the AFM. To confirm the inner assembly of the collagen fibrils, the AFM was used as a microdissection tool. Native collagen type I fibrils were dissected and the inner core uncovered. To determine the elastic properties of collagen fibrils the tip of the AFM was used as a nanoindenter by recording force–displacement curves. Measurements were done on the outer shell and in the core of the fibril. The structural investigations revealed the banding of the shell also in the core of native collagen fibrils. Nanoindentation experiments showed the same Young's modulus on the shell as well as in the core of the investigated native collagen fibrils. In addition, the measurements indicate a higher adhesion in the core of the collagen fibrils compared to the shell.

© 2006 Elsevier Inc. All rights reserved.

Keywords: AFM; Microdissection; Force spectroscopy; Collagen

Collagen molecules consist of three polypeptide chains (α -chains), which form a unique triple-helical structure. More than 20 genetically distinct collagens exist in mammalian tissue, where collagen types I, II, III, V, and XI self-assemble into D-periodic cross-striated fibrils. Collagen molecules, forming the fibril, consist of an uninterrupted right handed triple helix called tropocollagen [1], approximately 300 nm in length and 1.5 nm in diameter. The collagen self-assembles in cross-striated fibrils that normally occur in the extracellular matrix of connective tissues. These fibrils are stabilized by covalent cross linking of specific lysines and hydroxyllysines of the collagen molecules which are ordered parallel in a D-periodic pattern [2]. The stagger of molecules gives rise to a characteristic band pattern of light and dark regions when negatively stained and viewed using an electron microscope [3].

An improvement in the field of imaging molecular structures was accomplished by the invention of the Atomic Force Microscope (AFM) by Binnig et al. [4]. AFM investigations carried out by Paige et al. [5] show native fibrils and fibrous long spacing fibrils (FLS-fibrils) [6]. Cocoon-like fibrils, which are in the range of hundreds of nanometers in diameter and 10–20 nm in length, were found to coexist with mature FLS fibrils. On the basis of detailed AFM studies a stepwise process in the formation of FLS collagen was proposed. Gutschmann et al. [7] observed that collagen fibrils from tendons behave mechanically like tubes. They concluded that the collagen fibril is an inhomogeneous structure. Moreover, it was observed that high strain lead to molecular gliding within the fibrils and ultimately to a disruption of the fibril structure [8]. Automated electron tomography studies, performed on corneal collagen fibrils showed that collagen molecules are organized into microfibrils (≈ 4 nm diameter) in a 36 nm diameter collagen fibril, which are tilted at $\approx 15^\circ$ to the fibril long axis

* Corresponding author. Fax: +49 89 3187 2942.

E-mail address: stefan.thalhammer@gsf.de (S. Thalhammer).

in a right handed helix. Analysis of the lateral structure demonstrated that the microfibrils exhibit regions of order and disorder within the 67-nm axial repeat of the collagen fibrils [9].

AFM nanodissection of big FLS-fibrils with a width of about 1.7 μm and a banding pattern of 270 nm showed the FLS banding also in the core of the fibril [10]. For FLS-fibrils a different assembly pathway and structure are postulated. The characteristic banding mainly arises from the attachment of $\alpha 1$ -acid glycoprotein in FLS-fibrils [11]. The characteristic banding of native fibrils is determined by the repetition of overlap and gap zones [12].

Several investigations using the AFM as a tool for measuring the tensile modulus of collagen fibrils and subunits revealed details in the protein assembly. Graham et al. calculated force elongation/relaxation profiles of single collagen fibrils using the AFM. The elongation profiles showed, that in vitro assembled human type I collagen fibrils are characterized by a large extensibility. It was shown that the fibrils are robust structures with a significant conservation of its elastic properties [13]. Gutschmann et al. probed the crosslinks on a lower level of organisation using an AFM cantilever to pull substructures out of the assembly. Two different rupture events were determined; the first with a strong bond and a periodicity of 78 nm (bonds between subunits) and a second weaker one with a periodicity of 22 nm (between molecules) [14]. Bozec and Horton [15] studied trimeric type I tropocollagen molecules by AFM, both topologically and by force spectroscopy, showing multiple stretching peaks on the molecular level similarly as shown by Gutschmann et al. [14]. Fratzl et al. and Puxkandl et al. [8,16] investigated the fibrillar structure, viscoelastic and mechanical properties of collagen by recording stress-strain curves. The stress-strain curves can be divided into several regions [28]. At first crimps [17] and kinks [18], are removed, before a linear region is seen where the collagen triple helices are stretched, along with increase of the gap zones compared with the overlap zones. Slippage is first seen within fibrils at crosslink deficient collagen [16], and then higher strains lead to a disruption of the fibril.

Here we used the AFM as a microdissection tool and a tool for probing local elasticity. The mechanical behaviour of native single fibrils was tested by recording force-distance curves on the shell and in the core of the fibrils to gain insights into the collagen assembly and mechanical properties.

Materials and methods

Preparation of the collagen fibrils. The collagen solution was prepared from calfskin (Sigma). Approximately 1 mg of the compound was dissolved in 1 ml of 0.5% acetic acid over night at 4 °C. The solution was sonicated for 1 h at 0 °C to dissolve any collagen aggregates. Finally, the mixture was centrifuged at 4000 rpm for 90 min at 4 °C and the supernatant was filtered through a 0.2 μm filter unit (Sigma), (modified protocol according Paige et al. [5]). The final dialysis mixture is composed of 0.5 mg/ml collagen, and 0.2 mg/ml $\alpha 1$ -acid glycoprotein.

For the preparation a dialysis tubing (Serva, visking 8/32) with a molecular weight cut off (MWCO) of 12–14 kDa and a tube diameter of 6 mm was used. The received solution was diluted 10-fold after dialysis and dried in 10 μl aliquots on freshly cleaved mica. A detailed procedure for the dialysis procedure can be found in reference [19].

AFM microscopy. For morphological characterization a Topometrix Explorer (AtoS, Germany) was used. It was operated in non-contact mode under ambient conditions, with 35% relative humidity, using NSC12 B (non-contact silicon cantilever) cantilevers (Mikromasch, Estonia). The spring constant of the non-contact probe (NSC) was 14 N/m. The resonant frequency of the NSC cantilever was 315 kHz. The nominal tip radius was specified <10.0 nm. Image analysis was performed using SPIP software (Image Metrology, Lyngby, Denmark).

AFM microdissection. To reveal the core of the collagen fibril, the AFM (Bioprobe, Park Scientific, USA) was used as a microdissection tool. For this the feedback of the z-piezo was switched off and the cantilever approached to the sample surface until the tip touched the sample. In order to apply the correct force to cut the fibril approximately in the upper half of the fibril diameter several pre-test were done using cantilevers with a spring constant of 56 N/m.

Force spectroscopy and data analysis. Elasticity measurements were carried out by recording force-distance curves using a NanoWizard AFM (JPK Instruments, Germany). Imaging and force spectroscopy were done in contact mode using CSC 37 A (nominal spring constant $k_c = 0.65$ N/m, nominal resonant frequency $f_R = 41$ kHz). The elasticity was measured both inside the fibril and on the outer shell at the same thickness of the sample. To evaluate the Young's moduli and the adhesion forces the force-displacement curves were processed using the software Microcal Origin and Microsoft Excel. To calculate the Young's moduli a suitable model has to be fitted to the contact region (above the zero line) of the force-distance curves. For the determination of the adhesion forces the height of the snap out of the retrace curve was calculated using the force spectroscopy data.

The indentation of an AFM tip into soft or hard samples can be modelled using the Hertzian contact mechanics [20]. The indentation of an infinitely hard body into a hard elastic half space (small indentations with the parabolic part of the tip) with a normal force F leads with this theory to [21–23]:

$$F_{\text{paraboloid}} = \frac{4}{3} \cdot \frac{E}{(1-\nu^2)} \cdot \delta^{3/2} \cdot \sqrt{R}, \quad (1)$$

where δ is the indentation depth, E is the Young's modulus, ν is the Poisson ratio and R is the tip radius. For incompressible materials the Poisson ratio is at 0.5. The applied force can be calculated with the deflection of the cantilever, which is considered as a tightened spring by Hook's Law:

$$F = k_c \cdot d, \quad (2)$$

where k_c is the spring constant and d is the deflection of the cantilever.

The deflection of the cantilever depends on the indentation of the tip into the elastic half space or rather the sample. The z-piezo extends and the distance of the extension z is split into the deflection and the indentation depth (δ) by

$$z = d + \delta \quad (3)$$

With these Eqs. (1)–(3) the Young's modulus can be expressed for hard samples as

$$E_{\text{paraboloid}} = \frac{3 \cdot k_c \cdot (d - d_0) \cdot (1 - \nu^2)}{4 \cdot \sqrt{R} \cdot [(z - z_0) - (d - d_0)]^{3/2}}, \quad (4)$$

where d_0 and z_0 are the corresponding values of the cantilever deflection and the z-piezo extension at the contact point. For soft samples in the contact regime Eq. (4) can be written as

$$z = \left[\frac{3 \cdot k_c \cdot (d - d_0) \cdot (1 - \nu^2)}{4 \cdot E \cdot \sqrt{R}} \right]^{2/3} + (d - d_0) + z_0. \quad (5)$$

To calculate the Young's modulus, the model (Eq. (5)) was fitted to every recorded force–distance curve. The spring constant ($k_c = 0.7 \text{ N/m}$) was determined by the Sader method [24,25], and the radius of curvature ($R \approx 20 \text{ nm}$), defining the tip shape, was determined by SEM microscopy.

Results and discussion

AFM imaging and microdissection

For AFM microscopy the samples can be investigated immediately after self-assembly and drying on freshly cleaved mica. The described collagen preparation technique [19] allows the reproducible production of single collagen fibrils with different banding patterns (Fig. 1).

Thereby we were also able to detect collagen fibrils with kinks. Gutschmann et al. [7] suggested that this mechanical behaviour corresponds to a strong deformation of a tube. The combination of probing sample properties by doing force spectroscopy as well as the manipulation of the specimen with a high-resolution imaging tool is very useful in material characterization applications. The AFM as a nanoindenter proved its applicability for elasticity measurement and material classification in different applications [26,27]. We used the AFM to probe the sample properties of the centre and the surface of the fibril to compare the morphological investigations with directly measured mechanical values. The AFM based microdissection was applied to reveal the inner structure of the specimen. During manipulation the shell and upper parts of the fibril were scratched away, to image the remaining core in a high-resolution mode (Fig. 2). The dissection was carried out in a defined angle to the fibril axis in order to exclude artefacts originated by an orthogonal or parallel (to the fibril axis) scratching procedure. It could be shown

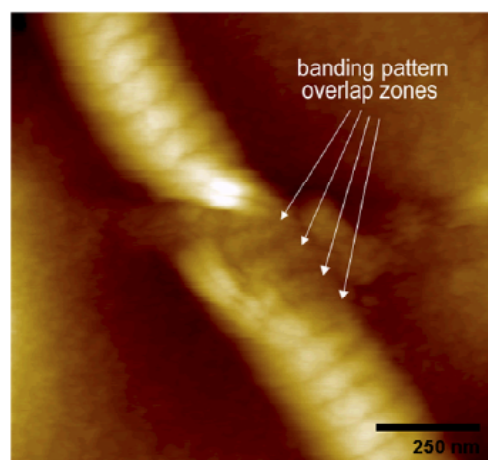


Fig. 2. High resolution AFM image of a microdissected collagen fibril. The core of the collagen fibril is revealed and the banding pattern can be recognized inside the fibril. The arrows indicates the overlap zones of the collagen molecules that arise during the self-assembly process of the collagen fibril (topography signal, scalebar 250 nm).

that there are no major geometrical differences of the banding on the shell and in the core of native single collagen fibrils. The banding pattern inside the fibril fits to that on the shell in width and distance. The fibril has a banding pattern of 78 nm, a height of 30 nm, and a width of 270 nm. The cutted area, shown in Fig. 2, is located in the core of the fibril, which was confirmed by line measurements (Fig. 3). Between the measured distance A and B the banding can be recognized on the shell as well as in the core. Among points C and D the height difference between

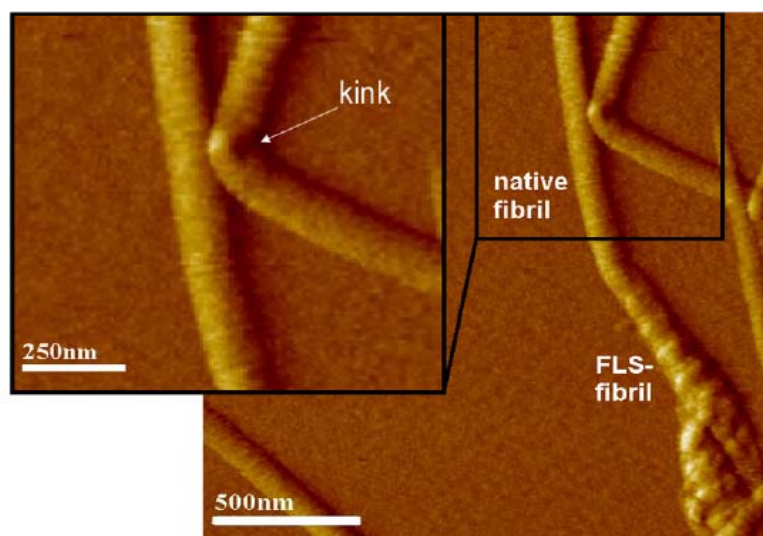


Fig. 1. High resolution AFM image of a single collagen fibril with kink. Due to kinks collagen are sometimes compared to tubes. The other fibril displays the polymorphism of collagen with native and FLS-parts in one fibril (error signal, scalebar 500 nm).

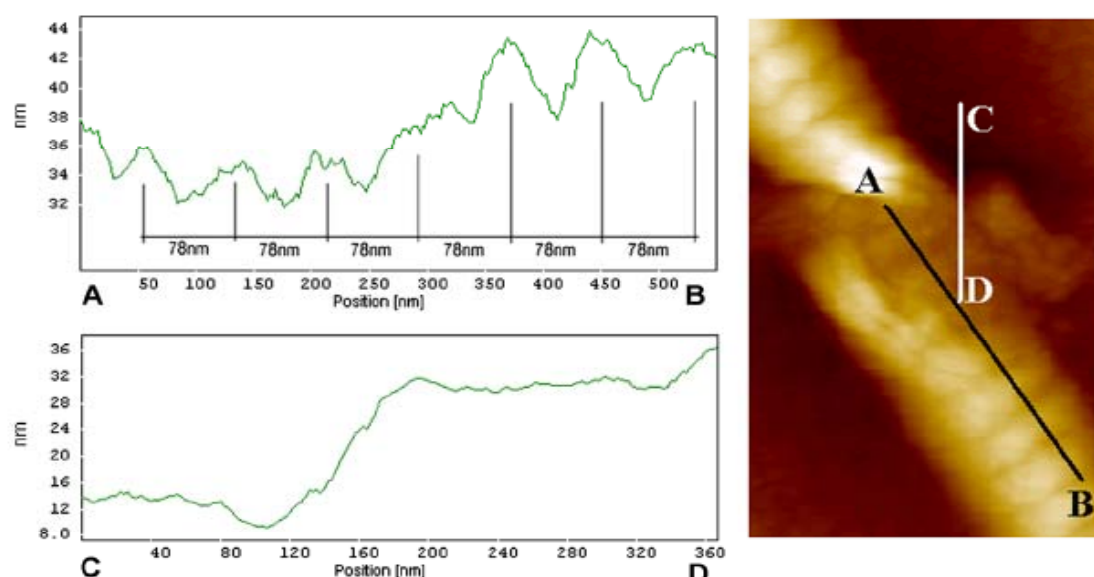


Fig. 3. Line measurements on the microdissected collagen fibril (Fig. 2). Between point A and B the banding can be recognized on the shell as well as in the core. The banding pattern can be determined to be approximately 78 nm. Between point C and D the height difference of around 16 nm between the substrate and the level of the cut area can be seen.

the substrate and the level of the cut area can be seen. The height difference between the substrate and cut area was determined to be 16 nm. These results are in concordance with Wen and Goh [10] who also showed a similar morphological structure of core and shell in FLS-fibrils, with a different assembly pathway and structure compared to native single collagen fibrils [11]. In a recently published work they further confirmed the differences of FLS fibrils to native collagen fibrils on the base of the superhelical structure and hierarchical organisation of disrupted fibrils [28]. Based on the model, that aligned tropocollagen molecules build the mature fibril by crosslinking with neighbour molecules in native collagen fibrils [14], it has to be taken into consideration that during microdissection complete layers are removed (Fig. 2). However, the scratching process can lead to a rupture of molecules and destruction of cross-linking. Different elastic properties of core and shell could be generated during the manipulation process. This is a major problem when probing inhomogeneous biological samples in the molecular range and influences during manipulation could not be completely excluded.

Force spectroscopy

For core and shell, respectively, more than 100 force–distance curves were recorded. The displayed data are representative for several experiments. The indentation depth on both areas was limited with a set-point-force for every force–distance curve. The maximal force of about 6 nN, corresponding to a cantilever bending of 8.5 nm, led to an indentation depth of about 0.5 nm both on the shell

and core of the fibril. Exemplary force–distance curves recorded on the shell and the core are displayed in Fig. 4A. The dark curve shows a spectroscopy curve on the shell, whereas the grey dashed curve was recorded in the core. The indentation experiments were repeatedly performed on several collagen fibrils. The slope of both curves recorded on the shell and the core showed no major differences indicating a comparable elasticity. The evaluation of the spectroscopy data was done at the positive cantilever deflection range above the zero line. The histogram in Fig. 4B displays the Young's moduli of the force–distance curves. The Young's moduli were calculated applying a fit of the Hertzian model to the contact range of the individual force–distance curves. The average values indicate no significant difference in elasticity between core and shell. The indentation experiments, performed on the shell and the core of dissected collagen fibrils could not verify different Young's moduli of core and shell. This is also well in line with our morphological results in Fig. 2 which shows a homogeneous assembly of the fibril. The average values were calculated to approximately 1.2 GPa. The maximum of the distribution lies at 1 GPa. The results of indentation experiments of thin samples can also be influenced by the underlying hard substrates. Samples can be compressed under the tip and the measured Young's modulus is maybe upper estimated, shown by Domke et al. [23]. In order to avoid this effect, the force curves were recorded on areas with the same sample height. It is also likely possible that the sample preparation especially the α 1-acid glycoprotein concentration influences the mechanical properties of the collagen fibrils. It was proposed that proteoglycans have

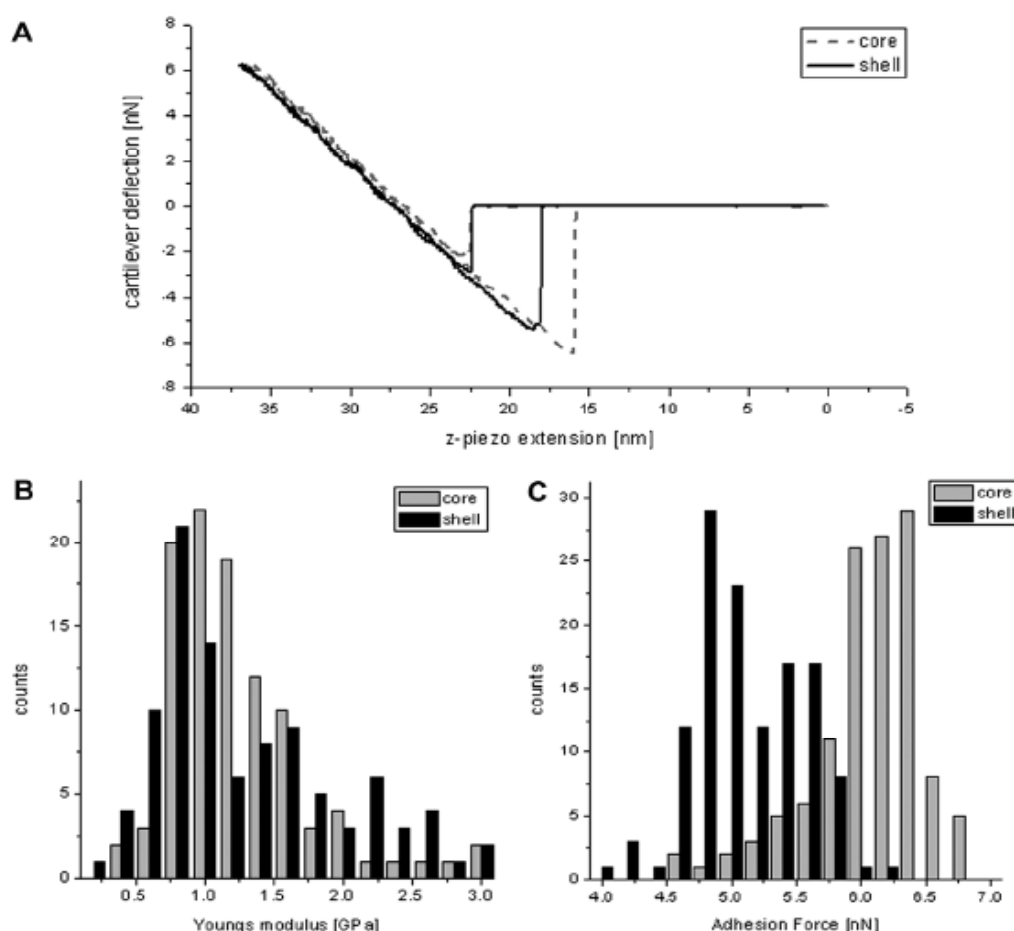


Fig. 4. (A) Typical sample of a force–distance curves recorded on the shell and the core of a single collagen fibril. The dark curve shows a spectroscopy curve on the shell, whereas the grey dashed curve was recorded in the core. The slope of both curves is nearly the same and indicates identical elasticity. Measurements on the shell and in the core have to be performed in the same sample height to exclude “thin layer effects”. The Hertzian model was fitted to the positive cantilever deflection range. (B) Elasticity measurement of a single collagen fibril. Force distance curves were recorded on the shell and the exposed core. On both measuring points more than 100 curves were recorded. The diagram displays the Young’s moduli of the force distance curves versus the frequency. The nanoindentation experiment indicates no measurable difference between core and shell. (C) Adhesion measurement on a single collagen fibril. The data display the evaluation of the adhesion forces calculated from the height of the snap out of the retrace curve, see also the figure. The values show a higher adhesion in the core of the microdissected fibril.

an important influence on mechanical properties of the fibrils [7]. This could explain the difference between the measured and the literature value of 1 GPa [29]. Since the same cantilever was used for both sets of force curves, the comparison between core and shell is still valid.

The evaluation of the adhesion forces of the spectroscopy data indicates a higher adhesion in the core of the fibril. This can be already seen in Fig. 4A where typical spectroscopy data for core and shell are displayed. In Fig. 4C the height of the snap out effect calculated from the retrace curves is shown. The average value was calculated for the shell to 5 nN and for the core to 6 nN which points to a higher adhesion in the core of the fibril. Gutschmann et al. [7] suggested the presence of more highly crosslinked colla-

gen molecules near the fibril surface compared to the central region. This could lead to a higher amount of binding capacity for the tip and cause higher adhesion forces during the measurement. However, the results could have been also influenced by the scratching process which could have led to a rupture of molecules and destruction of crosslinks. The destroyed crosslinks and ruptured molecules could stick to the tip and increase the measured adhesion force. Moreover, the collagen fibrils were investigated in a dried state of preservation, which could have also an influence on the mechanical properties.

The mechanical properties of this collagen rich tissues, e.g., tendons, are largely determined by the collagen structure [8]. An inhomogeneous assembly of collagen fibrils

was published by several authors; Sarkar et al. [30] proposed that fluid domains in the collagen allow molecules to slip relative to one another, which was shown by Mosler et al. [31], in order to relieve applied stress. It has been proposed that, in case of high forces, the stiff outer shell of the collagen fibrils could break while the fluid core remains intact and might be used in the repair of the shell [7]. Our morphological results as well as the statistical evaluation of the Young's modulus using the indentation measurements could not confirm a "fluid" core or different structures of core and shell. Solely the adhesion measurements show differences between core and shell.

Acknowledgments

We thank Prof. Dr. Achim Wixforth, Dr. Matthias Schneider, and Daniel Steppich for their help and opportunity to perform the force spectroscopy measurements at the Lehrstuhl für Experimentalphysik II of the University of Augsburg.

References

- [1] G.N. Ramachandra, G. Karthan, Structure of collagen, *Nature* 176 (1955) 593–595.
- [2] K.E. Kadler, D.F. Holmes, J.A. Trotter, J.A. Chapman, Collagen fibril formation, *Biochem. J.* 316 (1996) 1–11.
- [3] B.R. Williams, R.A. Gelman, D.C. Poppke, K.A. Piez, Collagen fibril formation, *J. Biol. Chem.* 253 (1978) 6578–6585.
- [4] G. Binnig, C.F. Quate, C. Gerber, Atomic force microscope, *Phys. Rev. Lett.* 56 (1986) 930–933.
- [5] M.F. Paige, J.K. Rainey, M.C. Goh, Fibrous long spacing collagen ultrastructure elucidated by atomic force microscopy, *Biophys. J.* 74 (1998) 3211–3216.
- [6] V.J. Morris, A.R. Kirby, A.P. Gunning, *Atomic Force Microscopy for Biologists*, Imperial College Press, London, 1999. ISBN:1860941990.
- [7] T. Gutsmann, G.E. Fantner, M. Venturoni, A. Ekani-Nkodo, J.B. Thompson, J.H. Kindt, D.E. Morse, D.K. Fygenson, P.K. Hansma, Evidence that collagen fibrils in tendons are inhomogeneously structured in a tubelike manner, *Biophys. J.* 84 (2003) 2593–2598.
- [8] P. Fratzl, K. Misof, I. Zizak, G. Rapp, H. Amenitsch, S. Bernstorff, Fibrillar structure and mechanical properties of collagen, *J. Struct. Biol.* 122 (1998) 119–122.
- [9] D.F. Holmes, C.J. Gilpin, C. Baldock, U. Ziese, A.J. Koster, K.E. Kadler, Corneal collagen fibril structure in three dimensions: Structural insights into fibril assembly, mechanical properties, and tissue organization, *Proc. Natl. Acad. Sci. USA* 98 (2001) 7307–7312.
- [10] C.K. Wen, M.C. Goh, AFM nanodissection reveals internal structural details of single collagen fibrils, *Nano. Lett.* 4 (2004) 129–132.
- [11] J.K. Rainey, C.K. Wen, M.C. Goh, Hierarchical assembly and the onset of banding in fibrous long spacing collagen revealed by atomic force microscopy, *Matrix Biol.* 21 (2002) 647–660.
- [12] J.A. Petruska, A.J. Hodge, Subunit model for tropocollagen macromolecule, *Proc. Natl. Acad. Sci. USA* 51 (1964) 871–876.
- [13] J.S. Graham, A.N. Vomund, C.L. Phillips, M. Grandbois, Structural changes in human type I collagen fibrils investigated by force spectroscopy, *Exp. Cell Res.* 299 (2004) 335–342.
- [14] T. Gutsmann, G.E. Fantner, J.H. Kindt, M. Venturoni, S. Danielsen, P.K. Hansma, Force spectroscopy of collagen fibers to investigate their mechanical properties and structural organization, *Biophys. J.* 86 (2004) 3186–3193.
- [15] L. Bozec, M. Horton, Topography and mechanical properties of single molecules of type I collagen using atomic force microscopy, *Biophys. J.* 88 (2005) 4223–4231.
- [16] R. Puxkandl, I. Zizak, O. Paris, J. Kockes, W. Tesch, S. Bernstorff, P. Purslow, P. Fratzl, Viscoelastic properties of collagen: synchrotron radiation investigations and structural model, *Philos. Trans. R. Soc. Lond. B Biol. Sci.* 357 (2002) 191–197.
- [17] J. Diamant, R.G.C. Arridge, E. Baer, M. Litt, A. Keller, Collagen—ultrastructure and its relation to mechanical properties as a function of aging, *Philos. Trans. R. Soc. Lond. B Biol. Sci.* 180 (1972) 293–315.
- [18] P. Fratzl, N. Fratzl-Zelman, K. Klaushofer, Collagen packing and mineralization—an X-ray-scattering investigation of turkey leg tendon, *Biophys. J.* 64 (1993) 260–266.
- [19] S. Strasser, A. Zink, W.M. Heckl, S. Thalhammer, Controlled self-assembly of collagen fibrils by an automated dialysis system, *J. Biomech. Eng.* (2006).
- [20] H. Hertz, Über die Berührung fester elastischer Körper, *J. Reine angewandte Mathematik* 92 (1882) 156–171.
- [21] I.N. Sneddon, The relation between load and penetration in the axisymmetric Boussinesq problem for a punch of arbitrary profile, *Int. J. Eng. Sci.* 3 (1965) 47–57.
- [22] K.L. Johnson, *Contact Mechanics*, Cambridge University Press, Cambridge, 1994. ISBN-13: 9780521347969.
- [23] J. Domke, M. Radmacher, Measuring the elastic properties of thin polymer films with the atomic force microscope, *Langmuir* 14 (1998) 3320–3325.
- [24] J.E. Sader, J.W.M. Chon, P. Mulvaney, Calibration of rectangular atomic force microscope cantilevers, *Rev. Sci. Instrum.* 70 (1999) 3967–3969.
- [25] J.L. Hutter, J. Bechhoefer, Calibration of atomic-force microscope tips, *Rev. Sci. Instrum.* 64 (1993) 1868–1873.
- [26] J.B. Thompson, J.H. Kindt, B. Drake, H.G. Hansma, D.E. Morse, P.K. Hansma, Bone indentation recovery time correlates with bond reforming time, *Nature* 414 (2001) 773–776.
- [27] S. Strasser, A. Zink, G. Kada, P. Hinterdorfer, O. Peschel, W.M. Heckl, A.G. Nerlich, S. Thalhammer, Age determination of blood spots in forensic medicine by force spectroscopy, *Forensic Sci. Int.* (2006), doi:10.1016/j.forsciint.2006.1008.1023.
- [28] C.K. Wen, M.C. Goh, Fibrous long spacing type collagen fibrils have a hierarchical internal structure, proteins: structure, *Funct. Bioinform.* 64 (2006) 227–233.
- [29] Y.C. Fung, *Biomechanics—mechanical properties of living tissue*, second ed., Springer, New York 1993. ISBN: 0387979476.
- [30] S.K. Sarkar, Y. Hiyama, C.H. Niu, P.E. Young, J.T. Gerig, D.A. Torchia, Molecular-dynamics of collagen side-chains in hard and soft-tissues—a multinuclear magnetic-resonance study, *Biochemistry-U S* 26 (1987) 6793–6800.
- [31] E. Mosler, W. Polkhard, E. Knorzer, H. Nemetschekgansler, T. Nemetschek, M.H.J. Koch, Stress-induced molecular rearrangement in tendon collagen, *J. Mol. Biol.* 182 (1985) 589–596.

5.3 Implant Surface Coatings with Bone Sialoprotein, Collagen and Fibronectin and their Effects on Cells derived from Human Maxillar Bone

H. Hilbig, M. Kirsten, R. Rupietta, H. L. Graf, S. Thalhammer, S. Strasser, F. P. Armbruster

European Journal of Medical Research (2007), 12, 6-12

IMPLANT SURFACE COATINGS WITH BONE SIALOPROTEIN, COLLAGEN, AND FIBRONECTIN AND THEIR EFFECTS ON CELLS DERIVED FROM HUMAN MAXILLAR BONE

H. Hilbig¹, M. Kirsten², R. Ruppert¹, H.-L. Graf², S. Thalhammer³, S. Strasser³, F. P. Armbruster⁴

¹Institute of Anatomy, Leipzig University, Germany,

²Department of Oral-, Maxillo-, Facial- and Reconstructive Plastic Surgery, University Hospital, Leipzig, Germany

³Center for NanoScience, GeoBioCenter, Department of GeoSciences, München, Germany

⁴Immundiagnostik AG, Bensheim, Germany

Abstract

The interaction between implant material and surrounding tissues is believed to play a fundamental role in implant success. Although bone sialoprotein (BSP) has been found to be osteoinductive when coated onto femoral implants, collagen and fibronectin are the most used compounds for preparation of pre-coated cell culture slides at present.

In this study, the support of BSP-, collagen- and fibronectin-coated and non-coated implant material for the development of adult human maxillar bone *in vitro* was studied and compared. The expression of bone turnover markers like BSP and osteocalcin as well as osteonectin, transforming growth factor beta (TGF-beta) and CD90 during different time periods of cell cultivation (3, 5, 10, 15, 20 and 25 days) was visualized immunohistochemically. The distribution patterns of the cells were examined on a rough surface of the titanium-hydroxyapatite dental implant material TIGER and on a total smooth surface of the technical implant material glimmer.

Significantly different values were found for glimmer at the 15. and the 20. Div, exclusively, indicating that a smooth surface was more improved than a rough ceramic surface by pre-coatings. The White-test using rankings of the median values gave evidence for BSP-coatings at position 1 followed by collagen.

Our experiments were designed to use very low concentrated BSP coating solution with the aim to reduce the healing time with a minimal effort and minimal risks for the patients.

Key words: Bone, implants, non-collagenous proteins

INTRODUCTION

Aseptic loosening of implants remains an unsolved orthopedic problem. The interaction between implant material and surrounding tissues is believed to play a crucial role in implant success or failure. Adaptive cellular responses to the implant material include alterations in the cytoskeleton, integrin expression and synthesis of extracellular matrix proteins. Beside osteocalcin and osteonectin, bone sialoprotein (BSP) is the major non-collagenous protein of the extracellular

bone matrix (Fisher 1985; Fisher and Termine 1985; Marks and Popoff 1988). BSP is a highly glycosylated and sulphated phosphoprotein with a molecular weight of 70-80 kDa (Ganss et al. 1999) that is found almost exclusively in mineralized connective tissues. Characteristically, polyglutamic acid and arginine-glycine-aspartate (RGD) motifs with the ability to bind hydroxyapatite and cell-surface integrins, respectively, have been conserved in the protein sequence of different species. BSP expression coincides with initial bone mineralization and it serves as a center of crystallization for hydroxyapatite (Hunter and Goldberg 1993; 1994; Hoshi and Ozawa 2000). Furthermore, expression of the BSP gene, which is induced in newly formed osteoblasts, is up-regulated by hormones and cytokines that promote bone formation, e.g. transforming growth factor-beta (TGF-beta). In addition, the morphological induction and maintenance of hydroxyapatite nucleation during bone formation has been shown to correlate with TGF-beta expression.

Recently, O'Toole et al. (2004) demonstrated that BSP is osteoinductive when coated onto femoral implants. On the other hand, osteoblasts have been found to adhere on BSP-coated surfaces in the similar way as on collagen- and fibronectin-treated ones.

Therefore, the aim of the present study was to compare BSP-, collagen- and fibronectin-coated and non-coated implant material in enhancing the development of adult human maxillar bone at different time intervals: 3, 5, 10, 15, 20 and 25 days *in vitro* (Div). As the cascade of bone cell differentiation is initiated by the TGF-beta supergene family and develops as a mosaic structure, antibodies against TGF-beta, BSP, osteocalcin and osteonectin were used to characterize osteoblast-like cells. For immunohistochemical staining of fibroblasts and non-differentiated osteoblasts, the antibody against human CD90 was applied.

MATERIAL AND METHODS

TISSUE PREPARATION

All procedures used in the present study were approved by the Ethics Committee of the University of Leipzig. The rules of the Declaration of Helsinki 1964

(NIH publication no. 86-23, revised 1985) were followed. Human maxillar bone samples without any clinical or radiographic evidence of pathology were obtained from two male donors (40 and 45 years old) undergoing dental surgery at the Department of Oral-, Maxillo-, Facial- and Reconstructive Plastic Surgery, University Hospital of the University of Leipzig. In each case, the bone samples were placed in a sterile tube containing sterile 0.05 M phosphate buffered saline (PBS), pH 7.4, and penicilline/streptomycine, 10 000 IU/ml each (PromoCell, Germany). Thereafter, all samples were processed under sterile conditions. The maxillar bones were cut in 0.1-0.2 cm pieces. After several rinses in PBS, the material was incubated with 0.25% collagenase type IV (166 U/mg, Biochrom AG, Germany) for 3 hours at 37 °C, washed and cultured in Dubelcco's modified Eagle's medium (PromoCell, Germany) supplemented with 10% fetal bovine serum (PromoCell, Germany) in an atmosphere of 5% CO₂ – 95% air at 37 °C. The medium was changed twice weekly. Cells were subcultured from the initially isolated primary cells and seeded at a density of 4000 cells/well in six-well plates. In all experiments cells were used at first passage.

IMPLANTS

The dental implant material TIGER and the technical material glimmer were used in the experiments. TIGER (ZL-Microdent, Germany), based on a material developed by Graf (1997) and described by Schreckenbach et al. (1999), consists of titanium with hydroxyapatite ceramic and has a roughened surface to improve the attachment, spreading, and growth of the bone cells on the metal implant (Hulbert et al. 1970; Schwartz et al. 1999). In contrast, glimmer has a total smooth surface. The implant samples with a size of 10 x 30 x 1mm were coated with BSP, collagen and fibronectin as follows: 10µg of BSP (His-Myc-Ek-BSP, Immundiagnostik, Bensheim, Germany) were dissolved as described by Wuttke et al. (2001), and 10µg of fibronectin (Biochrom, Germany) in 1 ml of 0.9M sterile PBS, pH 7.2. Collagen (Cohesion, USA) was used as VITROGEN 1% (bovine dermal collagen dissolved in 0.012 N HCl). Then twenty-four implants were incubated for two hours in 300 µl of BSP, fibronectin or collagen solution. The treated implants were removed from the coating solutions and allowed to dry under sterile conditions for 12 hours at room temperature. Thereafter, the coated implants were placed in six-well cell culture plates, the cells were seeded and grown for different days (3, 5, 10, 15, 20 and 25) *in vitro*.

IMMUNOCYTOCHEMISTRY

Cells were fixed with 4% PBS buffered paraformaldehyde for 15 minutes and rinsed in PBS. For immunohistochemical characterization, cells on the surface of the implant discs were treated for two hours with a blocking agent, 10% normal goat serum (Vector, Burlingame, USA) or a mixture of 10% normal goat and 10% normal donkey serum in PBS, and incubated overnight at 4 °C with 1:100 diluted primary antibodies

against BSP (monoclonal mouse anti-human BSP, Immundiagnostik, Bensheim, Germany), osteocalcin (monoclonal, rabbit-anti-human, Acris, Hiddenhausen, Germany), osteonectin (monoclonal, mouse-anti-human, Acris), TGF-beta (monoclonal, rabbit-anti-human, Chemicon, Temecula, USA) and CD90 (monoclonal anti-human CD90, FITC-conjugated, DIANOVA, Hamburg, Germany) according to Saalbach et al. (1997). For simultaneous detection of BSP and CD90 or osteonectin and TGF-beta, implants were treated with a mixture of the corresponding antibodies. After washing in PBS, the bound primary mouse antibodies were visualized by incubation with 1:50 diluted goat-anti-mouse-Cy3 (Jackson Immuno Research) in 4% PBS buffered bovine serum albumin (Serva, Germany) for two hours, whereas for visualization of the primary rabbit antibodies a donkey-anti-rabbit-Cy2 (Jackson Immuno Research) was used. After several rinsings with PBS, the cell preparations were counterstained using DAPI (Serva, Heidelberg, Germany), dried and coverslipped. Control sections were put through the same procedure with nonspecific mouse or rabbit antibodies (DAKO).

Immunostained cell preparations on the implant surfaces were analyzed using a motorized Zeiss Axio-pho2 microscope equipped with appropriated filters. Separate images for DAPI-, Cy3-, Cy2- and FITC-labeled cells were recorded digitally as color-separated components using an AxioCam digital microscope camera and AxioVision multi-channel Image processing (Zeiss Vision GmbH, Germany). Individual color images (blue for DAPI, red for Cy3, green for Cy2 and FITC) were merged, and the co-expression sites appeared in white-yellow color. Representative images of the experiments are shown in Figs. 2 and 3.

STATISTICAL ANALYSIS

DAPI-BSP, DAPI-osteocalcin, and DAPI-onectin labeled cells were counted on the borderline as well as in the middle of the corresponding implant surface. Three to ten successive sections were screened at 400x magnification on a frame of 350µm x 230µm. Only the values of analogous parts were used for averaging. The interactive measurements were carried out using the software of the Kontron-Videoplan-System (Kontron, Zeiss, Germany) and the "frozen image tool". The system software of the Videoplan provided the mean (average ± standard deviation) and the median values for each file. The U-test was used to compare the data sets of the different files and to determine the level of significance of the differences between the various coated surfaces. For a rapid approximation, ranks in a test of Wilcoxon (1945) and White (1952) were used.

AFM MICROSCOPY

The atomic force microscope (AFM) moves a very small sharp tip attached to a soft cantilever, which acts as a spring, in a raster pattern over the sample surface. Deflections in the tip corresponding to surface topography are recorded. The AFM can be operated in air and liquids. In routine diagnosis, it is often desirable to minimize cantilever deflections in order to protect the

sample from too large and potentially damaging forces. For this procedure, a feedback loop is used to adjust the sample height while imaging. The analysis was performed on an AFM (Topometrix Explorer) with 130 μm xy-scan range and 10 μm z-scanner. The AFM is mounted on the top of an inverted microscope (Zeiss Axiovert 135) in order to select the region of interest on the sample surface. For observations of the specimen under ambient conditions, soft cantilevers were utilized in constant force mode (sharpened microlevers, spring constant = 0.02 N/m, tip radius < 10 nm, Thermomicroscopes Sunnivalle CA USA). The forces applied during AFM measurements were 10-20 nN under ambient conditions (Thalhammer et al. 2001).

RESULTS

MORPHOLOGY

The BSP expression in cells settled on collagen- and BSP-coated TIGER surface (red color) was first detectable at day 5 *in vitro* (Fig. 2). Some of the cells were extremely large sized, especially at the BSP-coated implant surface. BSP was mainly localized within the non-mineralized matrix. Although at the beginning of the experiment the morphology of the cells was spheroidal, after one day it changed to the typical polygonal one (not shown). The CD90 marker (green color) indicated a co-localized expression of BSP and CD 90. In the control sample (Fig. 2), the dominance of the green color persisted until day 20 *in vitro*. The expression of osteocalcin and osteonectin was similar to that of BSP, whereas TGF-beta differed significantly. To a greater extent these features were seen also on the glimmer surface as shown in Fig. 3 for day 5 *in vitro*. The distribution patterns of cells on the implant surfaces varied widely as revealed using DAPI staining of nuclei. BSP expression in cells settled on the TIGER surface displayed a half-circular pattern at days 10 and 15 *in vitro* (Fig. 2). At days 20 and 25 *in vitro*, cells were homogeneously distributed on the implant surface including a random sample.

CELL COUNTS

Cell counts revealed that most of the survived cells are settled on the surface of the BSP-coated implants. Fig. 4 displays the median values and the standard deviations indicating only small differences between the various samples. Significantly different values were found at days 15 and 20 *in vitro*, especially for glimmer surfaces. Ranking of the median values gives evidence for BSP-coatings at position 1 followed by collagen. All glimmer samples, coated and non-coated, exhibit significantly smaller standard deviations in the number of settled cells than the TIGER ones. In summary, the observed promotion of cell settlement and/or enhanced cell proliferation on the TIGER surface was not significant.

The control experiment using non-coated materials revealed that TIGER is superior in number of adhered cells, especially at day 25 *in vitro*. That superiority was changed by pre-coating with BSP solution.

ATOMIC FORCE MICROSCOPY

The results of the atomic force microscopy revealed that the surface patterns of BSP-, collagen- and fibronectin-coated glimmer differed widely (Fig. 1, left column). The best results were found for collagen promoting cell settlement on the glimmer samples with a total homogeneous distribution pattern covering the whole surface. The BSP-coating results in very few drops of the BSP solution on the surface. Some more drops on the surface were revealed for fibronectin coating with the highest level of the z range. It can be summarized, that cells with different soma sizes and features were found, whereas the distribution patterns of the settled cells were identical for all coating types (Fig. 1, right column). The influence of the BSP coating on the glimmer surface with discontinuously moistened surface is shown in Fig. 5 which displays the borderline (see Fig. 1, BSP left column) of the coating. Here a disruption of cell number and BSP expression as well as cell features were revealed. Comparison of cell distribution patterns on the glimmer surface with these on the dental implant material surface demonstrates that cell attachment depends to a higher degree on the surface design than on its coating. In materials with identically designed surfaces, BSP-coating promotes cell settlement to a higher degree than the other used coating materials.

As a conclusion, we found 1) a benefit of BSP-coated smooth implant surfaces for the osteoinduction; 2) an enhancement of the osteoinductive effect of surface roughness by BSP-coating.

DISCUSSION

Successful attachment on artificial surface is prerequisite for inducing new bone formation locally at the site of implantation. Protein-coated surfaces may influence the biocompatibility of implant materials by initiating and supporting osteogenesis (Sodek and McKee 2000). Collagen, fibronectin, vitronectin or mixtures of natural extracellular matrix proteins are the mostly investigated proteins for this purpose (Meyer et al. 1998; Lacouture et al. 2002; Salih et al. 2002). BSP was found to be osteoinductive in bone repair (Wang et al. 2004) and sufficient to achieve healing in critical defects (Wang et al. 2002). Lacouture et al. (2002) compared type I collagen, fibronectin, and vitronectin in supporting adhesion of mechanically strained osteoblasts and found out that the major factor governing strain resistance was the number of integrin-extracellular matrix attachments when the number of molecules available for attachment was limited. At a low concentration of protein-coating density, collagen supported the highest attachment rate followed by fibronectin and vitronectin. At higher concentrations, vitronectin supported the highest attachment rate after 24 hours *in vitro*.

Nevertheless, the key of the success of implants is related to the initial healing process (Lekic et al. 1996). Most of the authors (Cook et al. 1985; Kieswetter et al. 1996; Leize et al. 2000) suggest that the larger surface area of rough material leads to an initially delayed, but then prolonged cell proliferation. The initial delay at the rough TIGER surface can be compensated by

January 31, 2007

EUROPEAN JOURNAL OF MEDICAL RESEARCH

9

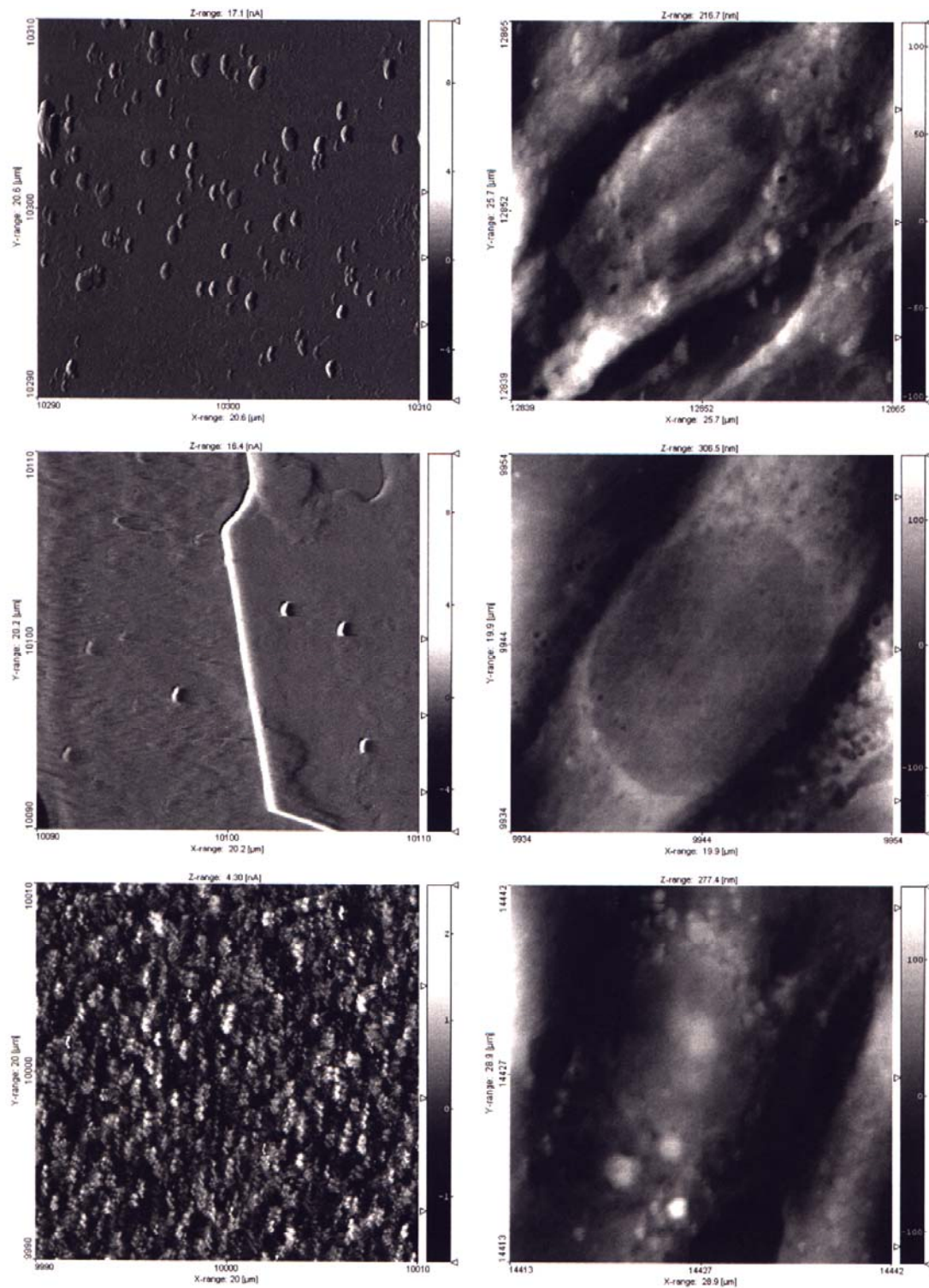
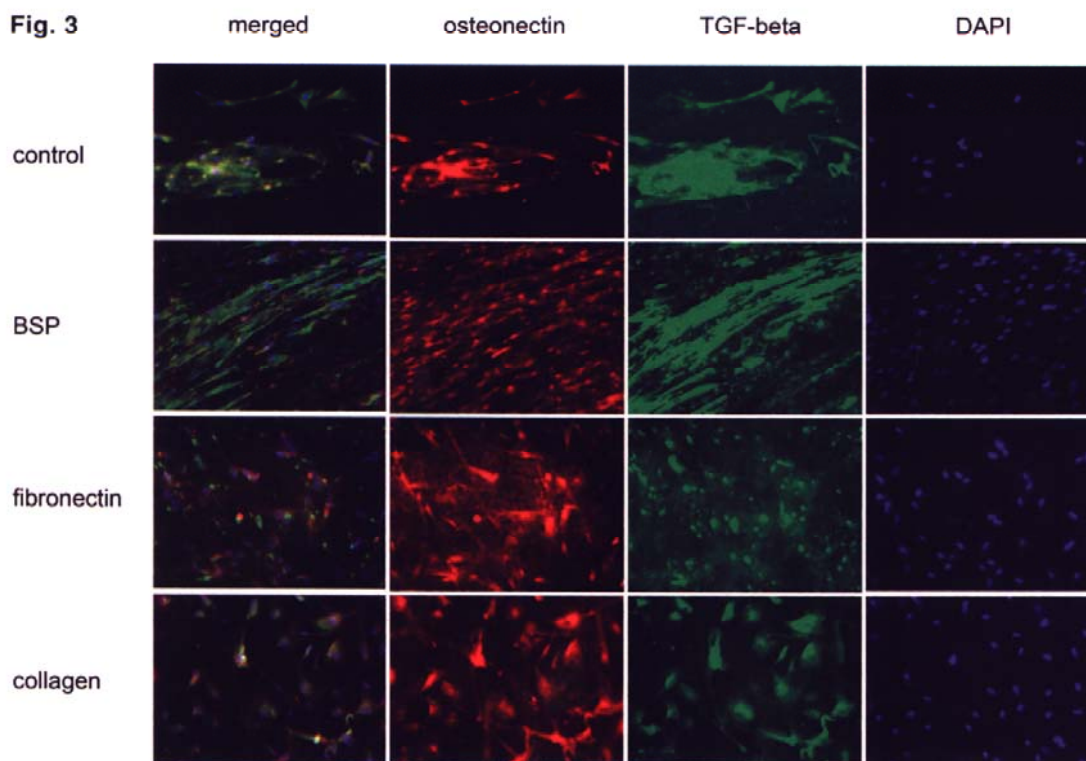
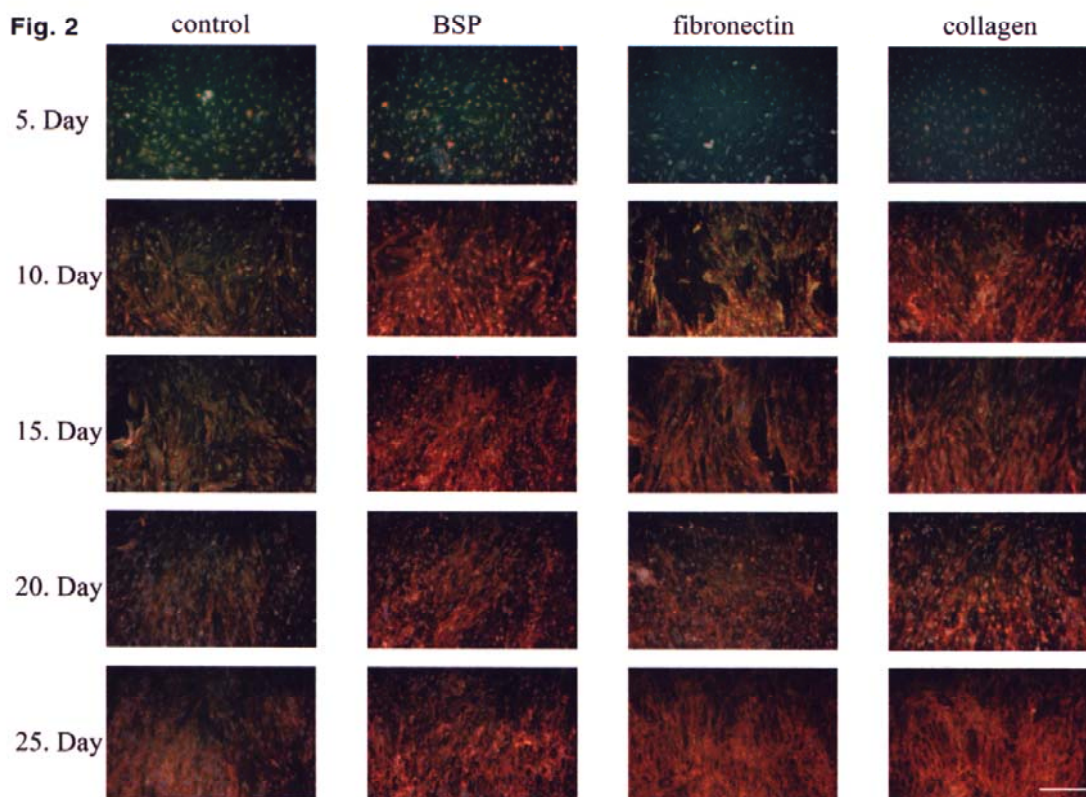


Fig. 1. Left column: Atomic force microscopic features of the glimmer surface coated with fibronectin (above), BSP (middle) and collagen (bottom). Right column: Features of the settled cells at the glimmer surface coated with fibronectin (above), BSP (middle) and collagen (bottom).



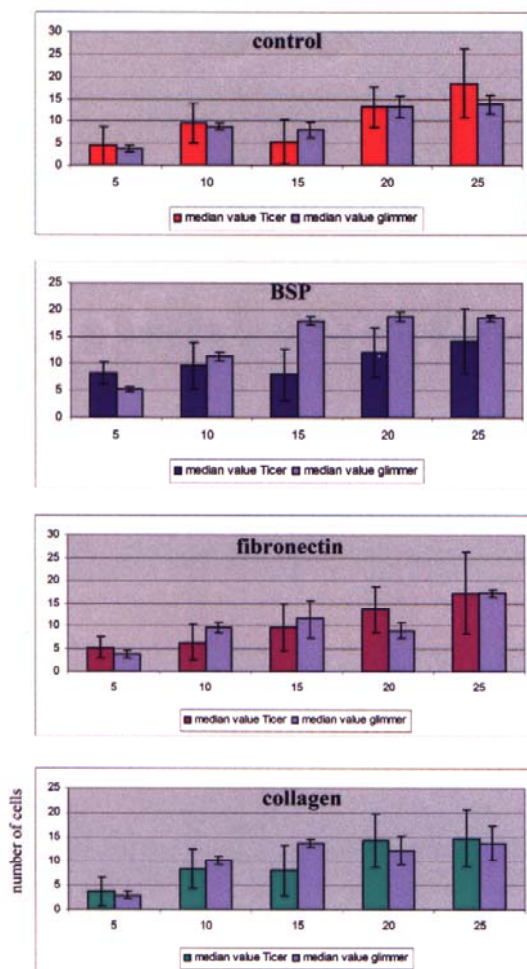


Fig. 4. Development of the number of cells settled the pre-coated surfaces from day 5. to day 25. *in vitro*.

BSP-coated surface. The deposition of BSP represents the first step of bone formation in ectopic transplantation systems *in vivo* (Riminucci et al. 2003). Chou et al (2005) reported the expression of BSP in relation to the provided inductive agents to the cell culture. That fact was supported by our results. The clinical superiority of human derived BSP (when compared with bovine collagen) based on the better histocompatibility of the former.

◀ Fig. 2. Expression of BSP (red immunofluorescence=BSP, blue=DAPI=nuclei of cells) and patterns of CD90 (green) in cells settled on the pre-coated surface of the implant material Ticer. Bar: 100µm.

◀ Fig. 3. Expression of osteonectin and TGF-beta in cells settled on pre-coated surface of glimmer at day 5 *in vitro* (DAPI= nuclei of cells). Bar: 50µm.

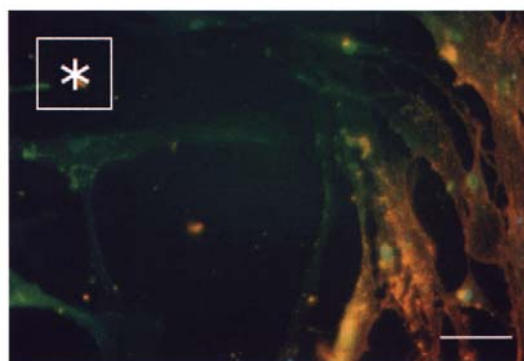


Fig. 5. Effect of coating visualized at the coating border on the glimmer surface by lacking BSP expression of settled cells, * indicates the part of the sample without BSP coating. Bar: 50µm.

Our experiments were designed to use very low concentrated BSP coating solution with the aim to reduce the healing time with a minimal effort and risks for the patients.

Acknowledgements: Many thanks to Dr. Stanka Stoeva for critical reading of the manuscript. We thank Ursula Troeger and Albrecht Rast for the excellent technical help.

REFERENCES

- Chou YF, Huang W, Dunn JCY, Miller TA, Wu BM (2005) The effect of biometric apatite structure on osteoblast viability, proliferation and gene expression. *Biomaterials* 26:285-295
- Cook SD, Walsh KA, Haddad RJ Jr (1985) Interface mechanics and bone growth into porous Co-Cr-Mo alloy implants. *Clin Orthop* 193:271-280
- Fisher LW (1985) The nature of the proteoglycans of bone. In: Butler WT (ed.) *The chemistry and biology of mineralized tissues*. EBSCO Media, Birmingham, Great Britain, pp.188-196
- Fisher LW, Termine JD (1985) Noncollagenous proteins influencing the local mechanisms of calcification. *Clin Orthop* 200:362-385
- Ganss B, Kim RH, Sodek J (1999) Bone sialoprotein. *Crit Rev Oral Biol Med* 79:79-98
- Graf HL (1997) *Zur Entwicklung und Charakterisierung eines neuen Implantatsystems*. Habilitationsschrift, Leipzig
- Hoshi K, Ozawa H (2000) Matrix vesicle calcification in bones of adult rats. *Calcif Tissue Int* 66:430-434
- Hulbert SF, Young FA, Mathews RS, Klawitter JJ, Talbert CD, Stelling FH (1970) Potential of ceramic materials as permanently implantable skeletal prostheses. *J Biomed Mater Res* 4:433-456
- Hunter GK, Goldberg HA (1993) Nucleation of hydroxyapatite by bone sialoprotein. *Proc Natl Acad Sci U S A* 90:8562-8565
- Hunter GK, Goldberg HA (1994) Modulation of crystal formation by bone phosphoproteins: Role of glutamic acid-rich sequences in the nucleation of hydroxyapatite by bone sialoprotein. *Biochem J* 302:175-179
- Karmatschek M, Maier I, Seibel MJ, Woitge HW, Ziegler R, Armbruster FP (1997) Improved purification of human bone sialoprotein and development of a homologous radioimmunoassay. *Clin Chem* 43:2076-2082

- Kieswetter K, Schwartz Z, Hummert TW, Cochran DL, Simpson J, Dean DD, Boyan BD (1996) Surface roughness modulates the local production of growth factors and cytokines by osteoblast-like MG-63 cells. *J Biomed Mater Res* 32:55-63
- Lacouture ME, Schaffer JL, Klickstein LB (2002) A comparison of type I collagen, fibronectin, and vitronectin in supporting adhesion of mechanically strained osteoblasts. *J Bone Miner Res* 17:481-492
- Leize EM, Hemmerlé J, Leize M (2000) Characterization, at the bone crystal level, of the titanium-coating/bone interfacial zone. *Clin Oral Res* 11:279-288
- Lekic P, Sodek J, McCulloch C (1996) Osteopontin and bone sialoprotein expression in regenerating rat periodontal ligament and alveolar bone. *Anat Rec* 244:50-58
- Marks SC, Popoff SN (1988) Bone cell biology: The regulation of development, structure, and function in the skeleton. *Am J Anat* 183:1-44
- Meyer U, Meyer T, Jones DB (1998) Attachment kinetics, proliferation rates and vinculin assembly by bovine osteoblasts cultured on different pre-coated artificial substrates. *J Mater Sci : Mater Med* 9:301-307
- O'Toole GC, Salih E, Gallagher C, Fitzpatrick D, O'Higgins N, O'Rourke SK (2004) Bone sialoprotein-coated femoral implants are osteoinductive but mechanically compromised. *J Orth Res* 22:641-646
- Riminucci M, Bianco P (2003) Building bone tissue: matrices and scaffolds in physiology and biotechnology. *Braz J Med Biol Res* 36:1027-1036
- Saalbach A, Aust G, Hausteil UF, Herrmann K, Andereg U (1997) The fibroblast-specific Mab AS02: a novel tool for detection and elimination of human fibroblasts. *Cell Tissue Res* 290:593-599
- Salih E, Wang J, Mah J, Fluckiger R (2002) Natural variation in the extent of phosphorylation of bone phosphoproteins as a function of in vivo new bone formation induced by demineralized bone matrix in soft tissue and bony environment. *Biochem J* 364:465-474
- Schreckenbach JP, Marx G, Schlottig F, Textor M, Spencer ND (1999) Characterization of anodic spark-converted titanium surfaces for biomedical applications. *J Mater Sci: Mater Med* 10:453-457
- Schwartz Z, Lohmann CH, Oefinger J, Bonewald LF, Dean DD, Boyan BD (1999) Implant surface characteristics modulate differentiation behavior of cells in the osteoblastic lineage. *Adv Dent Res* 13:38-48
- Sodek J, McKee MD (2000) Molecular and cellular biology of alveolar bone. *Periodontol* 24:99-126
- Thalhammer S, Zink A, Nerlich AG, Heckl WM (2001) Atomic Force Microscopy with high resolution imaging of collagen fibrils _ A new technique to investigate collagen structure in historic bone tissues. *J Archeol Sci* 28: 1061
- Wang J, Zhou H, Salih E, Hofstaetter JG, Glimcher MJ (2004) Bone Sialoprotein elicits biomineralization and ossification in a bone defect model. *J Bone Miner Res* 19: S221 Abstract
- Wang ML, Nesti IJ, Tuli R, Lazatin J, Danielson KG, Sharkey PF, Tuan RS (2002) Titanium particles suppress expression of osteoblastic phenotype in human mesenchymal stem cells. *J Orth Res* 20:1175-1184
- White C (1952) The use of ranks in a test of significance for comparing two treatments. *Biometrics* 8:33-41
- Wilcoxon F (1945) Individual comparisons by ranking methods. *Biometrics* 1:80-83
- Wuttke M., Müller S, Nitsche DP, Paulsson M, Hanisch FG, Maurer P (2001) Structural characterization of human recombinant and bone-derived bone sialoprotein. *J Biol Chem* 276:36839-36848

Received: November 12, 2006 / Accepted: December 12, 2006

Address for correspondence:

Prof. Dr. H. Hilbig
Institute of Anatomy
Leipzig University
Liebigstr. 13
04103 Leipzig
Germany
Phone: ++49-341-9722053
Fax: ++49-341-9722007
e-mail: hilbig@medizin.uni-leipzig.de

5.4 Age Determination of Blood Spots in Forensic Medicine By Force Spectroscopy

Stefan Strasser, Albert Zink, Gerald Kada, Peter Hinterdorfer, Oliver Peschel, Wolfgang M. Heckl, Andreas G. Nerlich, Stefan Thalhammer

Forensic Science International (2007), 170, 8-14

Available online at www.sciencedirect.com

Forensic Science International 170 (2007) 8–14

www.elsevier.com/locate/forensiint

Age determination of blood spots in forensic medicine by force spectroscopy

Stefan Strasser^a, Albert Zink^a, Gerald Kada^c, Peter Hinterdorfer^c, Oliver Peschel^d,
Wolfgang M. Heckl^{a,b}, Andreas G. Nerlich^e, Stefan Thalhammer^{a,f,*}

^aDepartment of Earth and Environmental Sciences, Ludwig-Maximilians-Universität, Munich, Germany

^bDeutsches Museum, Museumsinsel 1, Munich, Germany

^cInstitute for Biophysics, Johannes-Kepler-University, Linz, Austria

^dDepartment of Forensic Medicine, Ludwig-Maximilians University, Munich, Germany

^eDepartment of Pathology, Academic Hospital Munich-Bogenhausen, Germany

^fInstitute of Radiation Protection, GSF-National Research Center for Environment and Health, Germany

Received 16 February 2006; received in revised form 7 July 2006; accepted 30 August 2006

Available online 13 November 2006

Abstract

We present a new tool for the estimation of the age of bloodstains, which could probably be used during forensic casework. For this, we used atomic force microscopy (AFM) for high-resolution imaging of erythrocytes in a blood sample and the detection of elasticity changes on a nanometer scale. For the analytic procedure we applied a fresh blood spot on a glass slide and started the AFM detection after drying of the blood drop. In a first step, an overview image was generated showing the presence of several red blood cells, which could easily be detected due to their typical “doughnut-like” appearance. The consecutively morphological investigations in a timeframe of 4 weeks could not show any alterations. Secondly, AFM was used to test the elasticity by recording force–distance curves. The measurements were performed immediately after drying, 1.5 h, 30 h and 31 days. The conditions were kept constant at room temperature (20 °C) and a humidity of 30%. The obtained elasticity parameters were plotted against a timeline and repeated several times. The elasticity pattern showed a decrease over time, which are most probably influenced by the alteration of the blood spot during the drying and coagulation process. The preliminary data demonstrates the capacity of this method to use it for development of calibration curves, which can be used for estimation of bloodstain ages during forensic investigations.

© 2006 Elsevier Ireland Ltd. All rights reserved.

Keywords: AFM; Force spectroscopy; Forensic medicine; Age determination; Blood spots

1. Introduction

Blood analysis including blood cell measurement is one of the most basic items of hematological testing which is indispensable in health examination, disease diagnosis and treatment. The common lab test is used to diagnose and monitor the body's response to diseases. Some tests measure the components of blood itself and others examine substances found in the blood to identify abnormal function of various organs. In forensic sciences the examination of bloodstains represents a major

application during crime scene investigation. There exists a lot of reliable methods for the detection and identification of blood spots. For the evaluation of suspected bloodstains solutions such as phenolphthalein, tetramethylbenzidine can be used, as they change color when they come into contact with peroxidase or hemoglobin in the blood [1]. For the detection of even minute amounts of blood traces the presumptive luminol chemiluminescence test is widely used in forensic practical work [2]. It is further possible to unambiguously attribute the blood to a certain individual by using molecular biological techniques, such as genetic fingerprinting [3].

However, the determination of the age of a blood spot remains an unsolved problem in forensic routine work. For more than hundred years forensic scientists are engaged in finding a methodology, which allows determining the exact age of a dried bloodstain. Since then several approaches were

* Corresponding author at: GSF-National Research Center for Environment and Health, Ingolstädter Landstraße 1, 85764 Neuherberg, Germany.

Tel.: +49 89 3187 2893; fax: +49 89 3187 2942.

E-mail address: s.t@lmu.de (S. Thalhammer).

proposed to have potentially solved this important problem during crime scene investigation, but none of these could ever be established in forensic practice. An attempt was undertaken by evaluating the time differences of the solubility of bloodstains of different ages [4]. In control experiments it turned out, that both methods considerably diverge from the real age of an investigated bloodspot. More recently, new methods were tested such as remission spectrophotometry [5] or electron-spin-resonance measurements [6], which can detect an age-dependent increase of signal intensity of meth-hemoglobin, non-hem-iron molecules and organic radicals. Concordantly, these methods proved to have a high error rate, which only allow a rough estimation of the age of a bloodstain and does not excuse the high technical expense. In more recent times chromatographic methods were tested for the use in dating blood spots. Inoue et al. [7] used high pressure liquid chromatography (HPLC) to measure the quantitative compound of the globin chains of the red blood dye hemoglobin. They found a decrease of the α -chains related to the heme, the color defining prosthetic group of the red blood dye hemoglobin, with increasing age of a blood spot. The measurements of the standardized bloodstains revealed high deviations and revealed not to be practicable for forensic routine work. Moreover, a mobile application of this method for the use directly at a crime scene investigation seems not to be realizable. Taken together, all described methods proved to be not applicable in forensic routine work, as the results of the age measurement of the bloodstains provided too high deviations compared to the real age. Most of these attempts rely on advanced technical equipment and, therefore, does not allow the application directly at a site of crime. Additionally, a part of the sometime rare trace material has to be consumed for the use of these approaches, so that it will be lost for further important analysis, like molecular genetic investigations.

We present a new methodology which could be used for the age determination of dried bloodspots during crime scene investigation. Therefore, an AFM was used as a nanoindenter to monitor age-related changes of the elasticity of bloodstains under standardized conditions.

Since the invention of the AFM by Binnig et al. [8], indentation experiments are generally applied in measuring elastical properties. Nanoscaled materials are probed with the AFM due to its high lateral and vertical resolution down to 0.01 nm. In contrast to other hardness tester the force resolution of the AFM can reach ranges of 10^{-4} nN [9]. The application of AFM–force spectroscopy is widespread and used for measuring polymer systems [10,11], bone elasticity [12], collagen [13] or cells [14–16].

To investigate the alteration of the elasticity of blood samples with the AFM by force spectroscopy, force–distance curves were applied to the blood spot. To compare two samples it is sufficient to calculate the slopes in the upper linear part of the force–distance curves (see Fig. 1). For calculation of the Young's modulus a model has to be fitted to the measured data. A detailed calculation procedure can be found in the next section.

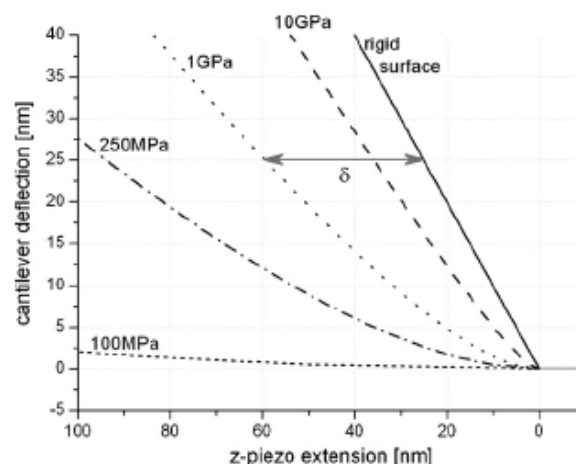


Fig. 1. Force–distance curves of various elastic samples calculated with the Hertzian theory. At rigid surfaces the AFM tip cannot penetrate into the sample, therefore the cantilever deflection corresponds to the extension of the z -piezo. The softer the sample the more penetrates the tip into the sample, therefore the slope is very smooth. To get the elasticity modulus (Young's modulus, E) the Hertzian or similar models have to be fitted to the measurement curves.

2. Materials and methods

2.1. Preparation of the blood samples

For the AFM investigations a few drops of capillary blood from a healthy human volunteer was drawn from the fingertip by using blood lancets. The blood drops were applied to a glass slide and dried at room temperature.

2.2. AFM microscopy

For morphological characterization of the blood samples an AFM Topomatrix Accurex (Atos, Germany) was used. It was operated in contact mode under ambient conditions, with 35% relative humidity, using NSC12F (non-contact silicon cantilever) cantilevers (Mikromasch, Estonia). The spring constants of the non-contact probes (NSC) was 0.3 N/m (F). The nominal resonant frequency of the NSC cantilever was 21 kHz (F). The nominal tip radius was specified <10.0 nm. Image analysis was performed using SPIP software (Image Metrology, Denmark).

2.3. Force spectroscopy and data analysis

Force spectroscopy was carried out with an AFM of Molecular Imaging/Agilent using Si cantilever (special made NSC15 high force constant, pyramidal tip shape, cone half angle $\alpha = 15^\circ$, cantilever typical cantilever thickness 4.8–5.5 μm , resonant frequency nominal: 405 kHz, spring constant nominal $k_c = 80$ N/m, Mikromasch, Estonia). For determination of the effective spring constant the Sader method was applied [17]. This procedure can be easily applied using the length, the width and the resonant frequency in fluid, typically air, with the accompanying quality factor Q . In this case the spring constant k_c is independent from the thickness and the density. The exact measurement of both parameters is non-trivial and additionally defects in the material are taken into account because of the usage of the resonant frequency. All comparative experiments were carried out with the same cantilever in ambient conditions with a spring constant of $k_c = 74$ N/m. The detailed calculation procedure for calculating the Young's modulus is presented in the following.

The indentation of an AFM tip into soft or hard samples can be modeled using the Hertzian contact mechanics [18]. Indentations of an infinitely hard body into a hard elastic half space (small indentations with the

parabolic part of the tip) with a normal force F leads with this theory to [19,20]:

$$F_{\text{paraboloid}} = \frac{4}{3} \frac{E}{1-\nu^2} \delta^{3/2} \sqrt{R} \quad (1)$$

where δ is the indentation depth, E the Young's modulus, ν the Poisson ratio and R is the tip radius. For incompressible materials the Poisson ratio is at 0.5. The applied force can be calculated with the deflection of the cantilever which is considered as a tightened spring by Hook's Law:

$$F = k_c d \quad (2)$$

where k_c is the spring constant and d is the deflection of the cantilever.

The deflection of the cantilever depends on the indentation of the tip into the elastic half space or rather the sample. The z -piezo extends and the distance of the extension z is splitted into the deflection and the indentation depth (δ) by:

$$z = d + \delta \quad (3)$$

With these Eqs. (1)–(3) the Young's modulus can be expressed for hard samples as followed:

$$E_{\text{paraboloid}} = \frac{3k_c(d-d_0)(1-\nu^2)}{4\sqrt{R}[(z-z_0)-(d-d_0)]^{3/2}} \quad (4)$$

where d_0 and z_0 are the corresponding values of the cantilever deflection and the z -piezo extension at the contact point. Eq. (4) can now be written for soft samples in the contact regime as:

$$z = \left[\frac{3k_c(d-d_0)(1-\nu^2)}{4\sqrt{R}} \right]^{2/3} + (d-d_0) + z_0 \quad (5)$$

To calculate the Young's modulus the model (Eq. (5)) has to be fitted to every force–distance curve. For the evaluation the average of approach and retract curve was taken. The spring constant ($k_c = 74 \text{ N/m}$) was determined by the Sader method [17], the radius of curvature ($R, R \approx 200 \text{ nm}$), determining the tip shape was determined using an scanning electron microscopy (SEM) image.

In Fig. 1 typical force–distance curves calculated with the Hertzian theory are presented. The horizontal line on the right side shows the behaviour when the tip is far away from the sample. The tip approaches to the sample and a force between tip and sample arises. It could be either attractive or repulsive. In case of attractive forces a snap in of the tip to the sample surface occurs while with repulsive forces the cantilever is bent up. Both events are not the case with our blood samples.

The force–displacement curves were processed using the software Microcal Origin and Microsoft Excel, to evaluate the slopes and the Young's moduli. For calculation of the Young's modulus Eq. (5) was applied to the measured data as described before.

3. Results

3.1. AFM imaging of the bloodstains

The AFM imaging of the samples revealed no morphological differences between the bloodstains following drying and after 31 days (see Fig. 2). The first row displays a series of images recorded on the freshly dried specimen. In the subsequent rows the same region of the bloodstain is visualized after 1, 2 and 4 weeks. In the overview images some small cracks in the bloodstain can be observed, which are already present in the first images taken immediately after drying of the blood. In the detailed pictures the erythrocytes can be easily identified due to their typical doughnut-like shape. Most interestingly, neither the erythrocytes nor the cracks in the bloodstain showed any morphological alterations during the observation period of 31 days.

3.2. Elasticity measurements on the bloodstains

On three different aged bloodstains (immediately after drying, 30 h and 31 days), force spectroscopy was carried out with the AFM, using the tip as a nanoindenter. Force–distance curves were recorded on different areas of the blood spot. In Fig. 3A an AFM image with a typical area for recording force–distance curves on the blood spot is displayed. The measurements of the elasticity on the blood were carried out on the thick center area to exclude effects of the hard glass substrate. Fig. 3B shows a typical force–distance curve of the 31 days old sample.

Fig. 4 displays the calculated Young's modulus of the force–distance curves with the individual standard variations of the samples. The average values of the samples differ significantly from each other. This clearly shows, that the elasticity of the bloodstain decreased with the age of the sample.

However, with regard to the standard variation the Young's moduli are very similar and the error ranges show a slightly overlap mainly in the lower values. Fig. 5 shows the huge variation of the individual slopes of the force–distance curves. The values are highly dependent on the measuring point.

4. Discussion

The unique elastic properties of the red cell membrane and their ability to withstand deformation stresses during circulation have been characterized by biomechanical investigations as well as biophysical studies. While the biochemistry of the system including various protein and lipid components is well established, the structural basis of the components is still under debate [21]. First insight into the red cell network structure and its viscoelastic properties derived from investigations using micropipette aspiration [22]. In more recent studies the AFM played a major role in characterizing the membrane assembly and its nanomechanical properties. The unfolding of spectrin repeats, a major component of the red cell cytoskeleton, by using the AFM provided deep insight into the mechanical stability and the structure of this protein [23]. In medical research, the AFM was mainly used to investigate morphological alterations of red blood cells, which show a relation to a certain disease. Kamruzzahan et al. [24] observed the surface topography of red blood cells of patients with systemic lupus erythematosus and compared it to those of healthy donors. Thereby, they were able to detect characteristic circular shaped holes at the surface of the red blood cells from the patients under physiological conditions, which could correlate with described functional deficiencies in red blood cells [25]. In an earlier study Zachee et al. [26] visualized uremic red blood cells with the atomic force microscope. The ultra-morphological images confirmed the existence of uremic echinocytes and demonstrated the capability of the AFM to study cell surfaces.

The imaging of altered erythrocytes due to mechanical stress represents another application of the AFM in blood research. Under various physiological conditions artificial organs occasionally traumatize the blood cells, which can lead to the critical liberation of hemoglobin molecules of erythrocytes. Ohta et al. [27] were able to show that the fine structure of the

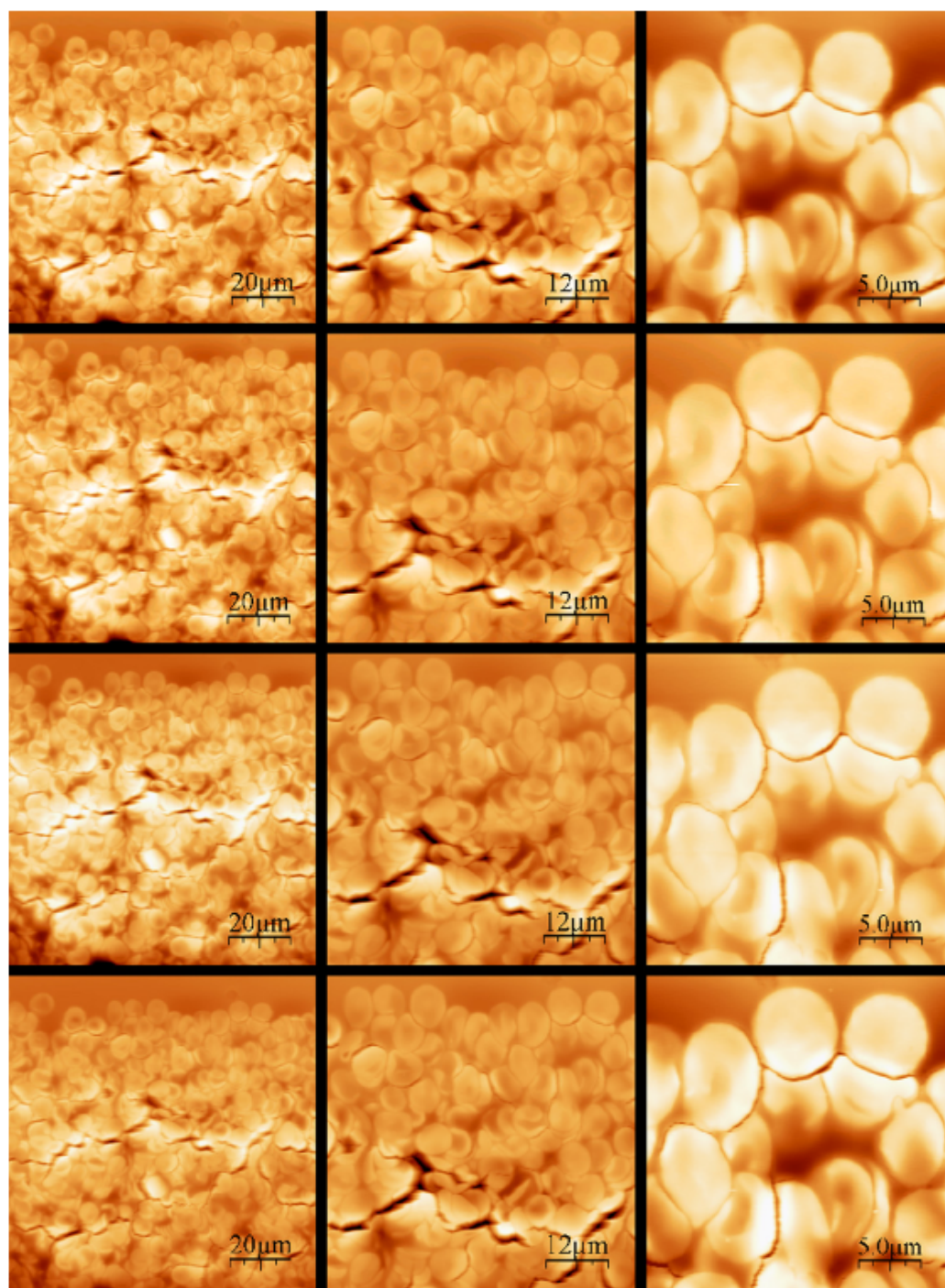


Fig. 2. Results of the morphological investigations of a dried blood spot by AFM. The illustration is divided into rows and columns. The AFM images in the rows correspond to the individual measuring days. The columns display identical scan areas depending on the alteration time of the blood spot. The first series (first row) was scanned after 1.5 h, the second series after 1 week, the third series after 2 weeks and the fourth series after 4 weeks. The morphology independent on the scan range (100, 60, 25 μm) does not change with the alteration time.

red blood surface was changed drastically by artificially induced shear stress. Moreover, they found that the surface roughness increased with the exposure time and could be correlated to the liberated hemoglobin concentration. In

another study the influence of different agents including phospholipids, low ionic strength media and drugs on the shape of human erythrocytes were investigated and characterized by the AFM [28]. The artificially produced abnormally shaped

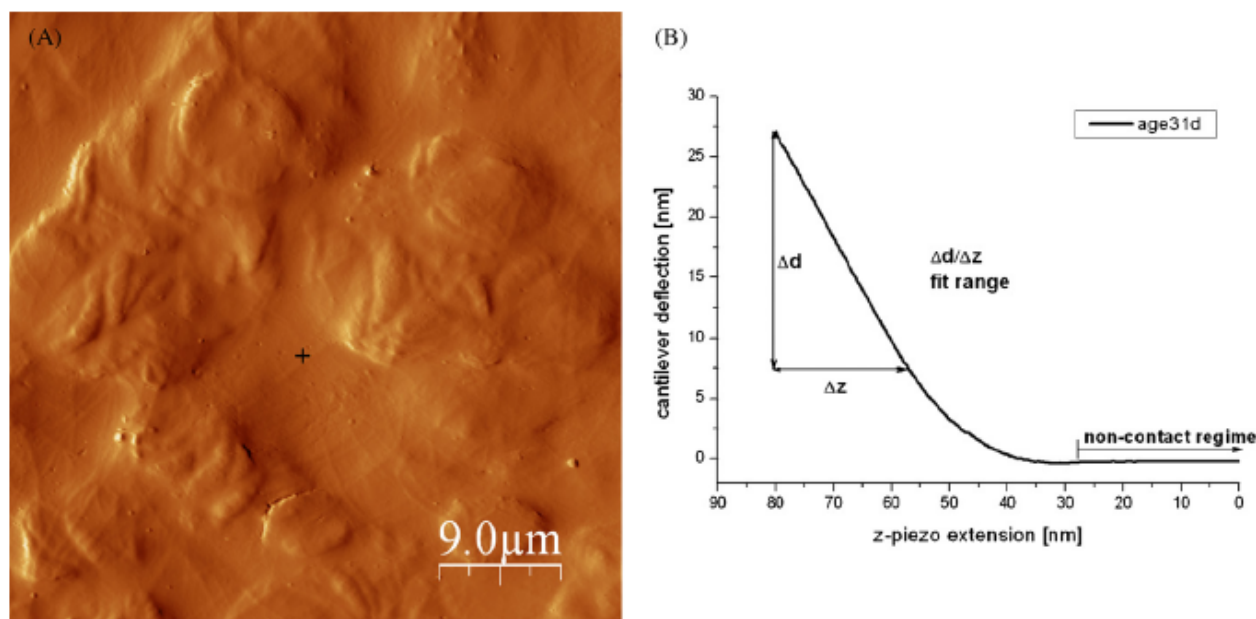


Fig. 3. Typical force–distance curve with corresponding AFM image showing the measuring spot. (A) AFM image of a typical area for recording force–distance curves on the blood spot. The measurements of the elasticity on the blood were carried out on the thick center area to exclude any effects of the hard glass substrate. The measuring points were distributed randomly over the sample. As an example, one of these measuring spots is marked on the AFM image (cross). (B) Typical force–distance curve of the 31 days old sample. The horizontal line on the right side of the curve is referred to as zero line, where tip and sample are not in contact. To exclude the influence of surface effects with unknown magnitude the fit is performed in the upper part of the curve marked as Δz and Δd . During the fitting procedure the Young's modulus E and the z -value of contact point z_0 are the calculated fitting parameter of Eq. (5).

erythrocytes were further compared with cells that occur with high incidence in blood pathologies, such as spherocytosis and anisopoichilocytosis. In all these medical related studies the AFM was used to image erythrocytes and detect differences in shape or cell wall surfaces. In only a few investigations the AFM was used to study elastic properties of cells by recording force curves and relate the differences of normal and altered cells to pathological conditions. Force spectroscopy of normal

and cancerous human bladder cells revealed a Young's modulus of about one order of magnitude higher of normal cells compared to the cancer cells [29]. The differences in elasticity could probably be attributed to changes in the cytoskeleton due to oncogenic transformation. In a further study Lekka et al. [29] probed the erythrocyte stiffness of red blood cells from patients suffering from coronary disease, hypertension and diabetes mellitus and compared it to erythrocytes derived from healthy donors. Analysis of the recorded force curves provided an

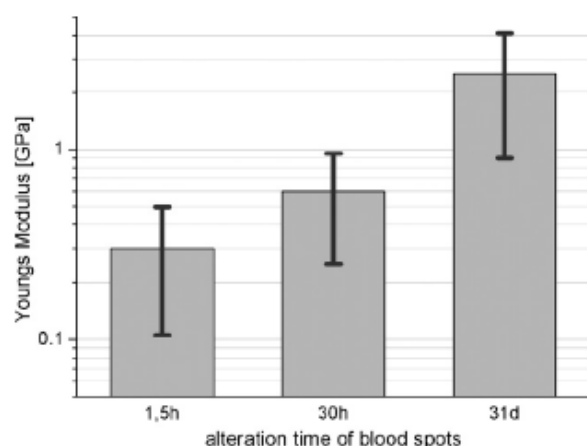


Fig. 4. Elasticity change vs. alteration time. The evaluation of the Young's moduli indicates an elasticity change depending on the alteration time. The bloodstain was measured after 1.5 h, after 30 h and after 31 days. Every column was calculated from more than 100 individual F – d curves. The whisker displays the standard deviation of the force curves.

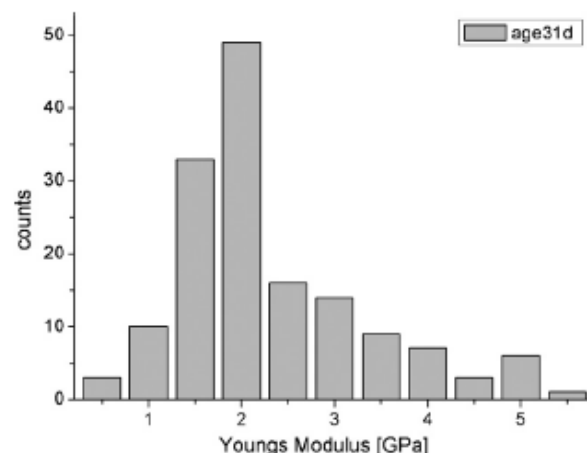


Fig. 5. F – d curve histogram of measurement day 31. The variation can be attributed to the inhomogeneous assembly of the blood spot. The F – d curves are recorded on the surface, influences from the bulk below cannot be excluded.

increase of the stiffness in samples from cigarette smokers and diabetes mellitus patients. This observation confirmed other biochemical studies, which have shown that chemical changes in the erythrocyte membrane, especially the ratio between phospholipids and cholesterol content can lead to an increase in cell wall rigidity in patients suffering from diabetes mellitus [30].

Until recently, the AFM was only introduced in a few specialized applications in forensic medicine, such as the examination of line crossings in documents [31]. In a recent study a first attempt was undertaken to detect time-dependent changes of the erythrocyte morphology [32]. The authors found cellular changes of erythrocytes after exposure in air for several days by using dynamic mode atomic force microscopy. They observed cell shrinking and fissures after 0.5 days and at 2.5 days of exposure nanometer scaled protuberances occurred which increased in number with time. Based on these results, Chen and Cai proposed that the alteration of the red blood cells could be used to estimate the time of death. However, the erythrocytes were not investigated under conditions to be found at a crime scene, but were mixed with an anticoagulant (EDTA), immunolabelled, deposited on mica and fixed manually. Therefore, it cannot be ruled out that the pre-treatment of the blood influences or enhances the observed cell wall alterations.

In contrast to this work, we investigated a bloodstain on a glass slide without any kind of pre-treatment or chemical modifications. Thereby, we could not detect any morphological alterations of the red blood cells over a time period of 4 weeks. The AFM images recorded during the whole observation period of the bloodstain showed no major differences (see Fig. 2). However, the recorded force–distance curves of our blood sample showed a clear increase of the stiffness with increasing age of the bloodstain. This represents the first application of force spectroscopy to investigate age related changes of dried blood, which could serve as a helpful tool in forensic science and serve as a new approach to solve a major problem during forensic casework, the age determination of dried bloodstains.

Nevertheless, we observed a few limitations during our investigations, which have to be clarified by further experiments. The measurements showed a high standard deviation, which can probably be explained by the non-homogeneous composition of the blood clot. During coagulation a fibrin network is generated in which platelets, erythrocytes, leukocytes and other blood components are embedded. Despite the fact, that the blood clot appears to be a homogeneous system, the single components seem to influence the elasticity parameters of the whole system in different ways. Moreover, there exists evidence that erythrocytes show some alteration in membrane elasticity and viscosity during *in vivo* ageing [33]. The age of the erythrocyte (1–120 days) could therefore have an influence on the measurements of the bloodspot. However, these differences are most probably negligible compared to the major elasticity changes during drying of the bloodstain. This holds particular true with respect to the fact, that we did not perform elasticity measurements on single blood cells, but considered the bloodstain as a complete system (see Fig. 3). The stiffness values of single erythrocytes and the influence of the measurement spot will be the major topic

of our further studies, in which we are planning to measure the single components of the blood and its elasticity parameters by force spectroscopy. Together with these upcoming data we hope to be able to establish a tool, which can be used for the age determination of dried blood spots in forensic routine applications.

Acknowledgement

This study was supported by a grant of the Excellence Network NanoBioTechnology (ENNAB).

References

- [1] M. Cox, A study of the sensitivity and specificity of 4 presumptive tests for blood, *J. Forensic Sci.* 36 (1991) 1503–1511.
- [2] T.I. Quickenden, P.D. Cooper, Increasing the specificity of the forensic luminol test for blood, *Luminescence* 16 (2001) 251–253.
- [3] P. Gill, Role of short tandem repeat DNA in forensic casework in the UK—past, present, and future perspectives, *Biotechniques* 32 (2002) 366–385.
- [4] W. Schwarzhäuser, Altersbestimmung von blutspuren, *Z. Ges. Gerichtliche Med.* 15 (1930) 119–124.
- [5] G. Lins, V. Blazek, The use of remission analysis for direct colorimetric determination of age of blood stains, *Z. Rechtsmed.: J. Legal Med.* 88 (1982) 13–22.
- [6] T. Miki, A. Kai, M. Ikeya, Electron-spin resonance of bloodstains and its application to the estimation of time after bleeding, *Forensic Sci. Int.* 35 (1987) 149–158.
- [7] H. Inoue, F. Takabe, M. Iwasa, Y. Maeno, Y. Seko, A new marker for estimation of bloodstain age by high-performance liquid-chromatography, *Forensic Sci. Int.* 57 (1992) 17–27.
- [8] G. Binnig, C.F. Quate, C. Gerber, Atomic force microscope, *Phys. Rev. Lett.* 56 (1986) 930–933.
- [9] N.A. Burnham, R.J. Colton, H.M. Pollock, Interpretation issues in force microscopy, *J. Vac. Sci. Technol. A: Vac. Surf. Films* 9 (1991) 2548–2556.
- [10] E. Tomassetti, R. Legras, B. Nysten, Quantitative approach towards the measurement of polypropylene/ethylene-propylene copolymer blends surface elastic properties by AFM, *Nanotechnology* 9 (1998) 305–315.
- [11] M.R. Vanlandingham, S.H. McKnight, G.R. Palmese, J.R. Elings, X. Huang, T.A. Bogetti, R.F. Eduljee, J.W. Gillespie, Nanoscale indentation of polymer systems using the atomic force microscope, *J. Adhes.* 64 (1997) 31–59.
- [12] J.B. Thompson, J.H. Kindt, B. Drake, H.G. Hansma, D.E. Morse, P.K. Hansma, Bone indentation recovery time correlates with bond reforming time, *Nature* 414 (2001) 773–776.
- [13] L. Bozec, M. Horton, Topography and mechanical properties of single molecules of type I collagen using atomic force microscopy, *Biophys. J.* 88 (2005) 4223–4231.
- [14] E. A-Hassan, W.F. Heinz, M.D. Antonik, N.P. D'Costa, S. Nageswaran, C.A. Schoenenberger, J.H. Hoh, Relative microelastic mapping of living cells by atomic force microscopy, *Biophys. J.* 74 (1998) 1564–1578.
- [15] W.H. Goldmann, Mechanical manipulation of animal cells: cell indentation, *Biotechnol. Lett.* 22 (2000) 431–435.
- [16] A. Touhami, B. Nysten, Y.F. Dufrene, Nanoscale mapping of the elasticity of microbial cells by atomic force microscopy, *Langmuir* 19 (2003) 4539–4543.
- [17] J.E. Sader, J.W.M. Chon, P. Mulvaney, Calibration of rectangular atomic force microscope cantilevers, *Rev. Sci. Instrum.* 70 (1999) 3967–3969.
- [18] H. Hertz, Über die berührung fester elastischer körper, *J. Reine Angew. Math.* 92 (1882) 156–171.
- [19] I.N. Sneddon, The relation between load and penetration in the axisymmetric Boussinesq problem for a punch of arbitrary profile, *Int. J. Eng. Sci.* 3 (1965) 47–57.
- [20] K.L. Johnson, *Contact Mechanics*, Cambridge University Press, Cambridge, 1994.

- [21] D.E. Discher, P. Carl, New insights into red cell network structure, elasticity, and spectrin unfolding—a current review, *Cell. Mol. Biol. Lett.* 6 (2001) 593–606.
- [22] E.A. Evans, New membrane concept applied to analysis of fluid shear-deformed and micropipet-deformed red blood-cells, *Biophys. J.* 13 (1973) 941–954.
- [23] M. Rief, J. Pascual, M. Saraste, H.E. Gaub, Single molecule force spectroscopy of spectrin repeats: low unfolding forces in helix bundles, *J. Mol. Biol.* 286 (1999) 553–561.
- [24] A.S.M. Kamruzzahan, F. Kienberger, C.M. Stroh, J. Berg, R. Huss, A. Ebner, R. Zhu, C. Rankl, H.J. Gruber, P. Hinterdorfer, Imaging morphological details and pathological differences of red blood cells using tapping-mode AFM, *Biol. Chem.* 385 (2004) 955–960.
- [25] Y. Richaud-Patin, B. Perez-Romano, E. Carrillo-Maravilla, A.B. Rodriguez, A.J. Simon, J. Cabiedes, J. Jakes-Ocampo, L. Llorente, A. Ruiz-Arguelles, Deficiency of red cell bound CD55 and CD59 in patients with systemic lupus erythematosus, *Immunol. Lett.* 88 (2003) 95–99.
- [26] P. Zachee, M. Boogaerts, J. Snauwaert, L. Hellemans, Imaging uremic red-blood-cells with the atomic-force microscope, *Am. J. Nephrol.* 14 (1994) 197–200.
- [27] Y. Ohta, H. Okamoto, T. Kanno, T. Okuda, Atomic force microscopic observation of mechanically traumatized erythrocytes, *Artif. Org.* 26 (2002) 10–17.
- [28] M. Girasole, A. Cricenti, R. Generosi, A. Congiu-Castellano, G. Boumis, G. Amiconi, Artificially induced unusual shape of erythrocytes: an atomic force microscopy study, *J. Microsc. (Oxford)* 204 (2001) 46–52.
- [29] M. Lekka, P. Laidler, D. Gil, J. Lekki, Z. Stachura, A.Z. Hryniewicz, Elasticity of normal and cancerous human bladder cells studied by scanning force microscopy, *Eur. Biophys. J. Biophys. Lett.* 28 (1999) 312–316.
- [30] M. Bryszewska, C. Watala, W. Torzecka, Changes in fluidity and composition of erythrocyte-membranes and in composition of plasma-lipids in type-I diabetes, *Brit. J. Haematol.* 62 (1986) 111–116.
- [31] S. Kasas, A. Khanmy-Vital, G. Dietler, Examination of line crossings by atomic force microscopy, *Forensic Sci. Int.* 119 (2001) 290–298.
- [32] C.J. Yong, Cai, Membrane deformation of unfixed erythrocytes in air with time lapse investigated by tapping mode atomic force microscopy, *Micron* (2005), (Epub ahead of print).
- [33] M. Baumann, Cell ageing for 1 day alters both membrane elasticity and viscosity, *Pflug. Arch. Eur. J. Phys.* 445 (2003) 551–555.

6. Outlook

In the past decade atomic force microscopy has developed very rapidly. Nowadays users benefit from high resolutions both in lateral and vertical direction, the handling was made much more user-friendly, thus the AFM became an established technique in different fields of science. Obviously the main advantage for biological, biophysical and medical applications is the ease of sample preparation.

As exemplified in this work, collagen fibrils exhibit a homogeneous structure and the elasticity of the core is similar to the shell. Hence, for elasticity measurements on collagen fibrils in bone sections it does not matter whether the measurements are performed in or outside the fibril. Since in cleaved samples it is difficult to distinguish between core and shell this knowledge is particularly useful. This is probably the most important prerequisite, when force spectroscopy on collagen fibrils is considered for the determination of degradation processes of different bone samples.

A supplementary method might be to measure the resistance of the “glue”-filaments between the organic and anorganic bone constituents. An alteration over time might be suitable for age determination. However, before such methods can be applied on a routinely basis much work remains to be done: first of all it needs to be checked under laboratory conditions, whether a detectable alteration occurs with time at all. Secondly, the influence of the soil, which surrounds the bone and the climate need to be studied very thoroughly.

In this context a conceivable application of AFM based force spectroscopy could be the age determination of skeletal remains. In the last decades many common graves have been revealed in conflict areas. In order to reconstruct incidents, precise dating of the grave is indispensable. One possibility is to investigate the degradation of the organic matrix in the remaining bones of the skeletons. Minute amounts would be sufficient for probing elastical properties by means of nanotechnological methods.

As presented in this thesis the AFM may serve as a novel tool in forensic science. It is useful to examine the alteration of blood spots for chronological reconstruction of crimes, thereby providing important evidence in crime scene investigation. However, before this method can be routinely applied, some issues remain to be solved. First of all, a possible influence of the inhomogeneous assembly within the blood spot has to be carefully verified, in order to exclude that the point of measurement determines the outcome. Besides that, it has to be checked whether elasticity changes are different when the blood spot ages on different substrates, for example wood, clothes or metal subsurfaces. A major impact on blood ageing presumably originates from environmental conditions like temperature, humidity, light irradiation or decomposition by organically driven processes. In order to characterize the influence of all these factors, many longterm studies where different conditions are compared need to be conducted.

7. Appendix

Visual Basic program for dialysis system control in combination with A/D converter card from Velleman K8005, USB Experiment Interface Board

```
Option Explicit
Dim DoNothing As Boolean
Dim n As Integer
Private Declare Function OpenDevice Lib "k8055d.dll" (ByVal CardAddress As Long) As Long
Private Declare Sub CloseDevice Lib "k8055d.dll" ()
Private Declare Function ReadAnalogChannel Lib "k8055d.dll" (ByVal Channel As Long) As Long
Private Declare Sub ReadAllAnalog Lib "k8055d.dll" (Data1 As Long, Data2 As Long)
Private Declare Sub OutputAnalogChannel Lib "k8055d.dll" (ByVal Channel As Long, ByVal Data As Long)
Private Declare Sub OutputAllAnalog Lib "k8055d.dll" (ByVal Data1 As Long, ByVal Data2 As Long)
Private Declare Sub ClearAnalogChannel Lib "k8055d.dll" (ByVal Channel As Long)
Private Declare Sub SetAllAnalog Lib "k8055d.dll" ()
Private Declare Sub ClearAllAnalog Lib "k8055d.dll" ()
Private Declare Sub SetAnalogChannel Lib "k8055d.dll" (ByVal Channel As Long)
Private Declare Sub WriteAllDigital Lib "k8055d.dll" (ByVal Data As Long)
Private Declare Sub ClearDigitalChannel Lib "k8055d.dll" (ByVal Channel As Long)
Private Declare Sub ClearAllDigital Lib "k8055d.dll" ()
Private Declare Sub SetDigitalChannel Lib "k8055d.dll" (ByVal Channel As Long)
Private Declare Sub SetAllDigital Lib "k8055d.dll" ()
Private Declare Function ReadDigitalChannel Lib "k8055d.dll" (ByVal Channel As Long) As Boolean
Private Declare Function ReadAllDigital Lib "k8055d.dll" () As Long
Private Declare Function ReadCounter Lib "k8055d.dll" (ByVal CounterNr As Long) As Long
Private Declare Sub ResetCounter Lib "k8055d.dll" (ByVal CounterNr As Long)
Private Declare Sub SetCounterDebounceTime Lib "k8055d.dll" (ByVal CounterNr As Long, ByVal DebounceTime As Long)
Private Declare Sub Sleep Lib "kernel32" (ByVal dwMilliseconds As Long)
```

"Set and clear digital output - manual"

```
Private Sub Command2_Click()
SetDigitalChannel (1)
End Sub
```

```
Private Sub Command3_Click()
ClearDigitalChannel (1)
End Sub
```

"Save data in Excel worksheet - manual"

```
Private Sub Command4_Click()
Dim Wo As Excel.Workbook
Dim Sh As Worksheet
Dim Ex As New Excel.Application
Set Wo = Ex.Workbooks.Add
Set Sh = Wo.ActiveSheet
Ex.ActiveWorkbook.Save
Ex.ActiveWorkbook.Close
End Sub
```

'Excel workbook
'Excel sheet
'Excel application

'Excel save
'Excel close

"Connect and disconnect A/D converter"

```
Private Sub Connect_Click()
    Dim CardAddress As Long
    Dim h As Long
    CardAddress = 0
    'CardAddress = 3 - (Check1(0).Value + Check1(1).Value * 2)
    h = OpenDevice(CardAddress)
    Select Case h
        Case 0, 1, 2, 3
            lblAusgabe_connect.Caption = "Card " + Str(h) + " connected"
        Case -1
            lblAusgabe_connect.Caption = "Card " + Str(CardAddress) + " not found"
    End Select
    'If h >= 0 Then Timer1.Enabled = True
End Sub
```

```
Private Sub disconnect_Click()
    CloseDevice
    lblAusgabe_connect.Caption = "Card disconnected"
End Sub
```

 "PH7-calibration_manual"

```
Private Sub pH7_Click()
    Dim ph_7 As Variant
    Dim Ausgabe_ph7 As Variant
    ph_7 = ReadAnalogChannel(2)
    Ausgabe_ph7 = ph_7 * 5 / 255
    lblausgabe_ph7.Caption = ph_7
    lblAusgabe_ph7_volt.Caption = Ausgabe_ph7
End Sub
```

'read out pH-value at pH 7
 'conversion in Volt
 'output in panel
 'output in panel in Volt

 "Starting control"

'Variable declaration

```
Private Sub Command1_Click()
    Dim t1 As String
    Dim t2 As String
    Dim t3 As String
    Dim t4 As Variant
    Dim wartezeit As Variant
    Dim t5 As Long
    Dim m As Variant
    Dim Zeitintervall As Variant
    Dim ph_anfang As Variant
    Dim ph_soll As Variant
    Dim ph_ist As Variant
    Dim ph_7 As Variant
    Dim ph_bei7 As Long
    Dim Anfangs_pH As Long
    Dim Ausgabe_ph7 As Variant
```

'start time
 'end time
 'actual time for calculation of the setpoint
 'elapsed time
 'delay time between measurements (Variable)
 'actual time
 'slope of set curve
 'dialysis time
 'start-pH-value
 'actual pH-set value
 'actual pH value
 'pH at 7 for calculation in Excel
 'start pH for calculation in Excel

'Variable declaration for data storage

```
Dim Wo As Excel.Workbook
Dim Sh As Worksheet
Dim Ex As New Excel.Application
Dim n As Long
Dim digout1 As Integer
Dim delta_delta_ph As Variant
Dim pH As Variant
```

'Excel Workbook
 'Excel worksheet
 'Excel application
 'counter for rod number

Dim delta_U As Variant
 Dim delta_ph As Variant
 Dim Start_ph As Variant
 Dim phsoll As Variant
 Dim delta_Usoll As Variant

'Programmroutine

ph_7 = 0 'blausgabe_ph7.Caption

'read pH-value at pH7

Zeitintervall = Dialysedauer.Text
 t1 = Now
 t2 = DateAdd("s", Zeitintervall, t1)
 ph_anfang = ReadAnalogChannel(2)

'dialysis period
 'start time
 'end time
 'read out start pH

'Open Excel

Set Ex = New Excel.Application
 Set Wo = Ex.Workbooks.Add
 Set Sh = Wo.ActiveSheet

'open new Excel workbook

'Loop for measurement and control

t3 = t1
 Do While t3 < t2
 t3 = Now
 t4 = DateDiff("s", t1, t3)
 m = (ph_7 - ph_anfang) / Zeitintervall
 ph_soll = m * t4 + ph_anfang
 ph_ist = ReadAnalogChannel(2)
 lblAusgabe_ph_ist.Caption = ph_ist * 5 / 255
 lblAusgabe_ph_ist.Refresh
 istph_b.Caption = ph_ist
 istph_b.Refresh
 sollph_v.Caption = ph_soll * 5 / 255
 sollph_v.Refresh
 sollph_b.Caption = ph_soll
 sollph_b.Refresh

'actual time
 'elapsed time
 'slope calculation
 'set point calculation
 'actual pH value
 'write pH value in panel

VScroll1.Value = ph_ist
 VScroll1.Refresh
 Label1.Caption = t4
 Label1.Refresh

'refresh Scroll

'Conversion of Volts in pH-value and write in panel

Start_ph = Anfang_pH.Text
 delta_ph = 6.5 - Start_ph
 delta_delta_ph = delta_ph / ph_anfang
 delta_U = ph_ist - ph_anfang
 pH = Start_ph - delta_U * delta_delta_ph
 lblAusgabe_Input.Caption = pH
 lblAusgabe_Input.Refresh
 delta_Usoll = ph_soll - ph_anfang
 phsoll = Start_ph - delta_Usoll * delta_delta_ph
 label2.Caption = phsoll
 label2.Refresh

'write actual pH value in scroll in panel

'Set and clear output

If ph_ist > ph_soll Then

'comparison set and actual value

```
SetDigitalChannel (1)                                'set output
lblAusgabe_digout1.Caption = 1                        'write output state in panel
lblAusgabe_digout1.Refresh
digout1 = 1
Else: ClearDigitalChannel (1)
lblAusgabe_digout1 = 0
lblAusgabe_digout1.Refresh
digout1 = 0
End If

'Save data in Excel
pH-Wert
n = n + 1                                              'increase counter (Excel)
With Sh
.Range("C" & n).Value = ph_ist                        'copy actual value in correct rod
.Range("A" & n).Value = t4                            'copy actual value in correct rod
.Range("B" & n).Value = ph_soll                       'copy actual value in correct rod
.Range("F" & n).Value = digout1                      'copy actual value in correct rod
.Range("D" & n).Value = pH
.Range("E" & n).Value = phsoll
End With

'Delay between measurments
t5 = Totzeit.Text * 1000
Sleep t5
lblAusgabe_ph_ist.Caption = ph_ist * 5 / 255          ' write actual pH value in panel
lblAusgabe_Input.Caption = ph_ist                    ' write actual pH value in panel in scroll
VScroll1.Value = ph_ist                              ' refresh Scroll
Loop

'Save and close Excel
Ex.ActiveWorkbook.Save                                'Excel save
Ex.ActiveWorkbook.Close                              'Excel close
Label1.Caption = "Regelung beendet"
Label1.Refresh
ClearDigitalChannel (1)
lblAusgabe_digout1.Caption = 0
lblAusgabe_digout1.Refresh
End Sub
```

8. Acknowledgements

I want to take the opportunity to thank all the people who were involved and supported me with explanations, discussions and new ideas.

I am greatly indebted to Prof. Dr. Wolfgang M. Heckl for the great opportunity to participate in his group, for the motivation and the granted freedom to realize own ideas.

I'm particularly grateful to Dr. Stefan Thalhammer for the supervision at all and assistance and support in the theoretical and the practical part of the dissertation.

For the endless discussions on all parts of the doctoral thesis, for his lectures in biology as well as inspirations for all kinds of physical and technical problems I want to thank in particular PD Dr. Albert Zink. I particularly appreciate the time he always had for enlightening discussions.

I am also very grateful to Dr. Thomas Wokusch and Dr. Peter Dreier from Siltronic AG for the opportunity to work part-time, thereby offering the time frame to explore the world of science. Moreover, I would like to thank Prof. Dr. Stefan Sotier for the opportunity to attend lectures at the LMU which eventually led to the preparation of this thesis.

I also want to acknowledge our collaboration partners in the hospital Bogenhausen, and the Universities of Augsburg and Linz, especially Prof. Dr. Andreas Nerlich, Prof. Dr. Achim Wixforth and Prof. Dr. Peter Hinterdorfer. I very much appreciate the opportunity to conduct some measurements in the laboratory of Prof. Dr. Hinterdorfer. Here I also want to thank Dr. Gerald Kada for devoting his time to my experiments and sharing his experience in handling the AFM with me. Furthermore I'm grateful to Daniel Steppich for sharing his limited measurement time at the AFM in Augsburg. I also want to mention the fruitful collaboration we had in the cell-interface project Prof. Dr. Heidegard Hilbig from the University of Leipzig.

Special thanks go to Dr. Markus Lackinger who helped me, particularly at the final stage.

I am also grateful of the support from Marek Janko on our measurement trips to Augsburg.

For sharing his expertise with the SEM image acquisition and contrast interpretation I want to express my gratitude to Mr. Macknapp from the Deutsches Museum.

I would like to thank Dr. Lilian Costa for her very helpful support. The discussions with her were very important for my basic understanding of biology. She also introduced me to the secrets of the AFM.

For her support and understanding, especially when I was exploring the scientific world, I am very much obliged to my partner Julia.

Last but not least, I want to thank my parents Wasti and Gerti for their support

9. Curriculum Vitae

Personally

Name: Stefan Sebastian Strasser
Day of birth: 04.01.1975 / Altötting
Address: Schatzhof 30 1/3, 84533 Marktl / Inn
E-mail: stefan.strasser@vr-web.de
Legal status: single

Education

1981-1987: Primary school, Zeilarn
1987-1991: Secondary school Simbach, secondary school level
1991-1993: Technical college Pfarrkirchen, vocational baccalaureate diploma
1994-1999: Undergraduate Study: physikalische Technik, University of Applied Sciences, Diplom (FH), final grade 1.6
2001-2004: Master Study: Mikro- u. Nanotechnik, University of Applied Sciences, Master of Engineering, final grade 1.4
since 2004: Ph.D. student / LMU München, Prof. Dr. Heckl

Practical courses

1995: Internship, Bosch-Siemens-Hausgeräte, Traunreut
1997: Internship, Wacker Siltronic AG, Burghausen

Military Service / Civil Service

1993-1994: Civil Service for handicapped people, Caritas Altötting

Professional employment

1999-2000: Development engineer, Daimler Chrysler Aerospace, Schrobenhausen
since 2000: Development engineer, Wacker Siltronic AG, Burghausen